Well name	m	R^2	β
Bujang-2	2.3787	0.9735	2.42
Sepat-1	2.5864	0.9932	2.82
Noring-2	2.8953	0.9994	4.03
Semangkok-1	1.4831	0.9973	1.60
Tangga-1	2.6048	0.9994	2.87
Inas-1	2.9482	0.9998	4.43

Table 6.4. β estimates at centre of the Malay Basin, based on the slope of subsidence *vs* (1-$e^{-t/\tau}$) plot in Fig. 6.27.

instantaneous stretching was assumed when estimating β in the central wells. This is not regarded as serious because a rifting duration of 10 Ma is well within the permissible range for the instantaneous rifting model to work (Jarvis and McKenzie, 1980). Another possible reason is that the gravity anomalies are sensitive only to the present-day crustal structure, whereas subsidence analysis incorporates a time-dependent thermal model, which assumes uniform thinning of the subcrustal lithosphere and the crust (McKenzie, 1978). The reliability of the subsidence analysis technique, therefore, depends on the quality of the biostratigraphic data used in the backstripping. The ages of the stratigraphic units, however, are believed to be reasonably accurate because they are based on a recently updated stratigraphic scheme which uses a large well data base in the Basin (Morley *et al.*, 1994).

The discrepancy between the values of β from gravity modelling and β from subsidence analysis could also be the result of non-uniform stretching (*cf.* Royden and Keen, 1980), whereby the amount of subcrustal stretching and/or thinning (β_m), perhaps by some other mechanism, is slightly greater than that in the crust (β_c). If β estimated from subsidence analysis represents the stretching factor for the whole lithosphere, the stretching factor in the subcrustal lithosphere, β_m, is given by

$$\frac{a - y_c}{\beta_m} = \frac{a}{\beta} - \frac{y_c}{\beta_c} \tag{6.13}$$

where a and y_c are the lithospheric and crustal thicknesses, respectively, and β_c is the crustal stretching factor. From the results, $\beta = 4.3$, $\beta_c = 2.3$ (minimum)

and, hence, β_m is 6.4. A greater, instead of lower, β_m at the centre of the Basin contradicts with the earlier model of nonuniform stretching used to explain the rift flank uplift. Also, if mantle stretching is much greater than the crustal thinning at the center of the Basin, we would expect massive uplift of the basin centre rather than subsidence.

The discrepancy in the β estimates is most probably the artefact of the different assumptions used in the two methods (Fig. 6.29). In Chapter 5, β was estimate

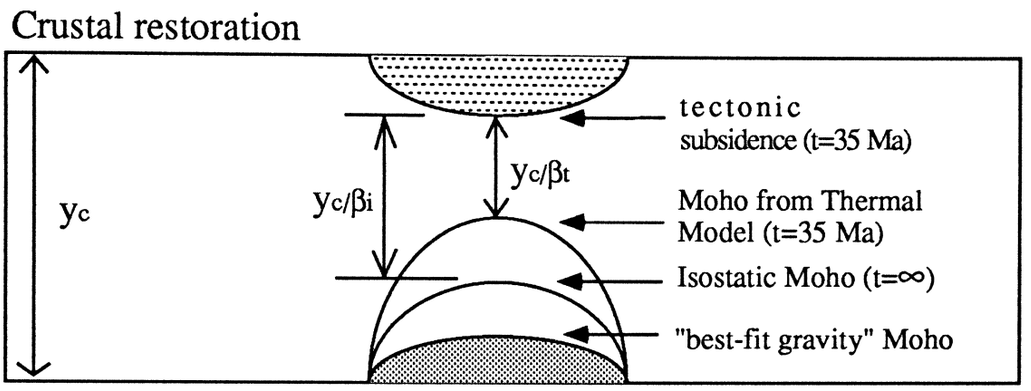

Figure 6.29. Diagram showing the difference in β values obtained using the two methods: β_i – from backstrip (isostatic) Moho (Chapter 5) and β_t – based on subsidence analysis (Chapter 6). Isostatic Moho calculated assuming $\rho_m = 3330$ kg m^{-3}. Note that $\beta_t > \beta_i$. The "best-fit" gravity Moho represents the Moho configuration that explains the free-air gravity anomaly.

from the crustal structure based on the backstrip Moho, which assumes Airy isostasy. As shown in Fig. 5.7 (p. 161), the Airy model underestimates the amount of thinning for a young basin because it ignores the fact that the stretched mantle may have a lower density than that assumed in the Airy model. The stretching factor obtained in this manner (β_i in Fig. 6.29) is, therefore, not the correct β, because the observed subsidence, from which it is derived, is less than the total subsidence (*i.e.* the subsidence when $t = \infty$). On the other hand, β determined from subsidence curves using the stretching model in Chapter 6 (β_t in Fig. 6.29) is more reliable because it incorporates a thermal model, which takes account of the transient nature of the subsidence. Because the Moho implied by the subsidence-derived, β_t (maximum 4.3), is shallower than the isostatic Moho, the degree of

isostatic compensation, C_m, of the Basins may be even lower than that determined previously in Chapter 5.

A maximum β_c value of 4.3 means that the crust underneath the centre of the Malay Basin has been thinned to about 7 km, assuming the initial crustal thickness was 30 km. The gravity data from across the central part of the Basin, however, suggest that the present crustal thickness is about 14 km, much greater than is indicated by the total subsidence. As discussed in Chapter 5, this could be the result of addition of lower crustal material by magmatic underplating. The underplating mechanism is, however, considered unlikely because the evidence for uplift, which should have occurred during the rifting phase, is lacking.

Without invoking the underplating mechanism, the β estimate of 4.3 already seems rather excessive for a basin that is still underlain by continental crust and filled, almost completely, with sediment. At stretching factors >2, there is an increasing chance of magma rising to the surface through dyke injection and volcanism; β>4 usually leads to continental splitting (Dewey, 1982). There is no evidence so far, despite extensive drilling for oil, of any intrusive or extrusive volcanics in the sedimentary fill. The available evidence, therefore, appears to be in favour of the alternative hypothesis suggested in Chapter 5, that part of the subsidence in the Malay and Penyu Basins is the result of strike-slip or upper crustal detachment faulting that did not involve the mantle. The total tectonic subsidence obtained by backstripping does not reflect the true stretching factor but includes subsidence resulting from other tectonic causes. The structural data presented in Chapters 3 and 4 have, indeed, shown the importance of strike-slip faulting in controlling basin formation.

6.3.5 Heat Flow

To test the estimates of β, the theoretical heat flow predicted by the β values are compared with the heat flow anomaly observed in the Basin. Data from 29 wells

were used, including those based on DST/PT data. Figure 6.30 shows a series of theoretical heat flow curves for various values of β between 1.2 and 4, as indicated by the subsidence analysis results. The figure shows that heat flow anomaly

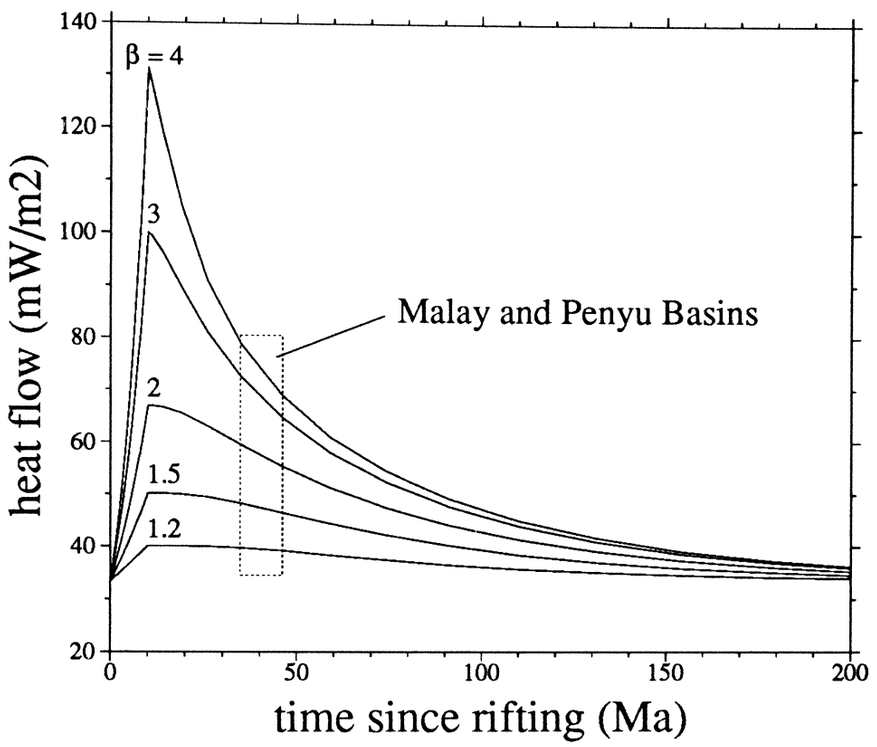

Figure 6.30. Theoretical heat flow history (1D model, uniform stretching) predicted by various β values for stretching duration of 10 Ma. Shown also is observed range of heat flow (35–80 mW m^{-2}) in the Malay/Penyu Basins (age ~35–40 Ma), excluding crustal heat flow of 33 mW m^{-2}.

resulting from lithospheric stretching decreases exponentially with time since the end of stretching (10 Ma) but, for young basins (<50 Ma), the anomaly is still significant. For example, the Malay and Penyu Basins, whose age is ~35–40 Ma, show present-day heat flows of 35–80 mW m^{-2} after the crustal contribution of 33 mW m^{-2} has been subtracted, which is comparable to the predicted basal heat flow. Table 6.5 compares the predicted and observed heat flow at some of the well locations, based on β derived from backstripped subsidence. The observed and predicted heat flows are plotted in Fig. 6.31, which shows a reasonable correlation and, thus, gives confidence in the β estimates from 1D backstripping.

Well name	β	heat flow observed	(mW m^{-2}) calculated
Anding-1	1.3	94	76
Anding-2	1.3	89	76
Angsi-1	1.9	94	95
Banggol-1	1.5	75	82
Bedong-1	3.6	72	110 *
Belumut-2	1.15	75	72
Besar-1	2.0	84	93
Bujang-2	2.4	70	99 *
Duyung 5H-2.1	1.6	91	85
Duyung Barat-1	1.6	85	84
Irong Barat-1	3.0	107	106
Palas-1	1.7	85	87
Resak-2	1.65	96	86
Tinggi-1	1.4	98	79 *
Tok Bidan-1	1.15	62	72
Sepat-1	2.8	86	104
Tujuh-1	4.0	66	112 *
Tangga-1	2.87	77	118 *
Sotong-1	1.3	89	76
Sotong-2	1.35	94	79
Sotong-5	1.3	86	76
Sotong 5G-5.1	1.3	94	76

Table 6.5. Comparison between observed and modelled heat flow based on β obtained from subsidence analysis. "Calculated" heat flow, here, includes the crustal heat flow of 33 mW m^{-2} estimated in Section 6.1. Bold well names denote DST/PT data. Calculation of heat flow assumes 35 Ma-old basin, stretched over a 10 Ma period. There is reasonable agreement between predicted and observed except for wells indicated by (*). The observed and calculated heat flows are plotted in Fig. 6.31.

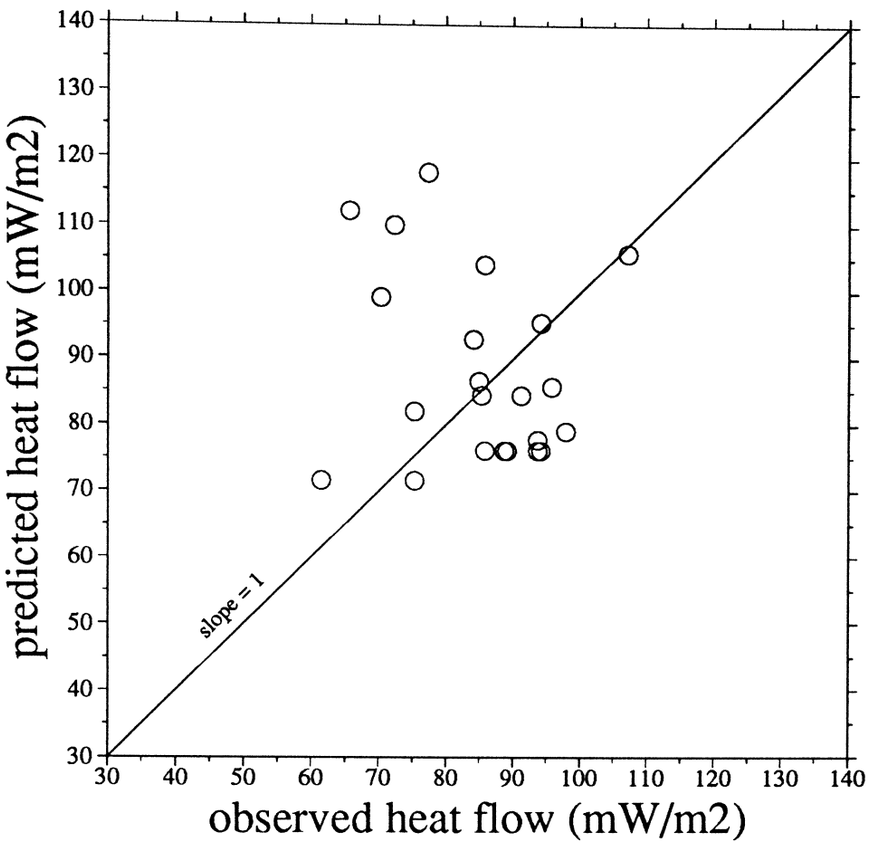

Figure 6.31. Plot of predicted *vs* observed heat flow data from Table 6.5. The diagonal line (slope = 1) represents perfect correlation.

For wells at the deepest central parts of the Basin, the predicted heat flow is higher than the observed. This could be the result of sediment blanketing, which may have reduced the observed surface heat flow significantly. The thick pile of sediment, especially at the centre of the Basin, acts as an insulator that prevents heat from escaping through the surface. Studies by de Bremaecker (1983) and Lucazeau and Le Douaran (1985), have shown that, for a moderately high sedimentation rate (350 mm Ma^{-1}) as in the Malay Basin, the reduction of surface heat flow resulting from sediment blanketing could be as high as 20–30%. If we assume, rather conservatively, a 25% reduction in the Malay Basin, a closer agreement between the predicted and observed heat flow is achieved.

6.4 Penyu Basin

In this section, the principles of subsidence analysis applied to the Malay Basin are used to examine the subsidence history in the Penyu Basin to determine the amount of stretching. Data from four wells were used (Table 6.6). The depths

Horizon	Ma	Penyu	Cherating	Rumbia	Merchong
1	0	52	72	66	62
2	3.5	400	530	480	560
3	7	720	840	820	880
4	13	800	990	900	1050
5	19	1150	1400	1330	1400
6	25	1700	2100	2000	1850
7	30	2350	2780	3050	2420
8	35	7230	5200	5950	4450

Table 6.6. Depth (in metres) to seismic horizons in Penyu Basin wells obtained by seismic-to-well correlation.

to the top of stratigraphic units are as defined in Chapter 3, based on seismic reflection data. The ages of the units are based on available biostratigraphic data (Appendix A.3). The approximate ages of the major unconformities in the Basin (Horizons 3 and 6) are based on correlation with the Malay Basin using the chronostratigraphic scheme of Morley *et al.* (1994). Horizon 3 is ~7 Ma, equivalent to the regional unconformity that marks the end of the basin inversion in both the Malay and West Natuna Basins (Ginger *et al.* 1993, Morley *et al.* 1994). Palynological studies by Rexilius *et al.* (1992) suggest that Horizon 6 corresponds approximately to the top of the Oligocene (~25 Ma). The ages of other horizons are much less certain and were determined by interpolation between the main marker horizons. As in the Malay Basin, rifting in the Penyu Basin is assumed to have been initiated at 35 Ma.

The backstripped subsidence and the corresponding best-fit theoretical curves are plotted in Figure 6.32. Airy isostasy was assumed in the backstripping. To fit the observed subsidence, a stretching duration of 5 Ma was assumed in all

wells. The results indicate β values between about 1.6 and 2.4 which, as expected, are lower than those obtained in the Malay Basin. Note that, in Penyu-1 for example, the slope of the observed subsidence curve is slightly less than that of the theoretical curve. This could be the result of the basin inversion phase (Chapter 3) which causes slight uplift of the basement during the later part of the Basin's development. The β values predict present-day surface heat flows, inclusive of crustal heat flow of 33 mW m^{-2}, between 80 and 92 mW m^{-2}, which agree rather well with the observed heat flow shown in Table 6.7.

Well	β	Heat flow predicted*	mW m^{-2} observed
Merchong-1	1.6	84	82
Cherating-1	1.75	87	89
Rumbia-1	2.0	92	82
Penyu-1	2.4	97	87

Table 6.7. Predicted *vs* observed heat flow in Penyu Basin based on the results of subsidence analysis (Fig. 6.32). (* – predicted heat flow includes the crustal contribution of 33 mW m^{-2}).

Gravity modelling results for the Penyu Basin (Chapter 5) have indicated that the effective elastic thickness, T_e, of the lithosphere is about 12 km. A finite T_e and flexural rigidity means that, for a given sediment load, less subsidence will occur compared to when the lithosphere has no rigidity ($T_e = 0$). By assuming Airy isostasy when backstripping the Penyu Basin well data, the contribution of sediment loading to the total observed subsidence may have been overestimated. This could have resulted in a slight underestimation of the tectonic subsidence and, hence, β. The β values obtained using Airy isostasy, therefore, represent the minimum stretching factors. However, because the T_e is relatively low, the underestimation may not be siginificant. The crustal stretching factor estimated from the gravity profile (Line A, Table 5.1, p. 183), which crosses the deepest part of the Basin, is about 2.3 and, therefore, agrees with the results of the Airy backstripping in this section.

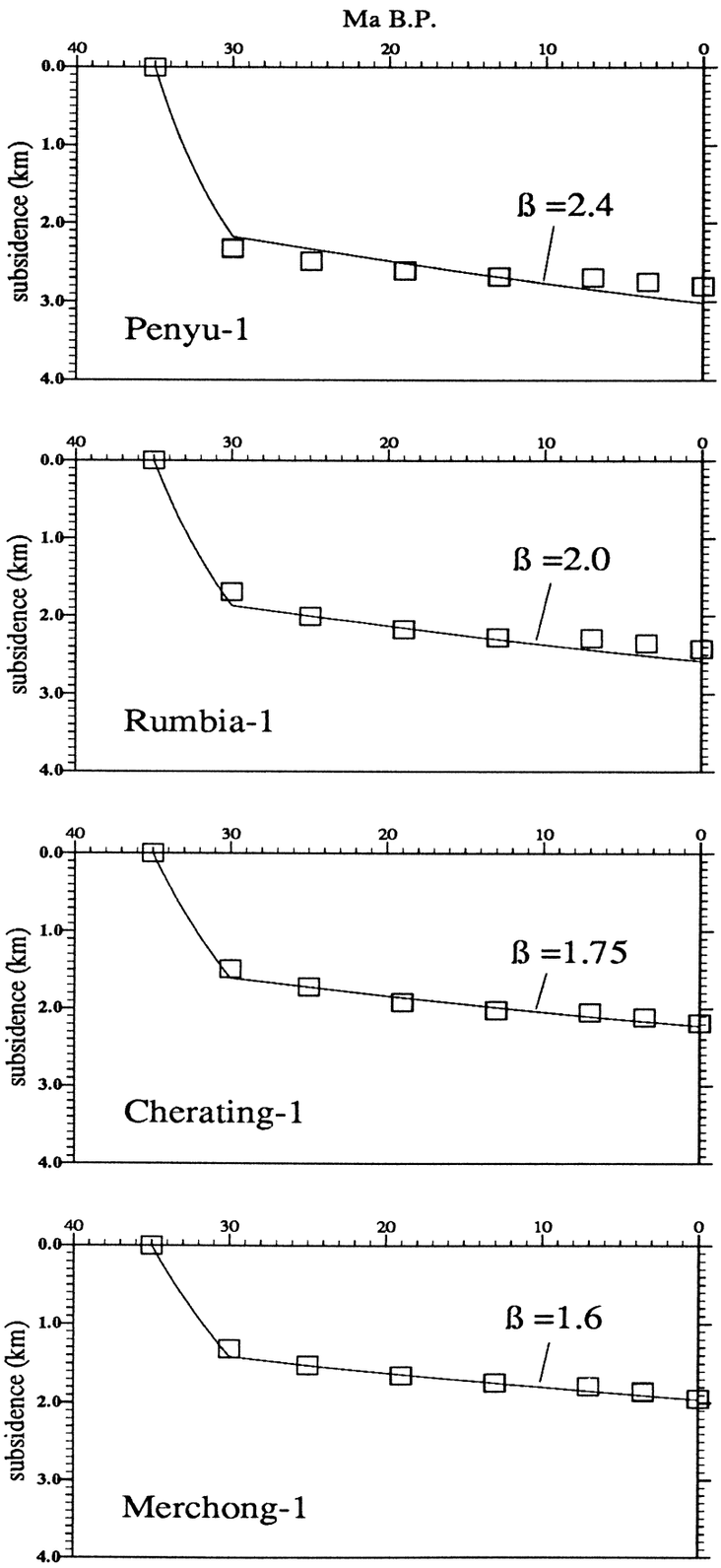

Figure 6.32. Subsidence in Penyu Basin wells. Best-fitting curves suggest rifting event from 35 to 30 Ma. Curves suggest β values between about 1.6 and 2.4.

6.5 Thermal History

In this section, sediment maturation data from the Malay Basin are used to investigate its heat flow history and compare it with the results of subsidence analysis and heat flow modelling. Only the Malay Basin is dealt with, because there are no data from the Penyu Basin. Determination of past heat flow is done, commonly, by extrapolating present-day heat flow back in time, using various indicators of temperature such as vitrinite reflectance, fission track annealing temperatures, and fossil biomarkers. Vitrinite reflectance is still the most common method of determining paleotemperatures in sediments. Below, an attempt is made to derive the heat flow history of the Malay Basin using vitrinite reflectance and fluorescence data. Vitrinite *fluorescence* measurement is a relatively new technique that has been applied successfully in basins where vitrinite reflectance is found to be suppressed because of various factors (Wilkins *et al.* 1992). Waples *et al.* (in press) used both types of vitrinite data in a recent study of the heat flow and maturity modelling study of the Malay Basin. Their work, however, did not address the tectonic mechanisms of basin formation. The objective of this section is to examine the heat flow history of the Basin using the available vitrinite maturity data and to test the models presented so far, which were based on analyses of gravity anomalies, subsidence, and heat flow data. Some of the maturity data used in the study have been analysed by Waples *et al.* (in press) but most were compiled from unpublished reports listed in Appendix A.3.

6.5.1 Maturity Modelling

Derivation of the temperature history of sediment from vitrinite reflectance (R_o) requires knowledge of the burial history, which may be obtained by 1D backstripping (Chapter 6). If the temperature gradient at a given time during the Basin's history is known, the maximum temperature attained by a sedimentary unit can be calculated. The temperature history so derived is then used to calculate the

time-temperature index (TTI) — an indicator of thermal maturity — from which R_o may be derived using one of the maturity modelling techniques described, for example, by Woods (1988). In this study, the "forward" modelling approach is used, whereby the present-day R_o-depth profile is calculated based on an assumed temperature -gradient history, and is then compared qualitatively with the measured R_o. This process is repeated until a reasonable fit is achieved.

The traditional method of calculating R_o from Lopatin's TTI (Waples, 1980) is now, generally, considered unsatisfactory and has been superseded by the more sophisticated techniques based on chemical kinetics (Waples, 1994). In this study, R_o is modelled using the simplified chemical kinetics method of Sweeney and Burnham (1990), called "EASY%R_o". As in other kinetics-based model, the maturation of kerogen in the EASY%R_o model is given by the Arrhenius rate equation

$$k = Ae^{-E/RT} \tag{6.14}$$

where A is the pre-exponential factor, E the activation energy, R the universal gas constant (0.008314 kJ mol^{-1} K^{-1}), and T the temperature in K. The main advantage is that, instead of using a single reaction specific to a particular kerogen type (*cf.* Hunt and Hennet, 1992), the model uses a set of 20 parallel reactions with different E's but the same $A = 1 \times 10^{13}$ s^{-1}. This is done to simulate a natural mixture of kerogens, each with a value of E weighted according to a predetermined stoichiometric factor, as shown in Table B.2 (p. 300). The Arrhenius equation is used to calculate the extent of reaction, F, which is related to R_o by

$$R_o = \exp(-1.6 + 3.7F)$$

where F is the fraction of reactants converted. Details of the calculations are given in Sweeney and Burnham (1990) and summarized in Appendix B.2.

6.5.2 Suppression of Vitrinite Reflectance

The possible suppression of vitrinite reflectance in the Malay Basin was investigated recently by Waples *et al.* (in press). They applied a new technique of

measuring vitrinite *fluorescence*, "Fluorescence Alteration of Multiple Macerals" (FAMM) (Wilkins *et al.*, 1992; Wilkins *et al.*, 1995), which measures the change in the peak fluorescence intensity of vitrinite when subjected to excitation by a constant-intensity light source over a specified period of time (700 s). Measurements are made with a laser Raman microprobe instead of the traditional fluorescence optical microscope. FAMM measurements are calibrated against a "standard" telocollinite sample for conversion of the fluorescence alteration ratio to the equivalent vitrinite reflectance, R_{eq}.

Waples *et al.* (in press) compared the FAMM results with R_o measured using the conventional method. They found significant suppression of vitrinite reflectance, particularly in the southwest and north-central parts of the Malay Basin. Some of the data from the southern part of the Basin are illustrated in Fig. 6.33 in which vitrinite reflectance (R_o) is plotted against equivalent reflectance (R_{eq}). The figure shows that the FAMM data plot, almost, in a straight line, with R_{eq} increasing with depth, whereas the R_o data plot to the left of the FAMM data, suggesting varying degree of suppression.

The cause of the suppression is unclear, although Waples *et al.* (in press) suggested that it may be the result of marine influence in the southeastern part of the Basin, where connection with the ancestral South China Sea may have been established. However, this does not explain the suppression of vitrinite in the far northwestern corner of the Basin. The chemical basis of vitrinite reflectance suppression has been investigated by a number of workers (Wilkins *et al.*, 1992; Pradier *et al.*, 1992) and is thought to be one or a combination of several factors, the most important being the hydrogen content of kerogen. Wilkins *et al.* (1992) have shown significant suppression of vitrinite reflectance on the NW Australian shelf, because of the presence of perhydrous vitrinite, abundant liptinite or both. These studies also suggest that vitrinite suppression could be related to source-plant type and environment of deposition.

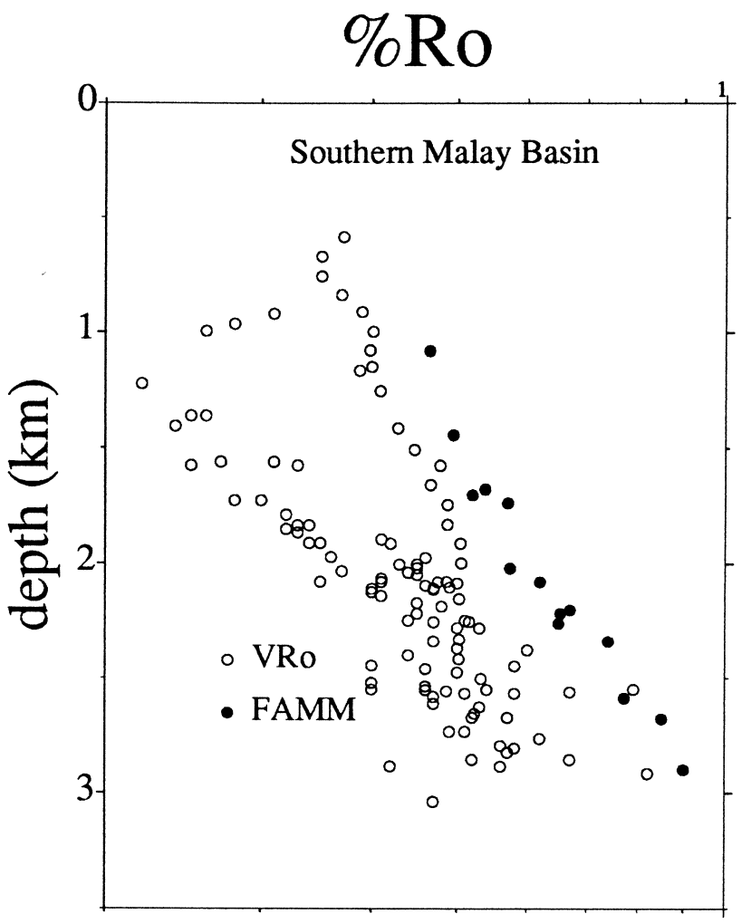

Figure 6.33. Plot of all available R_o and R_{eq} data from the southern part of the Malay Basin. Note that all the R_o data plot the left of the R_{eq} data, suggesting suppression of vitrinite reflectance.

6.5.3 Results from Malay Basin

The problem of using R_o data to invert heat flow history is illustrated in Fig. 6.34, which shows the results from three wells in the southern Malay Basin. The figure shows that, to fit the observed data, the temperature gradient is much lower than the present-day value throughout the history of the Basin. In Anding-1, for instance, the temperature gradient is <30 °C km^{-1}, corresponding to a heat flow of ~57 mW m^{-2}, which is lower than the estimated background heat flow (see Section 6.1). This conflicts with the evidence, which suggests that the Basin was formed by significant thinning of the lithosphere and, thus, would be expected to show exponential decrease in heat flow with time.

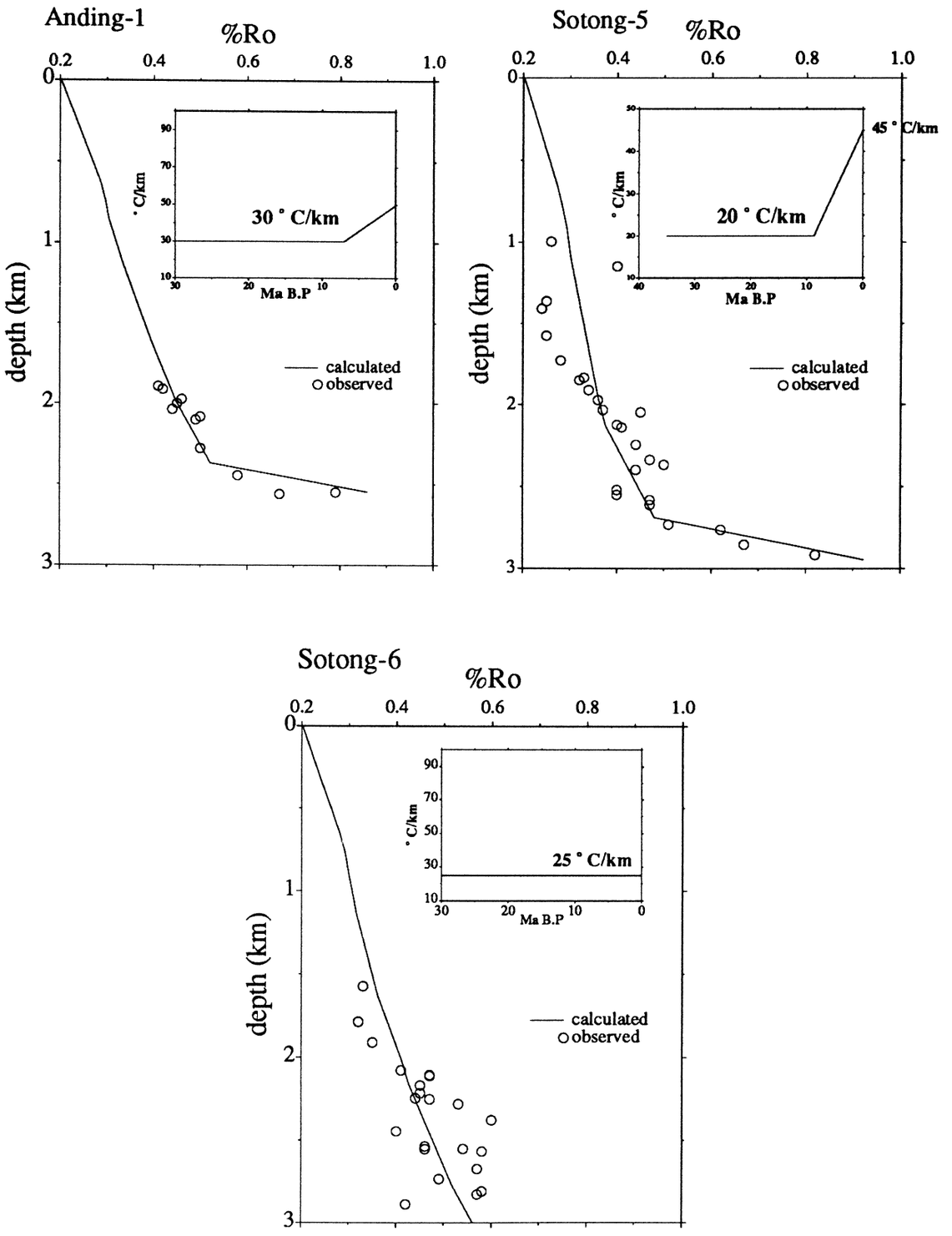

Figure 6.34. Result of modelling for Anding-1, Sotong-5 and Sotong-6 wells using conventional R_o data. The data requires the temperature gradient to be much lower than at present throughout the Basin's history.

Figure 6.34 shows a sudden increase in the temperature gradient within the last 10 Ma in two of the wells; note that these wells penetrate the pre-Tertiary basement, which contains sedimentary rocks. The spuriously high maturity of the bottommost sediment could be the result of overmature vitrinite, reworked from older rocks in the basement and incorporated into the Tertiary sediment. Waples *et al.* (in press) suggested that the apparently high maturity in the bottommost sediment could be the result of a recent regional "heat pulse". This is highly unlikely because, first, a recent heat pulse would have caused uplift of the entire Basin, for which no evidence has been found. In fact, subsidence appears to have been continuous since the end of the major inversion phase in late Miocene times, about 10 Ma ago. Secondly, a recent heat pulse would have affected the entire sediment column, not just the bottommost sediment. We should expect a steeper R_o-depth profile rather than a sharp "kick" at the bottom of the well column. Alternatively, the abrupt increase in R_o at the bottom of the well could be the result of an igneous intrusion emplaced at or near the sediment-basement interface during the later part of the Basin's history. This is difficult to prove, however, without further drilling.

Waples and coworkers concluded that a more plausible explanation for the apparent low maturity is the result of vitrinite suppression and, hence, recommended the use of FAMM-derived data wherever possible. FAMM data from five wells (see location in Fig. 6.8) were used to derive heat flow history to compare with the predictions of the stretching model. Figure 6.35 shows the results of modelling FAMM data from five wells.

Figure 6.36 shows the temperature gradients derived from FAMM data from the five wells modelled. All wells modelled show decreasing temperature gradients with time since rifting, assumed to be 35 Ma ago, from about 50–55 °C km^{-1} to 40–50 °C km^{-1}. Assuming an average sediment conductivity for the Basin's sediment (1.9 mW m^{-2}), the modelled present-day temperature gradients give surface heat flow values of 75–90 mW m^{-2}, which agree rather well with the observed heat flow

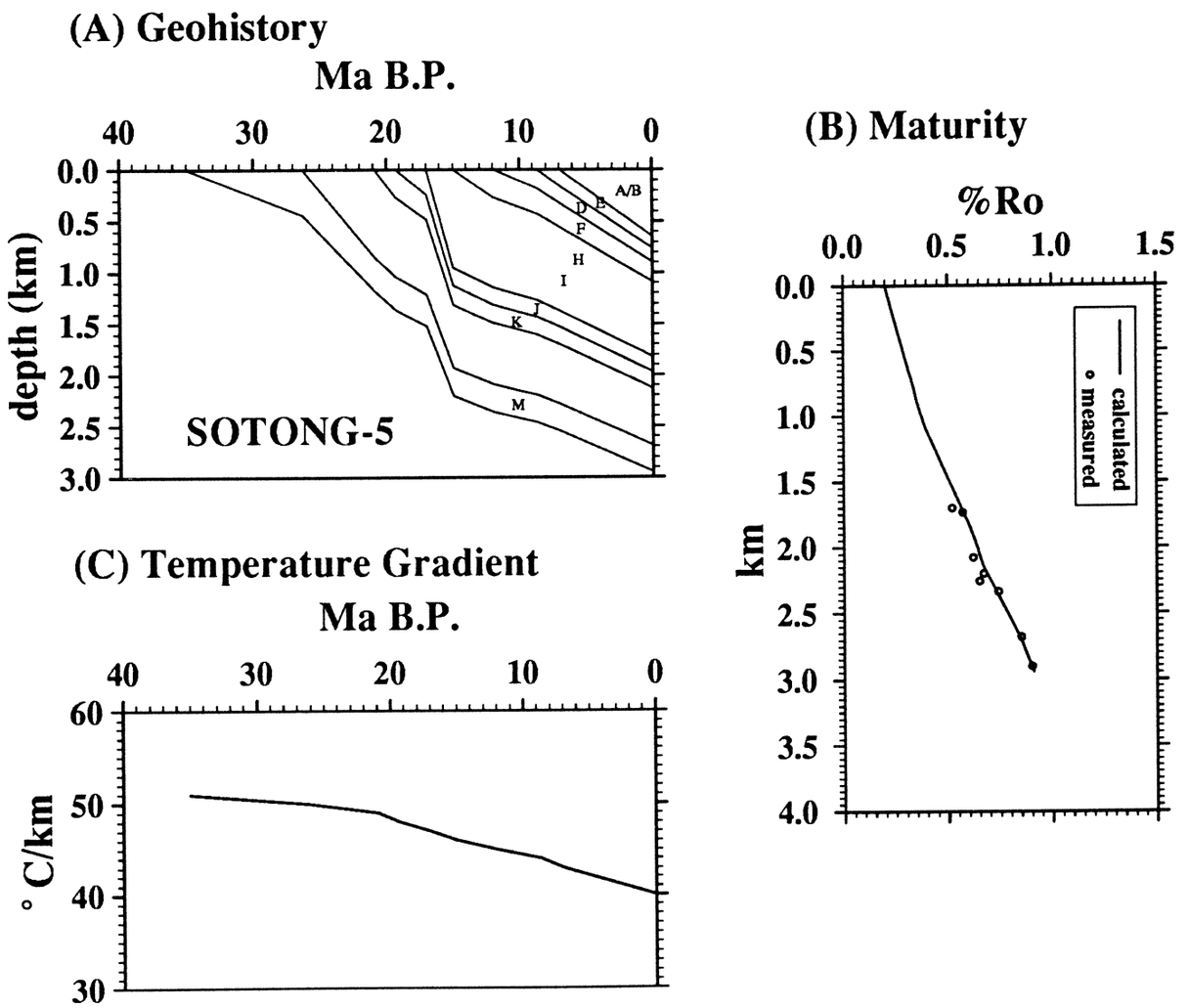

Figure 6.35. Result of R_o modelling for Sotong-5 (A) the Geohistory curve derived from backstripping, (B) Modelled R_o profile plotted against measured R_{eq}, and (C) Temperature-gradient history required to match the observed R_{eq}-depth plot, as shown in (B). Lines represent calculated R_o. Continued next page...

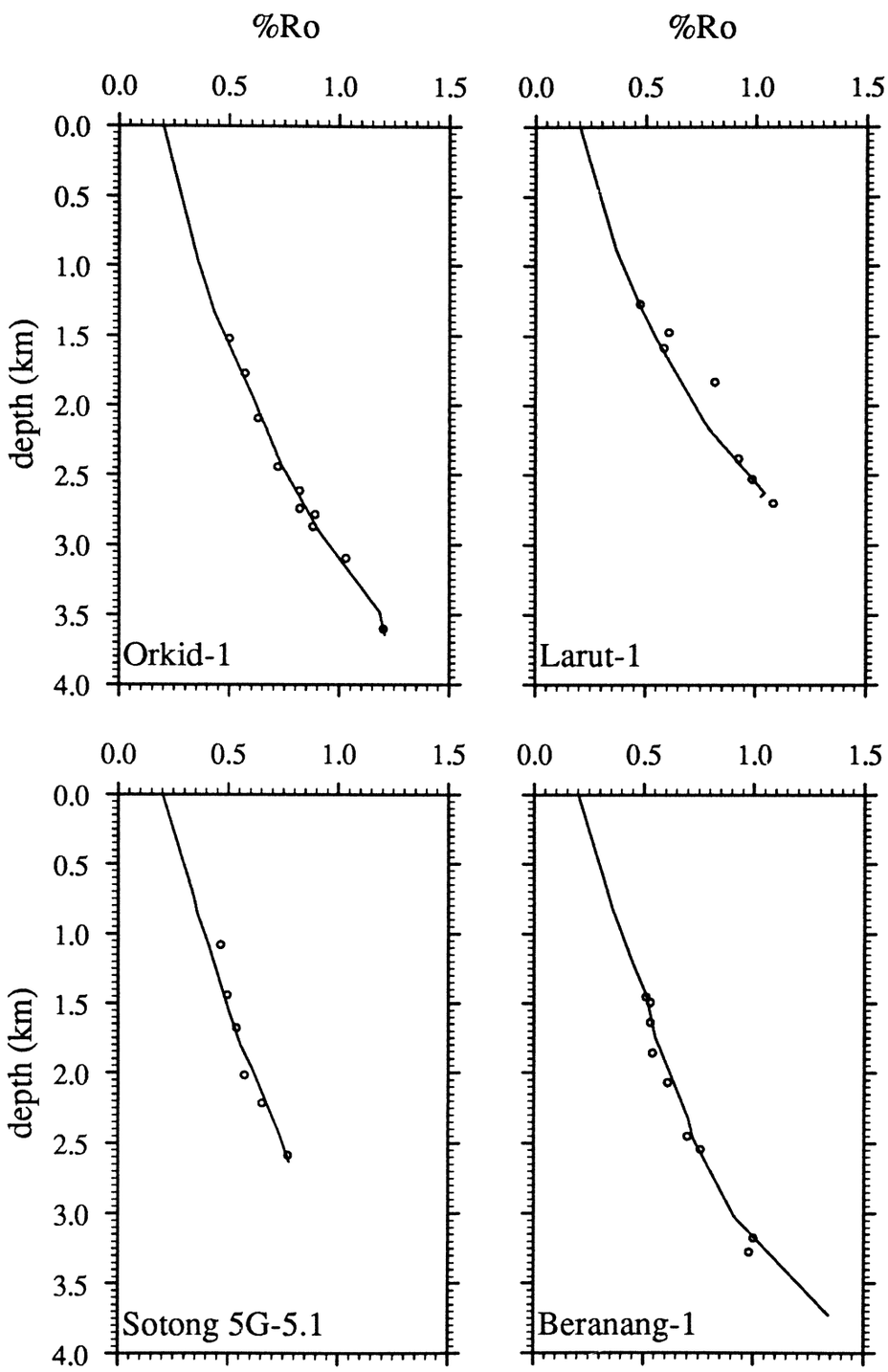

Figure 6.35 cont. Result of R_o modelling for Orkid-1, Larut-1, Sotong 5G-5.1 and Beranang-1 wells, using FAMM data (open circles).

(Table 6.1).

To estimate the heat flow variation with time from the temperature gradient, the thermal conductivity of the sediment, k_s, at any time was calculated by assuming a linear dependence of k_s on porosity, ϕ (Watts and Thorne, 1984):

$$k_s(z) = \phi k_w + (1 - \phi)k_g \tag{6.15}$$

where z is depth and k_w and k_g are the thermal conductivities of water and sediment grains, respectively, with values given in Table 5.2 (p. 196). ϕ is assumed to vary exponentially with depth (equation 5.13, p. 164) while lateral changes of ϕ and, hence, of k_s are ignored. The average conductivity of the sediment column at any time, t, is obtained by

$$k_{ave}(t) = [k_s(z_t) + k_s(0)]/2 \tag{6.16}$$

where z_t is the thickness of sediment at time t and $k_s(0)$ is the conductivity of surface sediment (1.3 mW m^{-2}). The results in Fig. 6.36 show relatively good agreement between the modelled heat flows and the heat flows derived from R_o data. All wells, except Larut-1, show initially-increasing heat flow with time since stretching, and decreasing gradually from about 22 to 15 Ma ago. The observed heat flow seems to decrease more rapidly after ~18 Ma, probably because of the increasing blanketing effect of sediment during the later part of the Basin's evolution. Absolute match between modelled and R_o-derived data could not be achieved because of uncertainties resulting from, for example, the variation in sediment thermal conductivity and in the background heat flow (crustal heat production) with time and the errors in estimating the stretching factors from subsidence analysis. Considering that the analysis is based on limited data from only a few wells, the heat flow history derived from sediment maturation data is reasonably well-matched by predictions of the stretching model.

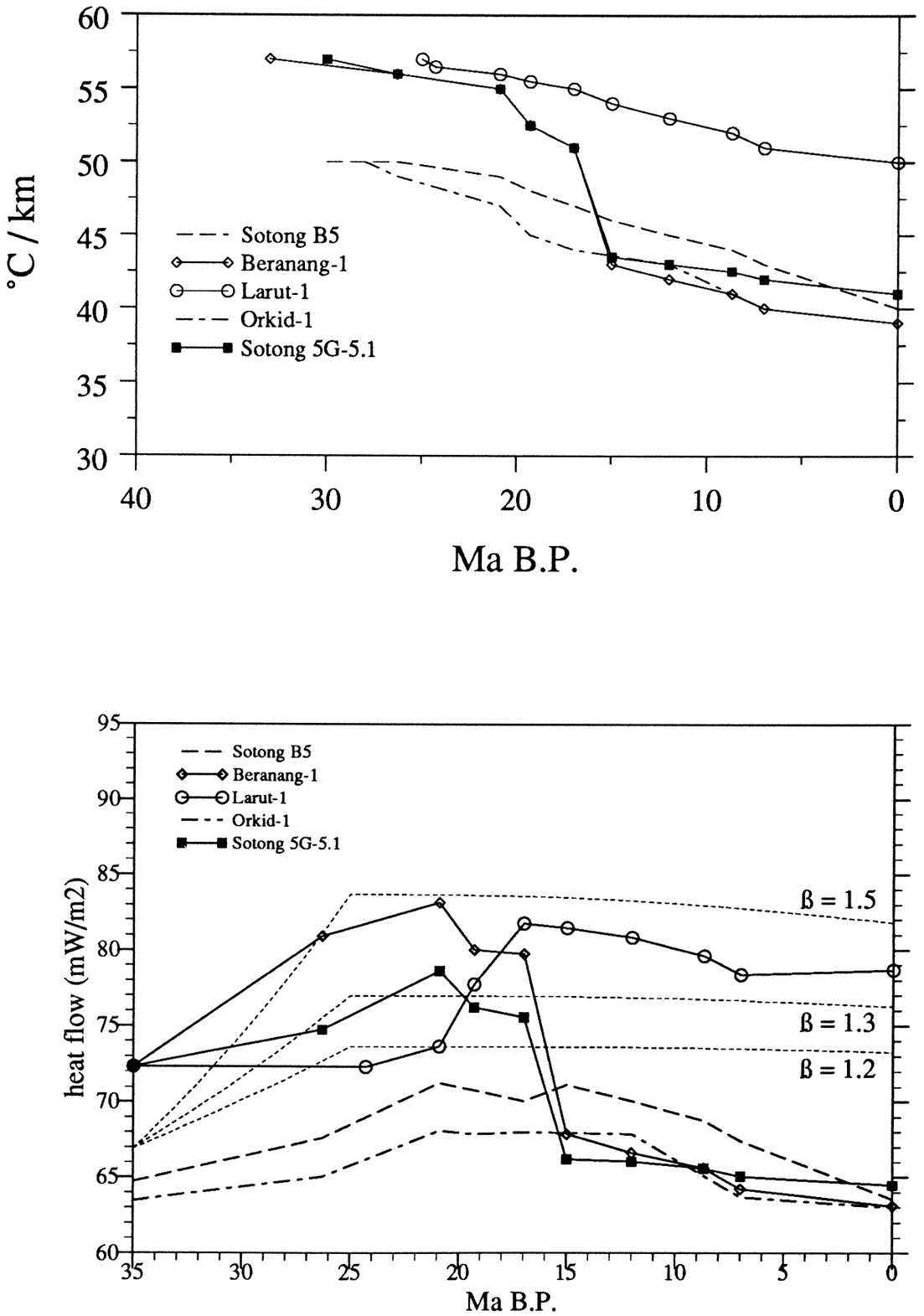

Figure 6.36. Geothermal gradient (top) and heat flow histories (bottom) derived from FAMM data in the five wells modelled (fine dashed lines) in Fig. 6.35. Modelled heat flow represents β= 1.2, 1.3, 1.5 based on backstripping results, with crustal heat flow of 33 mW m^{-2} added.

6.6 Conclusions

The subsidence and thermal histories of the Malay and Penyu Basins were investigated using well-established techniques of subsidence analysis and basin modelling. Stratigraphic data from 64 wells in the Malay Basin were backstripped using an Airy isostatic scheme. Application of the uniform finite-duration stretching model (stretching duration 10 Ma) based on the above information suggests that the stretching factor, β, in this Basin ranges from about 1.2 on the flanks to about 4.3 at the centre. Wells on the flanks of the Malay Basin show a delay in the subsidence, by about 10 Ma, relative to the time of rifting, possibly because of uplift of the basin flanks during the initial stages of rifting. The evidence suggests that the most plausible mechanism of uplift of the basin flanks during the initial rifting stages is by a form of nonuniform stretching coupled with lateral heat conduction.

The stretching factors estimated from the tectonic subsidence curves were used to predict the heat flow using the stretching model, for comparison with the observed heat flow. Compilation of heat flow data from the Malay and Penyu Basins and from the surrounding basins show that the area is now a high heat flow region, with an estimated heat flow anomaly of about 33–42 mW m^{-2} resulting from lithospheric stretching associated with the formation of the extensional basins. The Malay and Penyu Basins, like other basins in Sundaland, are generally less than 40 Ma and, hence, may still be undergoing thermal subsidence. This explains the relatively high heat flow observed in the region. The predicted heat flows based on the stretching factors, in general, agrees well with the observed heat flow. Backstripping well data from the Penyu Basin, also assuming Airy isostasy, shows maximum water-filled tectonic subsidence of about 3.0 km in the deepest part of the Basin, corresponding with a stretching factor of about 2.4. The β estimates from subsidence analysis were able to predict the present-day surface heat flows observed in the wells.

The subsidence results are further supported by the results of maturity mod-

elling based on vitrinite maturity data from a limited number of wells located on the flanks of the Basin. It is necessary to obtain, in future, good-quality maturity data from the central part of the Basin to better constrain its heat flow history.

Chapter 7

Conclusions

This study integrates various types of data, including structure (based on seismic interpretation), well stratigraphy, heat flow, and vitrinite maturity, to gain an understanding of the tectonic evolution of the Malay and Penyu Basins. In this chapter, the main conclusions of the various aspects of the study are summarized, and the implications for the origin and evolution of the Basins are discussed.

7.1 Regional Controls on Extension

The cause of the extension in central Sundaland during the early Tertiary seems to be related broadly to distributed shear deformation resulting from the indentation of India into Eurasia. Back-arc extension is thought to be unimportant on account of the large distance of the Malay and Penyu Basins from the Sumatra-Java subduction zone. Moreover, the oblique nature of the subduction beneath Sumatra has resulted in strong strike-slip partitioning of the deformation, aided by arc-parallel strike-slip faults and, thus, seems to have contributed little to the extension in Sundaland.

The regional geology (Chapter 2) suggests that strike-slip faulting and extension in Sundaland may have been in progress since Jurassic–Cretaceous times. We know, for instance, that the region was the site of a major collisional orogeny in the Late Triassic (The Indosinian), which must have resulted in thickening of the crust and lithosphere. Small intermontane basins controlled by major strike-slip faults,

such as the Gagau Formation of Peninsular Malaysia, are strong evidence for post-orogenic extensional tectonism in the region in pre-Oligocene times. Other evidence includes late Cretaceous–Paleocene basaltic extrusives and intrusives related to intraplate extension and, possibly, extension-related exhumation of high-grade metamorphic complexes in the Central Belt of Peninsular Malaysia. The Late Cretaceous was a time of widespread granite emplacement, which, apparently, was related to a major thermal event in the region. Many of the strike-slip faults initiated during this period were later reactivated during the Tertiary and have exerted strong control on rift basin development. Strike-slip faulting and crustal extension, accompanied by a regional thermal event in middle–late Cretaceous times, may have contributed to the weakening of the Sundaland lithosphere, which underwent a renewed phase of extensional tectonism in the early Tertiary.

The timing of widespread rift basin formation, some 35–40 Ma ago, seems to coincide, roughly, with the timing of the India–Eurasia collision. The main effect of the collision was to reactivate the pre-existing faults, depending on their orientation relative to the prevailing stress regime, and to cause localised extensional basin development. The Malay and Penyu Basins seem to have developed within one of these major fault systems. Structural evidence from the Basins, however, can not substantiate the idea of large-scale extrusion of crustal blocks resulting from the India-Eurasia collision. Although, on a regional scale, the fault system along which the Malay and Penyu Basin developed may be viewed as a discrete strike-slip fault, on a local scale, it represents a wide zone of distributed deformation involving smaller-scale fault-bounded blocks that responded passively to the relative motion of the plates either side.

7.1.1 Influence of Basement Structures

The formation of many rift basins are, commonly, influenced by pre-existing zones of weakness in the pre-rift basement (Dixon *et al.*, 1987; Daly, 1989). Hutchison (1989a) speculated on the possible importance of basement faults in controlling

the formation of Southeast Asian Tertiary basins. Indeed, the evidence from the Malay and Penyu Basin seems to suggest a strong basement influence. In the northern Sunda Shelf area, three main types of basement structures may have influenced Tertiary basin formation.

Indosinian collisional fabric The Indosinian Orogeny has left a strong predominantly N- to NNW-trending structural fabric in the region, manifested in the N-trending plutonic provinces in Thailand and Peninsular Malaysia, and NW-trending folds in Upper Triassic–Jurassic continental strata (Harbury *et al.*, 1990). The numerous N-trending Tertiary basins in northern Thailand and in the Gulf of Thailand are believed to have formed by E–W extension (McCabe *et al.*, 1988), and were probably influenced by the underlying Indosinian structures. In the Malay, Penyu and West Natuna Basins, however, N–S-trending structures are absent (Fig. 1.4) and, therefore, were probably not important in influencing Tertiary extension.

NW-trending fractures Numerous NW-trending strike-slip fault zones occur in Sumatra, Thailand, and Indochina and are believed to have played an important role in the development of Tertiary extensional basins (*e.g.* Tapponnier *et al.* 1982, 1986; Moulds, 1989; Polachan *et al.* 1989). NW-trending faults occur also on Peninsular Malaysia (Fig. 7.1) and show evidence for post-Early Cretaceous strike-slip displacement in the order of many tens of kilometres, some offsetting Lower Cretaceous sedimentary formations (Gobbett and Tjia, 1973). One example is the Kuala Lumpur–Endau Fault Zone, which is a left-lateral strike-slip fault zone that was active in late Cretaceous and early Tertiary times (Gobbett and Tjia, 1973). On the Bukit Tinggi Fault, which is a northern splay of the Kuala Lumpur Fault Zone, biotites from cataclastic granites have given K-Ar ages of 81–92 Ma (Late Cretaceous) (Gobbett and Tjia, 1973, p. 328). According to Stauffer (1968), the Tertiary Batu Arang Basin has steep dips near its northern edge, where the western extension of the Kuala Lumpur Fault is believed to be

located. This provides strong evidence for the influence of the NW-trending faults in Tertiary basin formation.

The NW-trending fabric in southern Peninsular Malaysia appears to continue offshore into the Singapore Platform, where NW-striking lineaments are observed in unpublished aeromagnetic anomaly maps. These lineaments represent, probably, the offshore continuation of the Kuala Lumpur–Endau strike-slip fault zones. Gobbett and Tjia (1973) interpreted the NW-trending faults on Peninsular Malaysia as major left-lateral strike-slip faults which represent Tertiary brittle deformation of Peninsular Malaysia, complementary to plastic deformation of the Andaman-Sumatra arc. Similar fault zones are expected and observed offshore east of the peninsula, for example in the West Natuna Basin and in the southern Malay Basin (Daines, 1985; Ginger *et al.*, 1993). North of the Penyu Basin, NW-trending faults such as the Dungun (Tjia, 1993) and Tenggol Faults occur on the southwestern margin of the Malay Basin. In the West Natuna Basin, major NW-trending transverse fault zones are believed to be reactivated basement wrench faults (Daines, 1985, Ginger *et al.* 1993). Further to the north in Thailand, Polachan *et al.* (1989) interpreted the major NW-trending faults as controlling the formation of pull-apart basins. The NW-trending faults in the West Natuna, Penyu and Malay Basins appear to be the offshore counterparts of the Late Cretaceous strike-slip faults of Peninsular Malaysia, the extensional basins must have been formed by reactivation accompanying the Tertiary deformation of Sundaland. Evidence from the Penyu Basin has been presented earlier to suggest that the NW-trending faults, such as the Merchong Graben boundary faults and the Trans-Penyu Fault, have had signifinicant strike-slip displacement.

E-trending fractures E-trending faults, which dominate the Penyu and West Natuna Basins, are generally absent in Peninsular Malaysia; however, there is evidence of approximately E-trending fractures associated with mafic intrusive activity. These have been documented in two areas. In northern Terengganu (Location A in Fig. 7.1), dolerite dykes fill joints in granites and trend N 75°E to N

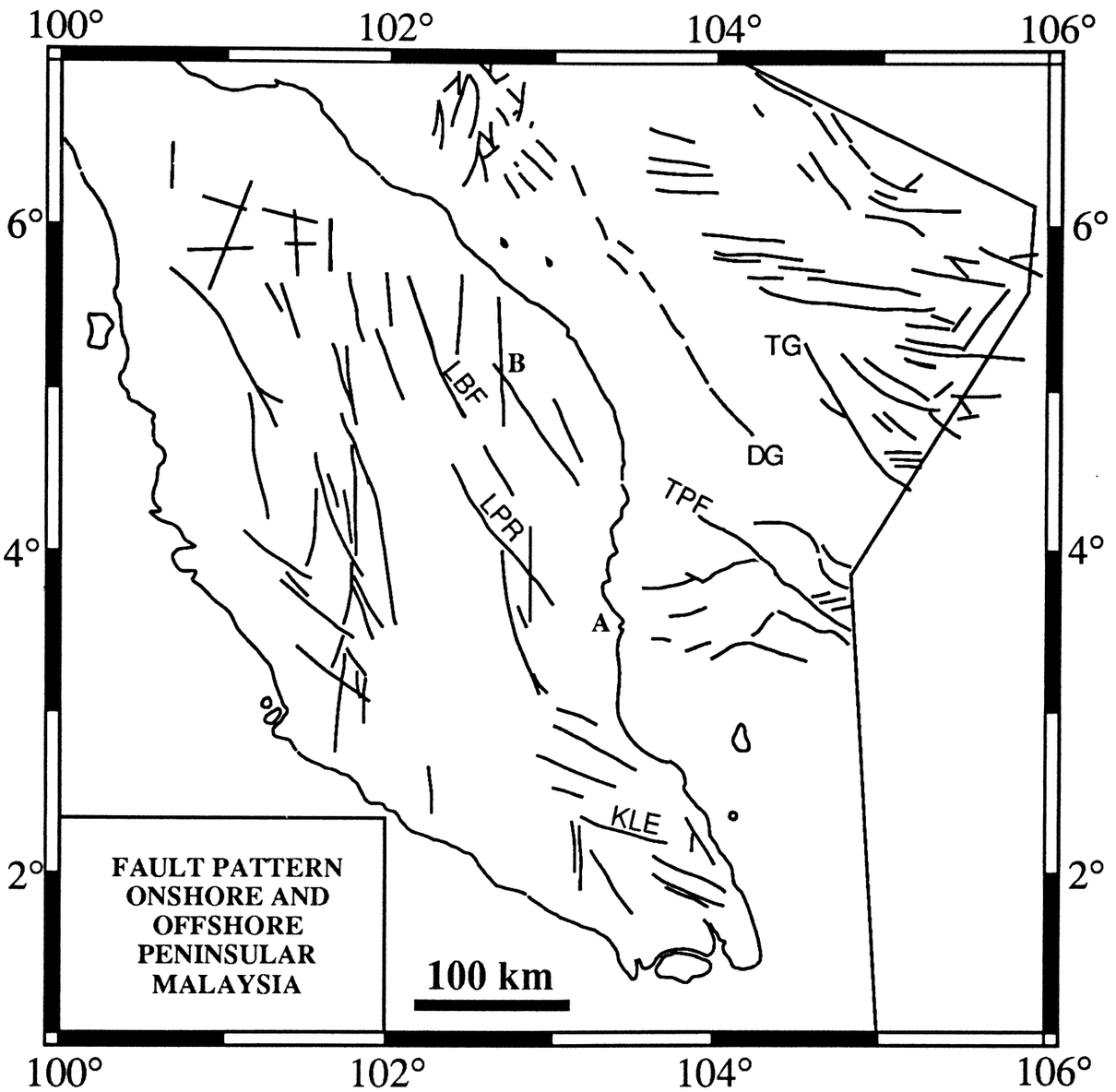

Figure 7.1. Map of the major faults on Peninsular Malaysia and adjacent offshore area, covering the Penyu and Malay Basins. Onshore structures compiled from Tjia (1989) and Geological Survey Map (1985); Offshore structures from unpublished PETRONAS maps, incorporating results of present study. Major NW-trending faults: KLE– Kuala Lumpur–Endau Fault, LBF– Lebir Fault, LPR– Lepar Fault, TPF– Trans-Penyu Fault, DF– Dungun Fault, TF– Tenggol Fault.

150°E. At Kuantan (Location B, Fig. 7.1) east-trending tholeiitic basalt dykes cut Late Permian–Early Triassic granites. The basalts at Kuantan have been dated as mid-Cretaceous (~110 Ma) (Haile *et al.*, 1983). These dykes, together with widespread Late Cretaceous granites, in the surrounding region (see Hutchison, 1989a, for review) imply a major middle to late Cretaceous extension and magmatic event in the area. It is quite likely, therefore, that the E-trending faults in the Penyu and Malay Basins may have formed along older structures.

7.1.2 Role of India-Eurasia Collision

In Chapter 2, the geological history of Sundaland was discussed from a phase of rifting and drifting associated with the break-up of Gondwanaland to a phase of continental collision and amalgamation at the southern margin of Eurasia, which moulded the present-day Southeast Asian continent. The region is, basically, the relict of a Late Mesozoic orogen, which seems to have been undergoing extension since as early as late Jurassic times, perhaps initially by gravitational collapse and, later, by back-arc extension and strike-slip related extensional tectonics. There is overwhelming geological evidence suggesting that the extensional tectonics in Sundaland is not exclusively a Cenozoic phenomenon— the occurrence of intermontane basins, formed probably by orogenic collapse (Dewey, 1988) and/or strike-slip faulting. Some of the evidence include the possible occurrence of metamorphic core complexes in the interior of Sundaland (MacDonald *et al.*, 1993), and the widespread evidence for intraplate basaltic magmatism (Flower *et al.*, 1992). Against this background of an overall extensional regime, the tectonic evolution of Southeast Asia was later influenced by the India–Eurasia collision at the beginning of the Tertiary. The most important effect of the collision, as far as Southeast Asia is concerned, was to reactivate pre-existing Late Cretaceous faults.

Dewey *et al.* (1989) have calculated the motion history of India relative to Eurasia. From the late Cretaceous to ~45 Ma B.P., India moved roughly northeastwards at an average velocity of ~10 cm a^{-1}, but changed to roughly north-

wards at the onset of the collision with Eurasia, with an average velocity of 5 cm a^{-1}. Before the collision, the convergence between India and Eurasia was roughly orthogonal and was accommodated by subduction beneath a volcanic arc along the southeastern margin of Eurasia. The change in relative motion at ~45 Ma, however, resulted in oblique convergence, which is accommodated, mainly, by lithospheric thickening in the frontal collision zone and by transpressional shear to the east and west of it (Dewey *et al.*, 1989). The indentation of India into Eurasia may have resulted, also, in oroclinal bending of the Sumatra-Java volcanic arc (Hutchison, 1992b).

Because the left-lateral faults in central Sundaland appears to have been active at least since the late Cretaceous, they may have originated during the orthogonal convergence phase prior to the India–Eurasia collision at 45 Ma. We may envisage the initiation of left-lateral faults using the plane-strain indentation model (Tapponnier and Molnar, 1976) where major slip lines radiate from the frontal collision zone (Fig. 7.2). However, when India collided with Eurasia, the change in relative plate motion caused dextral transpressional shearing in Southeast Asia adjacent to the eastern edge of the Indian continent. The effect of the dextral shear was to reactivate the existing faults that were created during the orthogonal convergence phase, thus causing internal clockwise rotation of the fault-bounded blocks. At the same time, the whole region underwent external clockwise rotation in response to the continuing indentation.

The intensity of the dextral transpression varies with distance from the collision zone. In central Sundaland, therefore, transpression was "felt" much later, probably in the late Oligocene–Miocene times, and may have been responsible, partly, for the widespread basin inversion during that time. Hence, the role of the India–Eurasia collision was not so much as to cause extrusion but regional transpressional shear in Southeast Asia, which affected the region in two ways: 1. Reactivation of the Late Cretaceous faults as left-lateral strike-slip faults whose motion was accommodated by clockwise rotation of fault-bounded blocks. Ter-

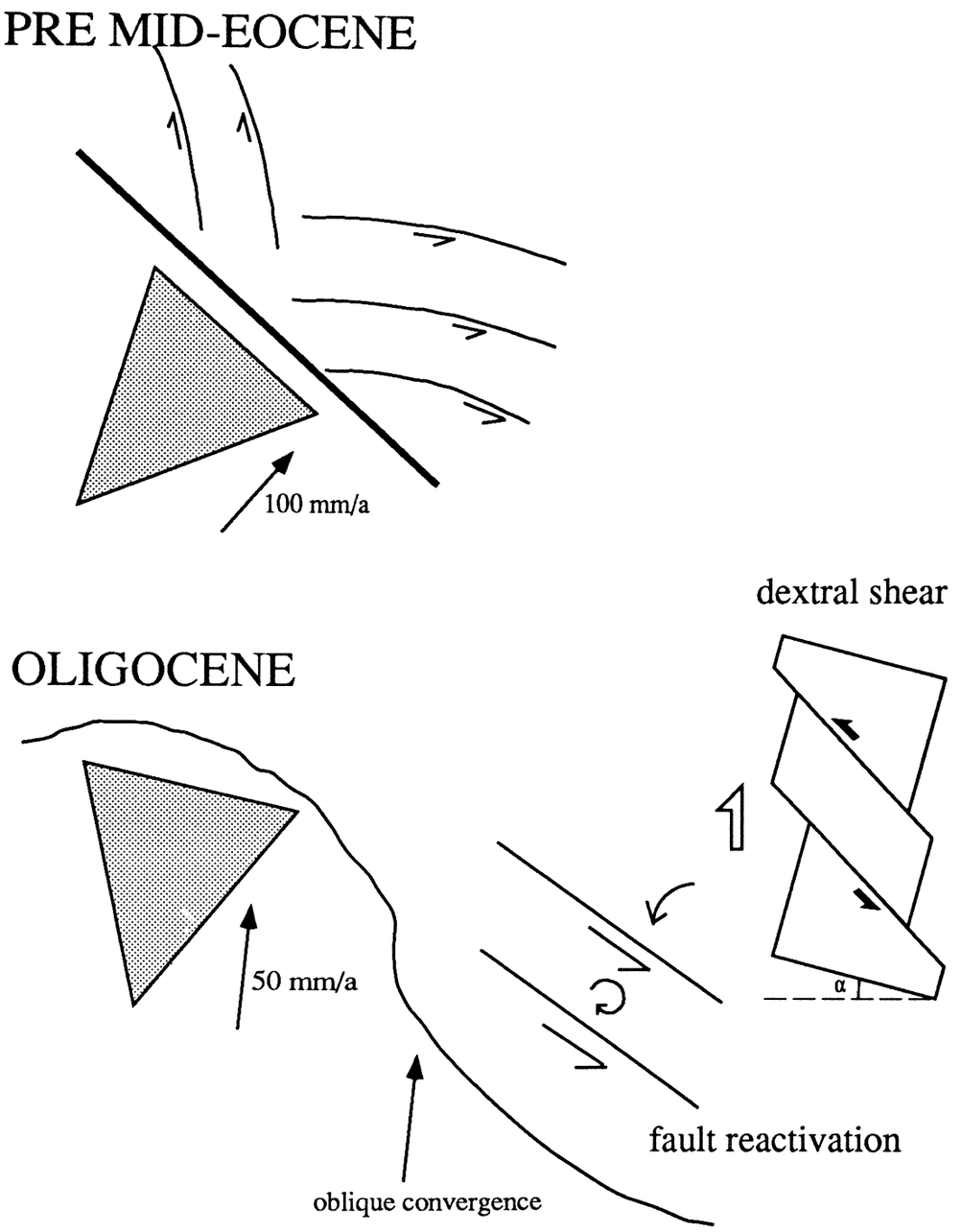

Figure 7.2. Sketch of tectonic model for Southeast Asia based on the regional geology discussed in Chapter 2. Pre-mid Eocene times: orthogonal convergence phase, as India moves northeastwards. Major left-lateral strike-slip faults initiated. Model for strike-slip faults based on slip-line field theory (Tapponnier and Molnar, 1976). Oligocene: India's motion northwards, resulting in oblique convergence in Southeast Asia. Dextral shear causes reactivation of pre-existing faults and shear zones. India's velocities from Dewey *et al.* (1989).

tiary extensional basins, including the Malay and Penyu Basins, may have developed along these reactivated strike-slip fault zones (Tapponnier *et al.*, 1982), and (2) Progressive dextral transpression and roughly N–S shortening across the region, causing inversion in the sedimentary basins.

The above hypothesis emphasizes the probable role of the India–Eurasia collision in influencing the Tertiary tectonics and basin development in Southeast Asia, without having to invoke large-scale extrusion of crustal blocks as a mechanism of extensional basin formation (*cf.* Tapponnier *et al.* 1982, 1986).

7.2 Structural Styles in the Penyu Basin

The first part of the study (Chapter 3) examines the structural styles and fault geometries in the Penyu Basin, based on newly-interpreted seismic reflection data, to understand its kinematic development. It was found that the Basin is not the "typical" rift basin bounded by normal fault zones but a complex extensional basin made up of a number of isolated subbasins, each controlled by one or more major basin-bounding faults. The Basin is interpreted to have developed by N–S extension, possibly related to a regional dextral shear induced by the India-Eurasia collision. The geometry of the individual subbasins is controlled by NW- and E-trending sets of pre-existing faults in the pre-rift basement. The fault geometry and its orientation relative to the regional stress field determine the style of faulting in the resulting basins. A fault at a high angle to the regional extension (N–S) resulted in a half-graben basin with a single bounding fault, as exemplified by the Kuantan Graben. Hence, approximately orthogonal extension in the Kuantan Graben was accommodated by dip slip on a relatively steep, planar normal fault. On the other hand, a fault that was oblique to the regional extension produced a pull-apart or rhomb graben, as a result of strike-slip partitioning of the extension. The Trans-Penyu Fault is one of several basin-bounding faults with a significant strike-slip history. The fault is probably related to late Cretaceous

strike-slip faults of similar orientation on land (Fig. 7.1). The Rumbia Graben, north of the Trans-Penyu Fault, is the result of oblique extension and pull-apart along the Fault. The importance of strike-slip tectonics in the Penyu Basin is indicated also by the structural style in the Merchong Graben, which is a pull-apart rhomb graben developed between two parallel NW-striking strike-slip faults.

Recognition of listric, low-angle half-graben border faults in the northeastern margin of the Rumbia Graben suggests the probable importance of upper-crustal detachment ("thin-skinned") faulting during extension in that part of the Penyu Basin, as a result of strike-slip reactivation of the Trans-Penyu Fault. Low-angle crustal detachments may have formed along pre-existing thrusts or shear zones in the Mesozoic basement. Thin-skinned extension has important implications for the isostatic compensation of the Basin. Because the mantle is not involved in the brittle extension in the upper crust, the Basin is undercompensated isostatically and shows a negative gravity anomaly (Chapter 5). Structural evidence suggests that a major change in the stress regime had affected the region, from N-S extension to N-S shortening, which is manifested as compressional anticlines formed over the half-grabens.

7.3 Extension and Inversion in the Malay Basin

The structural data from the Malay Basin (Chapter 4) suggests the importance of strike-slip faulting during basin formation. An idealized kinematic model is proposed based on the block model of McKenzie and Jackson (1986) to explain the main structural features in the Basin:

1. Lack of major strike-slip faults bounding the Basin

2. Predominantly E-trending basement faults, oblique to the basin trend

In the model, the Malay Basin is envisaged as a type of transrotational basin developed within a NW-trending zone of distributed deformation ~100 km wide. The E-trending basement faults were, probably, old basement faults that were reactivated by sinistral transtensional shear sometime during the early Oligocene (~35 Ma). Half-grabens were formed as the result of oblique transtension between fault-bounded crustal blocks which rotated passively in response to shear deformation.

During early–middle Miocene times (15–17 Ma) the half-grabens were inverted, apparently, as a result of reversal in the sense of shear. Oblique-slip reactivation of the E-trending bounding faults causes transpressive shortening across the half-grabens and the formation of *en echelon* anticlines. The change from extension to shortening, as has been observed in the Penyu Basin, indicates that a rotation of the regional stress field had taken place. A number of processes are likely to have caused this rotation, including intraplate stresses induced at plate boundaries (Letouzey *et al.*, 1990; Hutchison, 1992b) and the opening of marginal seas, such as the Andaman Sea (Daly *et al.*, 1991). Both are possible because the region is surrounded by active plate margins and back-arc spreading centres and, also, because the timing of inversion in the Basins coincides with the opening of the Andaman Sea and the Makassar Strait. Ridge-push forces generated by these spreading centres may have contributed to the overall compressional regime in the region during that time. Intraplate stresses induced by collision along the Sunda arc-trench to the south of the area may have been an additional factor which contributes to the inversion of Sundaland extensional basins (*cf.* Letouzey *et al.* 1990).

Some authors, such as Peltzer and Tapponnier (1988), Harder *et al.* (1992), and Huchon *et al.* (1994), have suggested that the progressive indentation of India into Eurasia since the mid-Eocene had caused rotation of the stress field across Southeast Asia. Figure 7.3 illustrates this idea schematically. During the initial stages of collision with India, the Eurasian margin is oriented roughly NW-SE.

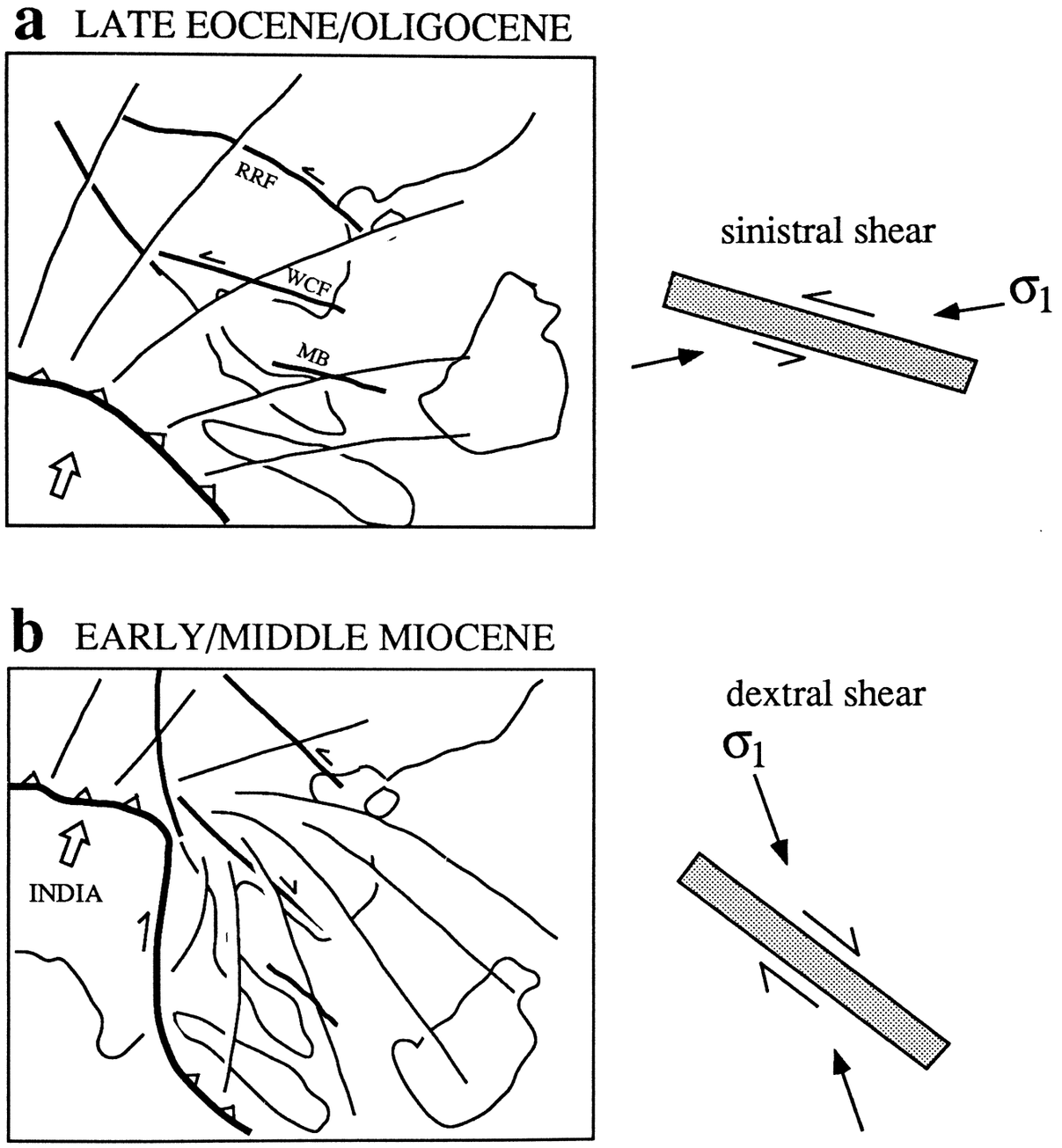

Figure 7.3. Rotating stress model for Southeast Asia, based on Huchon *et al.* (1994), to explain the development of the Malay Basin. (A) Late Eocene/early Oligocene onset of India-Eurasia collision. Radiating lines represent stress trajectories (σ_1 orientation). Sketch on the right shows the orientation of σ_1 and the shear zone, and the resulting shear couple. MB–Malay Basin. B) Early/middle Miocene — start of inversion. India has indented into Eurasia. Maximum compressive stress has rotated to N–S, while the shear zone orientation remained essentially NW-SE. WCF — Wang Chao Fault, RRF — Red River Fault.

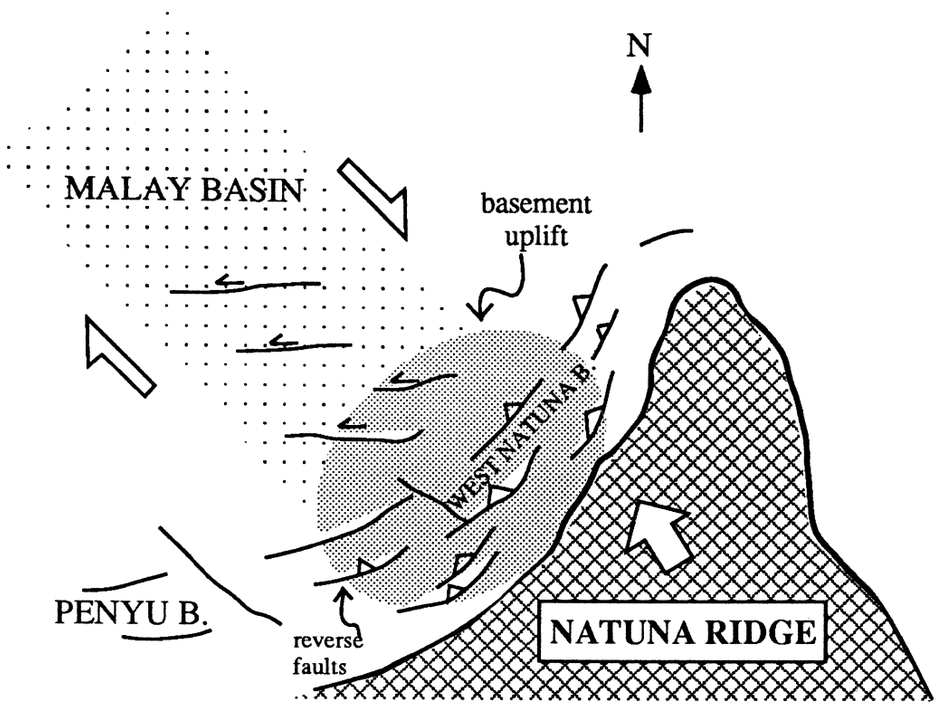

Figure 7.4. Sketch illustrating the cause of basement uplift in southern Malay Basin. Uplift was caused by crustal thickening between converging crustal blocks: 1. the northwestern side of the Malay Basin shear zone and 2. the Natuna Ridge, which acts as a buttress that resisted the southeastward motion of 1. Deformation in the sedimentary cover within the compressional zone (finely stippled area) is dominated by reverse and thrust faults, as documented by Ginger *et al.* (1993).

Hence, the stress trajectories (maximum compressive stress axes) would have been almost perpendicular to the collision margin, and roughly E-W between Peninsular Malaysia and Borneo, where the Malay Basin is located. As a result, pre-existing NW-trending shear zones in Sundaland, in which Malay Basin later developed, were reactivated as a sinistral shear zone (Fig. 7.3). This caused transtensional opening of the Malay Basin, accompanied by rotation of the interior fault-bounded crustal blocks (Fig. 4.16). As the indentation progressed, and India swept pass Southeast Asia, the stress trajectories rotated clockwise and become roughly N–S. Because the rotation of the stress field occurred at a much faster rate than that of the Sundaland continental block, the maximum compressive stress results in the reversal of shear along the Malay Basin shear zone (Fig. 7.3). This caused transpressional inversion of the originally transtensive basins (Fig. 4.16).

In Chapter 4, it was observed that the degree of basin inversion in the Malay Basin increases southeastwards as we approach the West Natuna Basin. In the northern Malay Basin, the inversion structures occur, commonly, as broad open folds, whereas in the southern part, the folds are tighter and commonly show wrench-related features with significant reverse dip-slip reactivation. In the West Natuna Basin, more intense deformation is indicated by the preponderance of reverse and, even, thrust faults (Ginger *et al.*, 1993).

Perhaps, the most obvious manifestation of the increasing deformation towards the southeast is the massive basement uplift, which resulted in thinning of strata and truncation by the regional middle–late Miocene Unconformity towards the southeast (Fig. 4.4, p. 124). Although this has been pointed out previously (ASCOPE, 1981), the cause of the uplift was not well understood. The available stratigraphic data suggest that the time of the uplift coincides with the basin inversion phase in the middle-late Miocene. Hence, basin inversion not only resulted in local inversion of half-grabens, but also a more regional basement uplift in the southeast. Because sedimentation seems to have been continuous in the northern part of the Basin, the uplifted region may have provided sediment to the subsiding basin to the northeast. This important feature of the Malay Basin, whereby rapid subsidence and deformation occur at the same time in different parts of the Basin, is typical of many strike-slip basins (Nilsen and Sylvester, 1995, p. 434).

Figure 7.4 illustrates a mechanism by which the southern Malay and West Natuna Basin may have been uplifted during the middle Miocene inversion phase. The inversion of half-grabens in the Malay Basin, as explained in the slat model, is the result of dextral shear. The increasing intensity of deformation in the south is caused by the buttressing effect of the Natuna Ridge which, effectively, resisted the dextral motion of the block on the northwestern side of the Malay Basin shear zone. Furthermore, the northward subduction of the Indian Plate beneath the Java Trench to the south may have contributed also to the deformation. The southern part of the Malay Basin and almost the entire West Natuna Basin are

situated, effectively, between two converging crustal blocks. This has resulted in large amounts of shortening, crustal thickening, and isostatic uplift of the region.

Chapters 5 and 6 investigate the state of isostasy and mechanism of subsidence in the Basins. The results suggest that basin formation may have involved a process of whole-lithospheric stretching and, partly, "thin-skinned" crustal extension. Although the structure indicates a strike-slip origin (Chapter 4), the general geometry and the subsidence history of the Basin seems to be typical of rift basins formed by homogeneous lithospheric stretching. The large thickness of sediment in the Malay Basin (>14 km) requires considerable crustal thinning which, curiously, is not reflected in the free-air gravity field. The low negative anomaly, of the order of −20 mGal, means that the crust underneath the Basin is not as thin as the sediment thickness implies.

The results of 1D-backstripping well data suggest a stretching factor, β, of up to ~4.0, which should have resulted in a large positive free-air anomaly. This estimate seems unrealistically high for a basin in continental crust. Indeed, the gravity data indicates maximum thinning of about 2.3, which means that β may have been overestimated by the backstripping method. The evidence suggests that magmatic underplating is an unlikely explanation for the apparent thickening of the crust, and that the most probable cause of the undercompensation in the Basin is some form of crustal extension that does not involve subcrustal lithosphere. Hence, although the dominant basin-forming process may have been homogeneous lithospheric stretching, part of the subsidence could have resulted from, possibly, upper-crustal detachment or "thin-skinned" extensional faulting.

The lithospheric stretching model (McKenzie, 1978), modified to take account of finite rifting duration and lateral heat flow, has been very useful, generally, in explaining the subsidence and thermal histories of the Malay and Penyu Basins (Chapter 6). Very high heat flows (85–100 mW m^{-2}) are observed because the Basins are young (<40 Ma) and, therefore, the thermal anomaly resulting from lithospheric thinning has not dissipated completely. Heat flows predicted using

stretching factors estimated from subsidence analysis agree rather well with the observed heat flows. The heat flow history in some Malay Basin wells derived by modelling vitrinite maturation is also comparable with the predictions of the stretching model.

7.4 Future Work

Although a better understanding of the origin and evolution of the Malay and Penyu Basins has been achieved from the integration of various geological and geophysical data, some areas of study require further investigation. The Malay Basin, in particular, is an active area of petroleum exploration and, hence, much of the data are confidential. More detailed structural information is needed to test further the kinematic model proposed for the Basin in Chapter 4. The deep structure of the Basin is also poorly known. In particular, much of the synrift structure is still hidden beneath the thick pile of postrift sediment in most parts of the Basin. A recent acquisition of deep seismic reflection data by PETRONAS will provide more information on the early synrift structural development of the Basin. Although the DMA data and Sandwell gridded data have produced some interesting results, the gravity data coverage in the region is very poor. More high-quality gravity data, perhaps already available in the oil industry, should provide a better constrain on the crustal structure underneath the Basins. Also lacking is seismic refraction data, which would be useful for determining the present Moho configuration and to test the gravity models discussed in Chapter 5. It is also important to obtain, in future, high-quality biostratigraphic and sediment maturation data for modelling of the subsidence and heat flow histories of the Basins. This will be of interest to the petroleum industry.

Appendices

Appendix A

Data and Methods

A.1 Velocity Data for Time-Depth Conversion

The seismic sections and structural contour maps illustrated in Chapter 3 were depth-converted based on velocity information from well "check-shot" surveys and stacking velocities. Five out of six wells used in the study of the Penyu Basin have velocity information. A time-depth ($t-z$) curve for each well was used to "tie" the seismic picks with the lithological and biostratigraphical boundaries. For depth-conversion, average interval velocities of the seismic units were used (Table A.1). The interval velocity of the oldest unit, P1, is based partly on stacking velocities, which are in the range 4100–4700 ms^{-1}, with an average of about 4350 ms^{-1}.

Well	Rhu-1/1A	Cherating-1	Rumbia-1	Pari-1	Penyu-1	Average
water	1500	1500	1500	1500	1500	1500
P7	1610	1710	1684	1696	1600	1660
P6	2207	2214	2267	2000	2133	2160
P5	2500	2307	2000	2545	2285	2328
P4	2567	2485	2529	2452	2592	2525
P3	3029	3043	3190	2960	3667	3178
P2	3702	3778	3684	3077	–	3560
P1	–	4136	–	4350	–	4350†

Table A.1. Interval velocities in ms^{-1} derived from check-shot surveys in Penyu Basin wells, and average velocities used in the depth conversion of seismic sections. †Estimates from stacking velocities have been included for better approximation of the velocity in the deeper synrift section.

Using the interval velocities in Table A.1, the thickness, ΔZ, of a seismic unit

is given by

$$\Delta Z = V \times \Delta t/2 \tag{A.1}$$

where V is its interval velocity and Δt is its apparent thickness in two-way travel time. Hence, the depth, Z_n, to seismic horizon n (n = 1,2,.. 8, downwards) is obtained by the total thickness of all units above it, plus the present water depth:

$$Z_n = \sum_{i=1}^{n} V_i \, \Delta t_i/2 \tag{A.2}$$

V_i and Δt_i are, respectively, the interval velocity and two-way time thickness of unit i.

A.2 Porosity-Depth Curve

This section discusses the derivation of the parameters governing the exponential porosity-depth relationship (equation 6.6), ϕ_o and c, based on sonic logs and porosity data from the Malay and Penyu Basins. Porosity data from the two basins were obtained from two sources: core plug measurements and sonic travel-time logs. The sonic log is probably the better source of porosity information because it gives an almost continuous coverage of the porosity over the entire depth of the well.

There are two common methods of obtaining porosity from sonic travel times. One method is by using the Wyllie's time-average equation (*e.g.* Asquith, 1980, p. 66–67).

$$\phi = \frac{\Delta t_{log} - \Delta t_{ma}}{\Delta t_f - \Delta t_{ma}} \tag{A.3}$$

where Δt_{log} is the sonic transit time (in μs/ft) from the log, Δt_{ma} is the transit time for the sediment grains (53 μs/ft), and Δt_f is the transit time for the fluid in the well bore (189 μs/ft for freshwater mud). For undercompacted sandstones occurring at depths above ~1000 m, the porosity calculated using the above formula is multiplied by a correction factor, $\frac{100}{\Delta t_{shale}}$, where Δt_{shale} is the transit time in the adjacent shale from the log.

Equation A.3 is widely used (*e.g.* Allen and Allen, 1990) although, generally, it is applicable only to clean, relatively unconsolidated sandstones (Helander, 1983, p. 154). Figure A.1 shows the porosity-depth data derived from the sonic log in Penyu-1 well, Penyu Basin, using equation A.3. Calculations were done using two values of Δt_{ma}, representing two extreme cases, one in which the lithology is entirely sandstone ($\Delta t_{ma} = 51\mu$s/ft), and the other in which the lithology is entirely shale ($\Delta t_{ma} = 67\mu$s/ft; Issler, 1992). Both curves show exponential decay of porosity but give unrealistically high values of surface porosities; 0.95 when $\Delta t_{ma} = 67\mu$s/ft and 1.18 when $\Delta t_{ma} = 51\mu$s/ft.

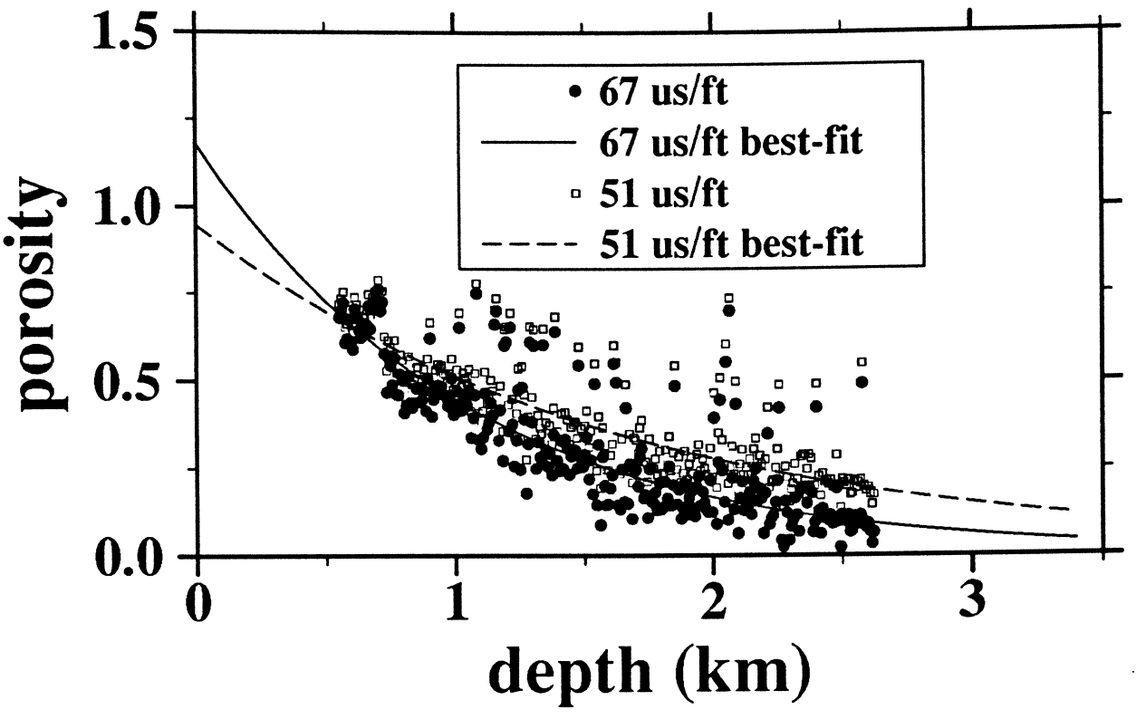

Figure A.1. Porosity vs depth plot derived from the sonic log in Penyu-1 well, using equation Wyllie's equation. To illustrate the range of possible porosity-depth curves, two sets of plots are shown, corresponding to different values of Δt_{ma}. The *best-fit* curves, obtained by regression, show unrealistic surface porosities.

An alternative to equation A.3 is the empirical formula given by Chapman (1983) and Raiga-Clemenceau *et al.* (1988)

$$\phi = 1 - \left(\frac{\Delta t_{ma}}{\Delta t_{log}}\right)^{1/x} \tag{A.4}$$

The value of x in the exponent is usually determined empirically but, because no data is available from the Malay and Penyu Basins to make a calibration, published values are used. Chapman (1983) suggested the value of 2 for sandstone, whereas Issler (1992) obtained a value of 2.19 for shale in the Beaufort-McKenzie Basin. As in equation A.3, the relevant values of Δt_{ma} were used.

Figure A.2A shows the result of applying equation A.4 to the sonic log in Penyu-1 well. A middle value for both Δt_{ma} and the constant x were used ($\Delta t_{ma} = 59\mu$s/ft, $x = 2.095$) for a mixed sandstone-shale lithology, which is appropriate for

the Malay/Penyu Basin sediments. The best-fit exponential curve gives $\phi_o = 0.49$ and $c = 0.50$ km^{-1}, which are more realistic and, also, are comparable to the values obtained by Sclater and Christie (1980) for the North Sea.

Well name	ϕ_o	c (km^{-1})
Anding Barat-1	0.55	0.55
Sotong 5G-5.1	0.56	0.56
Duyung 5H-2.1	0.51	0.47
Delah-1	0.51	0.48
Penyu-1	0.49	0.50
average	**0.52**	**0.51**

Table A.2. Values of constants for exponential porosity function obtained from sonic logs in 5 wells.

It is useful to compare the sonic-derived porosity with actual measurements from core A.2C. Quite a substantial amount of core porosity data are available from wells in the southern Malay Basin. Four of these wells — Anding Barat-1, Sotong 5G-5.1, Duyung 5H-2.1 and Delah-1 (their location shown in Fig. 6.8) — were chosen because continuous sonic logs throughout the well column have been recorded down to depths of ~3.5 km. As before, equation A.4 was used to obtain porosity from the sonic logs. Figure A.2B shows the result from Anding Barat-1 well, plotted with core porosities compiled from a total of 15 wells in the vicinity. Qualitatively, the two data sets seem to match quite well. The best-fit exponential curve through the sonic-derived data gives $\phi_o = 0.55$ and $c = 0.55$ km^{-1}. The porosity data gave a best-fit curve with $\phi_o = 0.57$ and $c = 0.61$ km^{-1}, which are somewhat higher than, but not significantly different from, those obtained from the sonic logs. Figure 6.5 shows the exponential curves from the four wells in the southern Malay Basin compared with the core data. The data indicate that equation A.4 gives relatively consistent result for the area and, therefore, justifies its use in the Malay and Penyu Basins. Table A.2 summarizes the values of ϕ_o and c obtained from the four Malay Basin wells and from the Penyu-1 well in the Penyu Basin. For the Malay Basin, the average value of ϕ_o and c based on the four wells shown in Table A.2 were used in the flexural backstripping and gravity

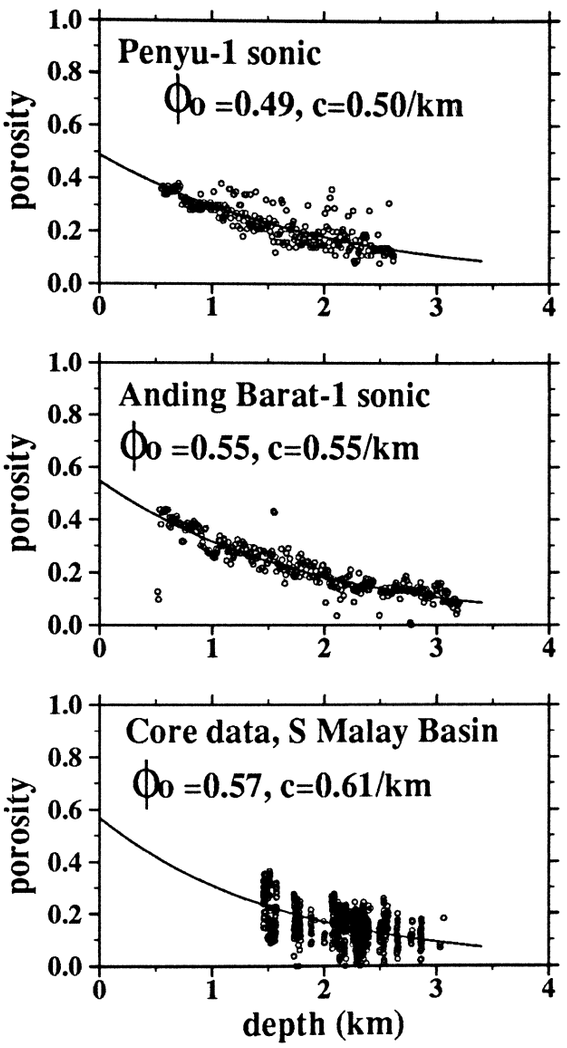

Figure A.2. Porosity vs depth plots using equation A.4 (A) derived from the sonic log in Penyu-1 well. (B) derived from the sonic log in Anding Barat-1 well. (C) Core data from southern Malay Basin for comparison. Both (A) and (B) uses $\Delta t_{ma} = 59\mu$/ft, $x = 2.095$.

modelling in Chapter 5 and in the subsidence analysis in Chapter 6.

A.3 Data Sources

Below is a list of unpublished reports, not cited in the text, from which various data have been compiled for the study. The data include biostratigraphy, borehole temperatures, velocity survey, well lithological description, vitrinite reflectance, and porosity-permeability measurements. Data supplied by PETRONAS.

1. Hall, M.E., Ahmad Din, and Mohd Zaki Othman, 1986. The PETRONAS Carigali PM12 Block Southern Malay Basin: A review of the petroleum geology.
   PETRONAS Carigali internal report.

2. Ho Kiam Fui, 1984. The biostratigraphic re-evaluation of southern Malay Basin, PM6 Block, and Penyu subbasin, offshore Peninsular Malaysia.
   PETRONAS Carigali internal report.

3. Well-completion Logs for Rhu-1A, Merchong-1, Cherating-1, Rumbia-1, Penyu-1, and Pari-1.

4. Well velocity survey reports for Rhu-1A, Merchong-1, Cherating-1, Rumbia-1, Penyu-1, and Pari-1.

5. Sonic logs of Rhu-1A, Merchong-1, Cherating-1, Rumbia-1, Penyu-1, Pari-1, Anding Barat-1, Duyung 5H-2.1, Sotong 5G-5.1, Delah-1.

6. Routine core analysis results (porosity and permeability data) for about 15 wells in the southern Malay Basin (PM12).

A.4 Malay Basin Well Stratigraphic Data

Below are the stratigraphical data used in the backstripping analysis in Chapter 6. Values represent the top of seismic units in metres.

No	Well Name	A	D	E	F	H	I	J	K	L	M	Basement
1	Abu-1	61			759	947	1149	1512	1639			1910
2	Anding Barat-1	76	639	744	864	1106	1572	1811	1975		2655	3167
3	Anding-1	74	677	794	911	1167	1651	1890	2026		2410	2587
4	Anding-2	74	666	774	890	1148	1645	1868	2000		2409	2658
5	Angsi-1	68				1213	1510	2006	2222	2626	2977	
6	Badak-1	56	811		1110	1234	1433	1981	2090			2295
7	Banggol-1	64			870	1283	1628	2224	2510			
8	Bedong-1	59	1299	1554	2054							
9	Belumut-2	72				571	605	881	1035	1207	1423	1463
10	Beranang-1	59	680	849	1227	1469	1778	2355	2498		3054	
11	Besar-1	70				684	851	1434				
12	Bintang-2	50	1062	1364	1722							
13	Bubu-1	62			718	875	1056	1406	1516			1609
14	Bundi-1	69	1053	1183	1563	1734	2366					
15	Bunga Orkid-1	55	1012		1368		1981	2446	2939		3511	3671
16	Bunga Pakma-1	56					2010	2473	2932			3522
17	Bunga Raya-1	55	846		1167	1340	1733	2110	2605		2854	2906
18	Cahaya-1	68					888	1160	1302	1469	1593	
19	Delah-1	78	705	828	925	1207	1716	2049	2155		2607	2928
20	Duyung 5H-2.1	75	530	571	647	727	1247	1800	1966	2440	2765	
21	Duyung Barat-1	70	626	726	852	1010	1548	1689	2155	2562		
22	E Belumut-1	72				605	766	1057	1215			1455
23	East Larut-2	62	890	947	1072	1227	1562	2192	2336			2725
24	East Raya-1	69			776	1053	1346	1831	2015	2271		2410
25	Feri-1	75	660	765	896	1126	1620	1863	1986		2451	2918
26	Gayong-1	74					444	938	1274			
27	Guntong-1	62			812	982	1317	2072	2449			
28	Irong Barat-1	65			572	696	1117	1851	2060			
29	Kepong-1	68			655	712	1021	1678	1994	2490		
30	Larut-1	62	923	1009	1105	1321	1566	2197	2554	2658		2686
31	Ledang Barat-1	66						365	526	1032	1417	
32	N Lukut-2	61		768	871	940	1166	1577	1687			1945

(continued next page...)

No	Well Name	A	D	E	F	H	I	J	K	L	M	Basement
33	Palas-1	63		797	939	1033	1361	1998	2376	2940		
34	Penara-1	60		925	1103	1227	1472	1946	2076	2314		2373
35	Pendera-1	83				555	714	1334	1636			
36	Piatu-1	63				1374	1635	2261	2402	2584	2784	
37	Relau-1	63		793	964	1063	1314	1770	1881	1967	2031	2177
38	Resak-2	64	674	880	1290	1648	1947	2546	2771			
39	Seligi-2	74				527	564	1117	1354	1754	2086	
40	Simpur-1	60				689	856	1108	1162			1309
41	Sotong 5G-5.1	76	680	789	918	1134	1598	1857	2013		2476	2675
42	Sotong-1	74	696	802	914	1126	1621	1903	2046		2525	2750
43	Sotong-2	72	688	798	917	1134	1601	1907	2050		2574	2911
44	Sotong-3	74	671	773	896	1094	1625	1918	2047		2630	3016
45	Sotong-4	73	642	741	855	1064	1557	1793	1914		2524	2635
46	Sotong-5	73	700	817	948	1141	1065	2012	2173		2729	2985
47	Sotong-6	73	705	814	944	1185	1681	2046	2199		2802	3177
48	South Raya-1	41			821	1081	1359	1838	2038			2261
49	Sumalayang-1	64			660	775	966	1283	1359			1438
50	Tabu-1	64			774	1004	1391	2217				
51	Tapis-10	64			606	749	1016	1800	2131			
52	Telok Barat-1	62		813	923	1188	1674					
53	Tembikai-1	69		893	1114	1292	1496	2267	2403	2702		
54	Tinggi-1	72				563	705	1216	1437	1766	1999	
55	Tiong Barat-1	64			678	812	1134	1789	2160			
56	Tiong-1	67				645	926	1571	1956	2536		
57	Tok Bidan-1	44	667	777	846		1657					2118
58	Inas-1	64	1252	1492								
59	Sepat-1	62	1201	1472	1740							
60	Noring-2	58	1263	1489	1934							
61	Bujang-2	65	1083	1325	1751							
62	Semangkok-1	62	704	847	1072	1415						
63	Tujuh-1	59	1332	1809	2138							
64	Tangga-1	66	1081	1325	1797							

Appendix B

Computer Programs

B.1 XRIFT

The program XRIFT calculates the subsidence and heat flow of a 1D or 2D basin based on the quantitative model of lithospheric stretching proposed by McKenzie (1978), modified to incorporate finite-duration rifting and horizontal heat conduction (Cochran, 1983). For the 1D model, only the vertical heat conduction is considered, whereas for the 2D basin model, effects of horizontal heat loss can, as an option, be included in the computation. The program is an adaptation of a FORTRAN version by J.R. Cochran, modified and re-written in the C programming language.

Basic 1D Model

The core of the program is the basic 1D uniform-stretching model of McKenzie (1978), which calculates the vertical temperature structure of the lithosphere following an instantaneous stretching event. The temperature structure of the lithosphere, $T = T(z,t)$, is calculated by solving the one-dimensional heat flow equation

$$\frac{\partial T}{\partial t} = \kappa \frac{\partial^2 T}{\partial z^2} \quad 0 \leq z \leq a \tag{B.1}$$

$$\left.\begin{aligned} T(0,t) &= 0 \\ T(a,t) &= T_o \end{aligned}\right\} \quad 0 \leq t < \infty$$

where z is the vertical coordinate measured positive downwards, t is time, and κ is the thermal diffussivity of the lithosphere. The initial and boundary conditions are such that the temperatures at the surface and at the base of the lithosphere are maintained at 0 °C and T_o=1333 °C, respectively. After instantaneous stretching by a factor β, the temperature structure becomes

$$\begin{aligned} T(z,0) &= \beta T_o z/a \quad \text{for} \quad 0 \leq z \leq a/\beta \\ &= T_o \quad \text{for} \quad a/\beta < z \leq a \end{aligned}$$

At infinite time after stretching, the temperature structure approaches the pre-stretching equilibrium temperature structure $T(z,\infty)$ (Fig. 6.6C). The solution to equation B.1 is made up of a steady state (solution when $t = \infty$) and a transient temperature solution $T^*(z,t)$:

$$T(z,t) = T(z,\infty) + T^*(z,t) \tag{B.2}$$

The steady-state solution is $T_o z/a$ whereas the transient solution is given by

$$T^*(z,t) = T_o \sum_{n=1}^{\infty} A_n \sin\left(\frac{n\pi z}{a}\right) \exp\left(\frac{-n^2 t}{\tau}\right) \tag{B.3}$$

where $\tau = a^2/\pi^2\kappa$ and A_n is the Fourier sine transform of the temperature anomaly, *i.e.* the difference between temperature structure at the onset of cooling, $T(z,0)$, and the equilibrium temperature structure, $T(z,t=\infty)$:

$$A_n = \frac{2}{aT_o} \int_0^a [T(z,0) - T(z,\infty)] \sin\left(\frac{n\pi z}{a}\right) \mathrm{d}z \tag{B.4}$$

Figure 6.6B and C shows that the temperature anomaly is given by

$$\begin{aligned} T(z,0) - T(z,\infty) &= (\beta - 1)T_o z/a \quad \text{for} \quad 0 \leq z \leq a/\beta \\ &= T_o(1 - z/a) \quad \text{for} \quad a/\beta < z \leq a/\beta \end{aligned}$$

B.4 is thus evaluated to give

$$A_n = \frac{2}{n\pi}\left(\frac{\beta}{n\pi}\right) \sin\left(\frac{n\pi}{\beta}\right) \tag{B.5}$$

Hence, the complete solution for the temperature structure is

$$T(z,t) = T_o \left[\frac{z}{a} + \sum_{n=1}^{\infty} A_n \sin\left(\frac{n\pi z}{a}\right) \exp\left(\frac{-n^2 t}{\tau}\right)\right] \tag{B.6}$$

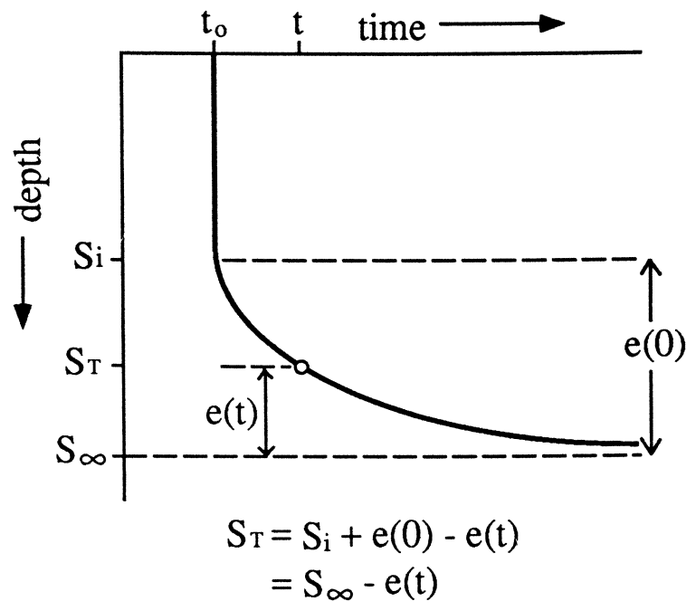

Figure B.1. Schematic diagram showing the calculation of total subsidence, S_T, at time t after instantaneous stretching.

The subsidence, S_T, at time t after stretching is the difference between the subsidence at infinite time, S_∞, and the elevation above that depth, $e(t)$ (Fig. B.1):

$$S_T(t) = S_\infty - e(t) \tag{B.7}$$

The approximation of S_∞ given by Hellinger and Sclater (1983, p. 8259) is used:

$$S_\infty = \frac{y_c(\rho_m - \rho_c)\,[1 - \alpha T_o y_c/2a]}{\rho_m(1 - \alpha T_o) - \rho_w}\left(1 - \frac{1}{\beta}\right) \tag{B.8}$$

while the expression for $e(t)$ is similar to that given by McKenzie (1978):

$$e(t) = \varepsilon_o \sum_{k=0}^{\infty} \frac{A_{2k+1}}{2k+1} \exp\left(\frac{-(2k+1)^2 t}{\tau}\right) \tag{B.9}$$

where

$$\varepsilon_o = \frac{2a\alpha T_o \rho_o}{\pi(\rho_o - \rho_w)} \quad \text{and} \quad \rho_o = \rho_m(1 - \alpha T_o)$$

The surface heat flux, Q, is found by differentiating B.6 for $z = a$:

$$\begin{aligned} Q &= k_o \frac{\mathrm{d}T}{\mathrm{d}z}\Big|_{z=a} \\ &= \frac{k_o T_o}{a}\left[1 + \pi \sum_{n=1}^{\infty} n A_n \exp\left(\frac{-n^2 t}{\tau}\right)\right] \end{aligned} \tag{B.10}$$

where k_o is the thermal conductivity of the lithosphere.

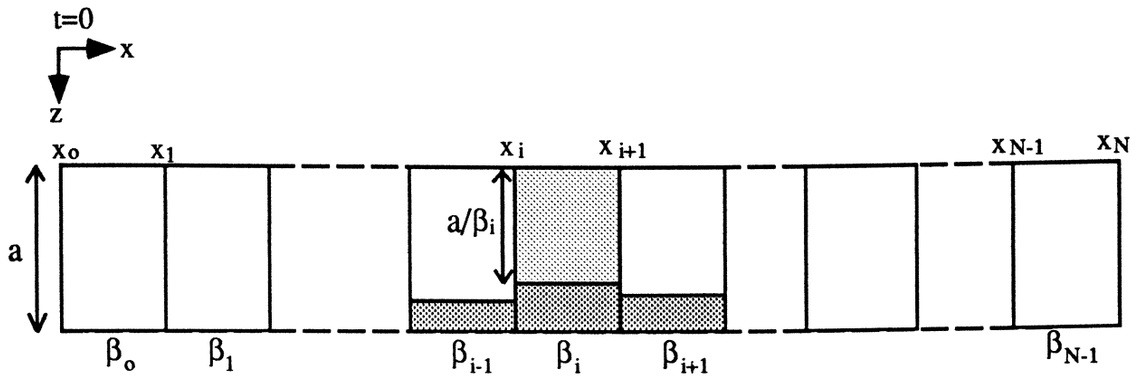

Figure B.2. Two-dimensional lithospheric model for subsidence/heat flow calculations. Lithosphere is divided into N blocks, each with a specified stretching factor, β_i. Blocks at either ends, which are distant from the rift zone, have $\beta = 1$. At $t = 0$ after instantaneous stretching, the lithospheric blocks will be thinned according to their respective β values, and the vertical temperature structure of each block is calculated. The temperature perturbation in each block as a result of lateral heat conduction from all other blocks is then calculated to correct for lateral heat loss.

2D Model With Lateral Heat Conduction

To include the effects lateral heat loss on the subsidence and heat flow histories of a two-dimensional basin, the 1D model is extended to 2D by considering the two-dimensional heat equation of the form

$$\frac{\partial T}{\partial t} = \kappa \left\{ \frac{\partial^2 T}{\partial x^2} + \frac{\partial^2 T}{\partial z^2} \right\} \tag{B.11}$$

where $T = T(x, z, t)$ is the vertical temperature distribution at a horizontal distance x. Watts *et al.* (1982) and Cochran (1983) have presented the analytical solution to equation B.11, which can be incorporated into the stretching model. In this model, the lithosphere is divided into a series of narrow blocks (Fig. B.2). The temperature structure of each block due to the vertical heat conduction from the base of the lithosphere will be modified by lateral conduction to and from the neighbouring blocks. Hence, the computation of the temperature structure, subsidence, and heat flow of a 2D basin that incorporates lateral heat conduction amounts to finding, first, the effects of vertical heat conduction for each block, as in the 1D model above, and then adding the effects of lateral heat conduction in each block due to all the other blocks.

The temperature structure of one block due to a stretching event may be written as

$$T(x,z,t) = X(x,t) \cdot Z(z,t)$$

where $X(x,t)$ and $Z(z,t)$ are the solutions of the one-dimensional equation in the horizontal (x) and vertical (z) directions, respectively. The solution for the z direction is the same as equation B.2. We can see that the solution of the two-dimensional equation is equivalent to the vertical solution, $Z(z,t)$, multiplied by some factor that is determined by the horizontal solution, $X(x,t)$. The solution in x direction is that of heat flowing into a semi-infinite medium (Carslaw and Jaeger, 1959, p. 58):

$$X(x,t) = \frac{1}{2\sqrt{\pi\kappa t}} \int_{-\infty}^{\infty} X(x',0) \exp\left[\frac{-(x-x')^2}{4\kappa t}\right] \mathrm{d}x'$$

For a single block between, say $x = x_i$ and $x = x_{i+1}$ (Fig. B.2), the initial condition is such that $X = 1$ between x_i and x_{i+1}, the horizontal limits of the blocks, and $X = 0$ otherwise. Hence, the above equation reduces to

$$X(x,t) = \frac{1}{2\sqrt{\pi\kappa t}} \int_{x_i}^{x_{i+1}} \exp\left[\frac{-(x-x')^2}{4\kappa t}\right] \mathrm{d}x'$$

Substituting $u = \frac{(x-x')}{\sqrt{4\kappa t}}$ gives

$$\begin{aligned} X(x,t) &= -\frac{1}{2\sqrt{\pi\kappa t}} \int_{x_i}^{x_{i+1}} \sqrt{4\kappa t} \exp(-u^2)\, \mathrm{d}u \\ &= -\frac{1}{\sqrt{\pi}} \int_{x_i}^{x_{i+1}} \exp(-u^2)\, \mathrm{d}u \end{aligned}$$

which is equivalent to

$$X(x,t) = \left[-\frac{1}{2}\mathrm{erfc}(u)\right]_{x_i}^{x_{i+1}}$$

where $u = \frac{(x-x')}{\sqrt{4\kappa t}}$. Hence, the solution for one box in the x direction is

$$X(x,t) = \frac{1}{2}\left[\mathrm{erfc}\left(\frac{x-x_i}{\sqrt{4\kappa t}}\right) - \mathrm{erfc}\left(\frac{x-x_{i+1}}{\sqrt{4\kappa t}}\right)\right]$$

Thus, the total solution for the temperature structure of a single block between $x = x_i$ and $x = x_{i+1}$ is

$$T(x,z,t) = T(x,z,\infty) + \frac{1}{2}\left[\mathrm{erfc}\left(\frac{x-x_i}{\sqrt{4\kappa t}}\right) - \mathrm{erfc}\left(\frac{x-x_{i+1}}{\sqrt{4\kappa t}}\right)\right] \cdot T^*(z,t) \tag{B.12}$$

where $T^*(z,t)$ is the transient solution for the vertical heat conduction given by equation B.6. As before, the steady-state temperature structure, $T(x,z,\infty)$, is simply $T_o z/a$.

Because the heat flow equation is linear, the law of superposition is used to determine the temperature distribution in all the lithospheric blocks. If N is the total number of blocks, the temperature structure is then

$$T(x,z,t) = T(x,z,\infty) + \frac{1}{2}\sum_{i=1}^{N}\left[\text{erfc}\left(\frac{x-x_i}{\sqrt{4\kappa t}}\right) - \text{erfc}\left(\frac{x-x_{i+1}}{\sqrt{4\kappa t}}\right)\right]\cdot T^*(z,t) \tag{B.13}$$

where x_i and x_{i+1} are the position of the edges of block i.

Finite-duration Rifting

The basic instantaneous stretching model, with or without lateral heat conduction, as described above, has been adapted for modelling finite-duration stretching. Following the approach made by Cochran (1983), a stretching period of length Δt_s is treated as a series of short rifting increments of 0.5 Ma duration. Assuming that the stetching factor increases exponentially during the stretching phase from 1 to β, the lithosphere is stretched incrementally by an amount, β_{inc}, given by

$$\beta_{inc} = e^{\mu\, t_{inc}}$$

where t_{inc} is the time step of 0.5 Ma duration and $\mu = \frac{1}{\Delta t_s}\log_e \beta$ is the constant governing the exponential increase in the stretching factor; β being the total stretching factor.

Because the temperature structure changes after each instantaneous stretching event, the initial temperature structure at the onset of cooling after each stretching increment is non-linear. Hence, after each stretching increment, the temperature structure of the lithosphere is evaluated using equation B.2, with the value of A_n obtained by performing the sine transform on the temperature anomaly

$[T(z,t) - T(z,\infty)]$ (equation B.4). A_n is evaluated at the end of each stretching increment and is used to calculate the subsidence (B.7) and heat flow (B.10) during the stretching phase. The value of A_n evaluated after the last stretching increment is used in the calculation of subsidence and heat flow throughout the post-stretching phase.

```
1     /*
2
3      XRIFT
4
5     This program calculates the thermal and subsidence histories across a
6     rift basin with FINITE RIFTING DURATION and LATERAL HEAT FLOW effects.
7     Ref: Watts et al (1982) and Cochran (1983).
8     Modified and translated into C by MAZLAN MADON from original Fortran program
9     SUBRIFT by J. R. COCHRAN  FEB 1982
10
11    Last modified 20 October 1995
12
13    Compile with FFT routines from Numerical Recipes in C (Press et al., 1992).
14
15    acc xrift.c four1.c realft.c sinft.c -o xrift
16
17    Input beta profile from file:
18            x       y
19    x - distance in km, y - beta factor
20
21    The profile will be padded on each side by 2*flexural parameter assuming a Te
22    of 5 km.
23    Calculations can be made with or without lateral heat flow effects.
24
25    An input file ''lithosphere.dat'' is required for specifying the constants used in th
      e calculation, e.g.
26
27    125.
28    31.2
29    3.28e-5
30    1333.0
31    8.0e-7
32    3.138
33    3330.
34    2800.
35    0.0
36
37    These figure correspond to the following parameters, in the same order:
38
39    Lithospheric thickness (km)
40    crustal thickness (km)\\
41    thermal expansion coefficient (\degrees C^{-1})
42    asthenosphere temperature (\degrees C)
43    thermal diffussivity (m^2/s)
44    thermal conductivity (W/mK)
45    density mantle at 0 \degrees C (kg/m3)
46    density crust at 0 \degrees C (kg/m3)
47    radiogenic heat component of heat flow (mW/m^2)
48
49    Outputs three files:
50    water loaded subsidence in km - <filename> specified by user
51    heat flow in h.f.u - in filename.htf
52    temperature structure of the lithosphere at center of basin - filename.tmp
53
54    ------------------------------------------------------------------------
55
56    MAZLAN MADON, Oxford, October 1995
57    */
58
59    #include <stdio.h>
60    #include <stdlib.h>
61    #include <string.h>
62    #include <math.h>
63
64    #define TRUE 1
65    #define FALSE 0
66    #define row 200
67    #define col 150
68
69    int     nbox, ia, i2;
70    double  yL, yC, alpha, t0, kappa, tau, kbase, rhom, rhoa, rhoc, rhow, hfc, airy, root
```



```
      k, te, dz;
71
72    int write_temp=FALSE;
73
74    main (int argc, char *argv[])
75    {
76    #define SECONDS 3.1536e13                /* converts m.y. to secs */
77
78            FILE * fpar, *fin, *fout, *fheat, *ftemp;
79            char    filnam[30], filnam2[30];
80            int     i, j, k, npts, itime;
81            int     lateral, profile, hfu, duration, linear, verbose, basin_age, reverse_
      time, square_time, abs_time, one_dim;
82            double  tend, time, tstep, stime, max_time, timeout, beta_crust;
83            double  temp[row][col], widthf;
84            double  pos[row], beta[row][3], subf[row], cons[row][3], t[row][col],
85            bcurr[row][3], bstep[row][3], width[row], An[row][150], z[150];
86            double  trift[200], subsid[row][200], heatf[row][200];
87
88            fin = fout = NULL;
89            lateral = profile = hfu = abs_time = TRUE;
90            duration = linear = verbose = reverse_time = basin_age = square_time = one_di
      m = FALSE;
91            for (i = 1; i < argc; i++) {
92                    if (argv[i][0] == '-') {
93                            switch (argv[i][1]) {
94                            case 'D':
95                                    sscanf(&argv[i][2], "%lf", &stime);
96                                    duration = TRUE;
97                                    break;
98                            case 'B':
99                                    sscanf(&argv[i][2], "%lf", &beta_crust);
100                                   one_dim = TRUE;
101                                   break;
102                           case 'O':
103                                   if ((fout = fopen(&argv[i][2], "w")) == NULL) {
104                                           printf("Cannot open output file\n");
105                                           exit(0);
106                                   }
107                                   strcpy(filnam, &argv[i][2]);
108                                   strcpy(filnam2, filnam);
109                                   break;
110                           case 'X':
111                                   lateral = FALSE;
112                                   break;
113                           case 'L':
114                                   linear = TRUE;
115                                   break;
116                           case 'P':
117                                   profile = FALSE;
118                                   break;
119                           case 'A':
120                                   abs_time = FALSE;
121                                   break;
122                           case 'S':
123                                   square_time = TRUE;
124                                   break;
125                           case 'W':
126                                   hfu = FALSE;
127                                   break;
128                           case 'M':
129                                   sscanf(&argv[i][2], "%lf", &max_time);
130                                   basin_age = TRUE;
131                                   break;
132                           case 'R':
133                                   reverse_time = TRUE;
134                                   break;
135                           case 'I':
136                                   write_temp = TRUE;
137                                   break;
138                           case 'V':
```

```
139                                     verbose = TRUE;
140                                     break;
141
142                             }
143                     } else
144                             fin = fopen(argv[i], "r");
145             }
146
147             if (argc < 4) errmess();
148             if (one_dim == 0 && fin == NULL) errmess();
149             if (fout == NULL) errmess();
150             if (!duration) {
151                     fprintf(stderr,"Error: Rifting duration not specified!\n\n");
152                     errmess();
153             }
154             if (stime < 1.0) {
155                     fprintf(stderr,"Duration of rifting assumed to be 1.0 Ma in calculati
    on..\n\n");
156                     stime = 1.0;
157                     }
158             if (!basin_age)
159                     max_time = 35.0;
160             if (one_dim) {
161                     nbox = 1;
162                     profile = lateral = FALSE;
163                     pos[1] = 70;
164                     beta[1][1] = beta[1][2] = beta_crust;
165
166             }
167
168
169             /* READ PARAMETERS FROM FILE */
170
171             if ((fpar = fopen("/home/users/mazlanm/src/lib/lithosphere.dat", "r")) == NUL
    L) {
172                     printf("Cannot open param.dat file\n Check...should be in /home/users
    /mazlanm/src/lib/lithosphere.dat\n");
173                     exit(0);
174             }
175
176             fscanf(fpar, "%lf", &yL);
177             fscanf(fpar, "%lf", &yC);
178             fscanf(fpar, "%lf", &alpha);
179             fscanf(fpar, "%lf", &t0);
180             fscanf(fpar, "%lf", &kappa);
181             fscanf(fpar, "%lf", &kbase);
182             fscanf(fpar, "%lf", &rhom);
183             fscanf(fpar, "%lf", &rhoc);
184             fscanf(fpar, "%lf", &hfc);
185             fclose(fpar);
186
187             if (verbose) {
188                     fprintf(stderr,"\nLithospheric parameters read from file \n<~mazlanm/
    src/lib/lithosphere.dat>:\n");
189                     fprintf(stderr," yL      : %.1f km\n yC  : %.1f km\n alpha       : %.2
    e K^-1\n To      : %.1f C\n kappa        : %.2e m^2/s\n k_b      : %.4f W/m*K\n rhom
     : %.f kg/m3\n rhoc      : %.f kg/m3\n hfc       : %.2f HFU\n",  yL, yC, alpha, t0, ka
    ppa, kbase, rhom, rhoc, hfc);
190             }
191
192             /* initialise */
193             tstep = 0.5;
194             rhow = 1030.;
195             ia = 128;
196             dz = yL / ia;
197             i2 = ia + 5;
198             rhoa = rhom * (1.0 - alpha * t0);
199             airy = rhoa / (rhoa - rhow);
200             tau = (yL*yL*1.0e6)/(M_PI*M_PI*kappa)/SECONDS;
201             rootk = yL / M_PI / sqrt(tau);
202             te = 5.;
```



```
203
204             fprintf(stderr," tau    : %.2f Ma\n\n", tau);
205
206             /* set up boxes and stretching history */
207
208             Set_up (fin, &one_dim, &stime, &linear, pos, beta, &widthf, width, cons, temp
    , z);
209
210             /* Set initial heat flow profile */
211
212             for (i = 1; i <= nbox; i++) {
213                     temp[i][3] = kbase * t0 / yL; /* units in mw/m2 */
214                     heatf[i][0] = temp[i][3];
215             }
216
217             fheat = fopen( strcat(filnam, ".htf"), "w");
218             if(write_temp) ftemp = fopen( strcat(filnam2, ".tmp"), "w");
219
220             /* Start of synrift loop */
221
222             tend = 0.0;
223             npts = 0;
224             while (tend < stime) {
225                     npts++;
226                     time = tend;
227                     tend = time + tstep;
228                     trift[npts] = tend;
229                     if (verbose)
230                             fprintf(stderr,"%d\tcalculating at %.2f Ma\n", npts, tend);
231                     for (i = 1; i <= nbox; ++i)
232                             Stept (&i, cons, &linear,  &time, &tend, bstep, bcurr, subf);
233
234                     /* calculate block widths after stretching increment */
235
236                     for (i = 1; i <= nbox; ++i) {
237                             width[i] *= bstep[i][2];
238                     }
239
240
241                     /* find new temperature distribution */
242
243                     for (i = 1; i <= nbox; ++i) {
244                             Stretch (&i,  t, &bstep[i][1], &bstep[i][2], temp);
245                     }
246
247                     /* let boxes cool through time step and calculate temperature structu
    re, subsidence, and heat flow at end of time step */
248
249                     for (i = 1; i <= nbox; ++i) {
250                             Sine_transform (&i, An, t, z);
251                             Tempers (&i, t, &tstep, An, &beta[i][2], subf, ftemp, pos, te
    mp, z);
252                     }
253
254
255                     /* add lateral heat flow effects */
256
257                     if (lateral) {
258                             for (i = 1; i <= nbox; ++i) {
259                                     Xflow (&i, t, temp, width, &tstep);
260                                     if (temp[i][1] < 0.f)
261                                             temp[i][1] /= airy;
262                             }
263                     }
264                     for (i = 1; i <= nbox; i++) {
265                             subsid[i][npts] = temp[i][1];
266                             heatf[i][npts] = temp[i][3];
267
268                     }
269             }
270
```

```
271
272             /* calculate An's at end of rifting phase */
273
274             for (i = 1; i <= nbox; ++i) {
275                     for (j = 1; j <= i2; ++j)
276                             *(t[i] + j) = *(temp[i] + j);
277                     Sine_transform (&i, An, t, z);
278             }
279
280             /* start of post rift loop ...
281             calculate temperature structure, heat flow and subsidence
282             at sqrt(time) intervals since end of stretching until max_time */
283
284             itime = 0;
285             while (trift[npts] < max_time ) {
286                     itime++;
287                     npts++;
288                     if (square_time)
289                             time = itime * itime;
290                     else
291                             time = itime;
292                     trift[npts] = stime + time;
293                     if (verbose)
294                             fprintf(stderr,"%d\tcalculating at %.2f Ma\n", npts, trift[np
    ts]);
295
296                     for (i = 1; i <= nbox; ++i) {
297                             Tempers (&i, t, &time, An, &beta[i][2], subf, ftemp, pos, tem
    p, z);
298                     }
299
300
301                     /* add lateral heat flow effects */
302
303                     if (lateral) {
304                             for (i = 1; i <= nbox; ++i) {
305                                     Yflow (&i, t, temp, &widthf, &time);
306                                     if (temp[i][1] < 0.f)
307                                             temp[i][1] /= airy;
308                             }
309                     }
310                     for (i = 1; i <= nbox; i++) {
311                             subsid[i][npts] = temp[i][1];
312                             heatf[i][npts] = temp[i][3];
313                     }
314             }
315             /*end of postrift*/
316
317
318
319             /* Output routines */
320
321             if (hfu) {
322                     for (j = 0; j <= npts; ++j) {
323                             for (i = 1; i <= nbox; i++) {
324                                     heatf[i][j] /= 41.84;
325
326                             }
327                     }
328
329             }
330
331             if (profile) {
332
333                     /* print subsidence and heatflow with time */
334                     if(verbose) fprintf(stderr,"\nOutput results for...\n");
335                     for (j = 0; j <= npts; j ++) {
336                             if (reverse_time)
337                                     timeout = max_time - trift[j];
338                             else
339                                     timeout = trift[j];
```



```
340                             if (verbose)
341                                     fprintf(stderr,"time = %.2f Ma\n", timeout);
342                             for (i = 1; i <= nbox; i++) {
343                                     fprintf(fout, "%.3f %.3f %.1f\n", pos[i], subsid[i][j
    ], timeout);
344                                     fprintf(fheat, "%.3f %.3f %.1f\n", pos[i], heatf[i][j
    ], timeout);
345                             }
346                             fprintf(fout, "\n");
347                             fprintf(fheat, "\n");
348                     }
349             } else
350              {
351                     /* print subsidence at a particular location with time */
352                     for (i = 1; i <= nbox; i++) {
353                             if (pos[i] == 70) {
354                                     for (j = 0; j <= npts; ++j) {
355                                             if (reverse_time)
356                                                     timeout = max_time - trift[j];
357                                             else
358                                                     timeout = trift[j];
359                                             if (verbose)
360                                                     fprintf(stderr,"time = %.2f Ma\tsubs
    = %.3f km\theat flow =%.3f HFU\n", timeout,subsid[i][j],heatf[i][j]);
361                                             if (abs_time) {
362                                                     fprintf(fout, "%.1f %.3f\n", timeout,
     subsid[i][j]);
363                                                     fprintf(fheat, "%.1f %.3f\n", timeout
    , heatf[i][j]);
364                                             } else {
365
366                                                     fprintf(fout, "%.1f %.3f\n", timeout
    - stime, subsid[i][j]);
367                                                     fprintf(fheat, "%.1f %.3f\n", timeout
     - stime, heatf[i][j]);
368
369                                             }
370                                     }
371                             }
372                     }
373             }
374
375             fprintf(stderr,"Done!\n");
376             fclose(fin);
377             fclose(fout);
378             fclose(fheat);
379             fclose(ftemp);
380             exit(0);
381     }
382
383
384     errmess()
385     {
386             fprintf(stderr,"\nxrift [-B<beta_crust/beta_mantle>] [<input file>]  -D<rifti
    ng duration> -O<output filename>\n");
387             fprintf(stderr,"\nCalculates theoretical subsidence and heat flow histories a
    cross rift basin, incorporating finite rifting duration and lateral heat conduction\n"
    );
388             fprintf(stderr,"Input file contains xy representing distance in km and beta f
    actor along profile. Need not be specified if the [-B] option is used.\n\n");
389             fprintf(stderr,"Options:\n");
390             fprintf(stderr,"[-B<beta_crust/beta_mantle>] : one-dimensional model, using s
    pecified beta values; if only beta_crust is specified, assumes uniform stretching - be
    ta_crust=beta_mantle.\n");
391             fprintf(stderr,"[-L] : linear stretching history; default is exponential\n");
392             fprintf(stderr,"[-X] : exclude lateral heat conduction for 2D model\n");
393             fprintf(stderr,"[-P] : output results at center of basin instead of whole pro
    file for 2D model\n");
394             fprintf(stderr,"[-A] : output time w.r.t time since end of rifting; default i
    s absolute time since start of rifting\n");
395             fprintf(stderr,"[-S] : calculate at square-root-time intervals after end of r
```

```
     ifting; default is at 1 Ma intervals\n");
396          fprintf(stderr,"[-M<max time>] : calculate to max time in Ma\n");
397          fprintf(stderr,"[-R] : reverse the time output from max time to 0\n");
398          fprintf(stderr,"[-W] : output heat flow in mW/m2; default in h.f.u.\n");
399          fprintf(stderr,"[-I] : output temperature profile of lithosphere at centre of
      basin to <filename.tmp>\n");
400          fprintf(stderr,"[-V] : verbose mode\n\n");
401          exit(0);
402  }
403
404
405  double  flex_par(double *fpar)
406  /* calculates flexural parameter */
407  {
408          static double   E = 1e11;
409          static double   p = 0.25;
410          static double   g = 9.80619203;
411
412          double  D, tmp;
413
414          D = E * pow(te * 1e3, 3) / ( 12 * (1 - (p * p)) );
415          tmp = 4 * D / ((rhom - rhow) * g);
416          *fpar = pow(tmp, 0.25);
417
418  }
419
420
421  int padbox(int *n, double *dx, double *fpar, double *x, double *z, double *xx, double
      beta[][3])
422  /* pad input boxes to 2 times the flexural parameter on both sides */
423  {
424          int     i, j, npad, m, nn;
425
426          nn = *n;
427          m = *n + 2 * npad;
428
429          npad = 2 * M_PI * *fpar / (*dx * 1e3);
430          if (npad > 0) {
431
432                  /*initialise left side pads*/
433                  for (i = 0; i < npad; i++) {
434                          xx[i] = x[0] - *dx * (npad - i);
435                          beta[i][1] = z[0];
436                          beta[i][2] = z[0];
437                  }
438                  /*renumber input boxes*/
439                  for (i = npad; i < nn + npad; i++) {
440                          xx[i] = x[i-npad];
441                          beta[i][1] = z[i-npad];
442                          beta[i][2] = z[i-npad];
443                  }
444
445                  /*initialise right side pads*/
446                  for (i = nn + npad; i < nn + 2 * npad; i++) {
447                          xx[i] = xx[i-1] + *dx;
448                          beta[i][1] = z[nn-1];
449                          beta[i][2] = z[nn-1];
450                  }
451          }
452
453          /* re-set number of boxes */
454
455          *n += 2 * npad - 1;
456          /*      for (i = 0; i < *n; i++)
457                  fprintf(stderr,"%.1f\t%.2f\t%.2f\n", xx[i], beta[i][1], beta[i][2]);
      */
458
459  }
460
461
462  int Set_up (FILE *ifp, int *one_dim, double *stime, int *itype, double *pos, double b
```



```
     eta[][3], double *widthf, double *width, double cons[][3], double temp[][150], double
     zz[])
463  /* read input file and set up boxes from input beta profile, set up initial temperatu
     re structure and stretching constants, */
464  {
465          int     i, j;
466          double  fparam, xinc;
467          double  x[110], z[110];
468
469          if (*one_dim == 0) {
470                  /* read input file containing beta profiles */
471                  i = 0;
472                  while ( (fscanf(ifp, "%lf %lf", &x[i], &z[i]) != EOF ) ) {
473                          ++i;
474                  }
475                  nbox = i;
476
477                  xinc = x[1] - x[0];
478                  *widthf = xinc;
479
480                  flex_par(&fparam);
481                  padbox(&nbox, &xinc, &fparam, x, z, pos, beta);
482
483                  /* find initial box width */
484
485                  *widthf = xinc;
486                  for (i = 1; i <= nbox; ++i) {
487                          width[i] = *widthf / beta[i][2];
488                  }
489          }
490          /* set up initial temperature structure */
491
492          for (i = 1; i <= nbox; ++i) {
493                  for (j = 1; j < 6; ++j) {
494                          *(temp[i] + j) = 0.f;
495                  }
496                  for (j = 6; j <= i2; ++j) {
497                          zz[j-5] = dz * (j - 5);
498                          *(temp[i] + j) = zz[j-5] * t0 / yL;
499                          /*      printf("%d %f\n",j-5,zz[j-5]);*/
500                  }
501          }
502
503          /* set up constants for stretching history
504          itype= 1 : linear function , itype= 0 : exponential */
505
506          switch (*itype) {
507          case 0:
508                  for (i = 1; i <= nbox; ++i) {
509                          for (j = 1; j <= 2; ++j) {
510                                  if (*(beta[i] + j) == 1)
511                                          *(cons[i] + j) = 0.0;
512                                  else
513                                          *(cons[i] + j) = log(*(beta[i] + j)) / *stime
     ;
514                          }
515                  }
516                  break;
517          case 1:
518                  for (i = 1; i <= nbox; ++i) {
519                          for (j = 1; j <= 2; ++j) {
520                                  *(cons[i] + j) = (*(beta[i] + j) - 1.0) / *stime;
521                          }
522                  }
523                  break;
524          }
525
526  }
527
528
529  int Stept (int *m, double cons[][3], int *itype, double *time, double *tend, double b
```

```
    step[][3], double bcurr[][3], double *subf)
530 {
531         int     j;
532         double  bold, bnew, sub;
533
534         /* exponential */
535
536         switch (*itype) {
537         case 0:
538                 for (j = 1; j <= 2; ++j) {
539                         if (*(cons[*m] + j) == 0.0) {
540                                 *(bcurr[*m] + j) = 1.f;
541                                 *(bstep[*m] + j) = 1.f;
542                         } else {
543                                 bold = exp(*time * *(cons[*m] + j) );
544                                 bnew = exp(*tend * *(cons[*m] + j) );
545                                 *(bstep[*m] + j) = bnew / bold;
546                                 *(bcurr[*m] + j) = bnew;
547
548                         }
549                 }
550                 break;
551
552                 /* linear stretching history */
553
554         case 1:
555                 for (j = 1; j <= 2; ++j) {
556                         bold = *(cons[*m] + j) * *time + 1.f;
557                         bnew = *(cons[*m] + j) * *tend + 1.f;
558                         *(bcurr[*m] + j) = bnew;
559                         *(bstep[*m] + j) = bnew / bold;
560                 }
561         }
562
563
564
565         /* calculate final asymptotic depth */
566
567         sub = yC * (rhom - rhoc) * (1 - alpha * t0 * yC / (yL * 2.0)) / (rhoa - rhow)
    ;
568         subf[*m] = sub * (1. - 1. / bcurr[*m][2]);
569
570 } /* Stept */
571
572
573 int Stretch (int *m, double t[][150], double *bstep, double *dstep, double temp[][150
    ])
574 /* calculate temperature profile of the lithosphere following an instantaneous stretc
    hing increment */
575 {
576         int     i, iz, j,  jz;
577         double  depth, yCnew, fract;
578
579         yCnew = yC / *dstep;
580         for (i = 1; i <= ia; i++) {
581                 j = i + 5;
582                 if (i <= yCnew)
583                         depth = i * *dstep;
584                 else
585                         depth = (i - yCnew) * *bstep + yCnew * *dstep;
586                 iz = depth;
587                 fract = depth - iz;
588                 iz += 5;
589                 jz = iz + 1;
590                 t[*m][j] = temp[*m][iz] + fract * (temp[*m][jz] - temp[*m][iz] );
591
592                 if (depth > yL)
593                         t[*m][j] = t0;
594
595         }
596
```



```
597 }
598
599
600 int Sine_transform (int *m, double An[][150], double t[][150], double zz[])
601 /* calculates fourier sine coefficients of the temperature structure xn from temperat
    ure anomaly after stretching event
602 tanom[] = dimensionless temperature anomaly after stretching increment
603 An[] = Fourier sine transform
604 calls sinft() to calculate sin transform */
605 {
606
607         int     i;
608         double  fact,tanom[256];
609
610         /* set up dimensionless temperature anomaly array */
611         fact=2./t0/ia;
612         tanom[0] = 0.;
613         for (i = 1; i <= ia; i++) {
614                 tanom[i] = fact*(t[*m][i+5] - t0 * zz[i] / yL);
615         }
616         /* calculate Fourier sine transform of temperature anomaly */
617         sinft(tanom-1, ia);
618
619         /*calculate An's*/
620         for (i = 1; i <= ia; i++) {
621                 An[*m][i] = tanom[i];
622         }
623 }
624
625
626 int Tempers (int *m, double t[][150], double *tstep, double An[][150], double *delta,
     double *subf, FILE *ftemp, double *pos, double temp[][150], double zz[])
627 /* calculates temperature, subsidence and heat flow for vertical heat conduction only
     */
628 {
629         int     i, j;
630         double  tim;
631
632         for (i = 1; i <= i2; i++)
633                 *(t[*m] + i) = 0.0;
634
635         tim = -1.0 * *tstep / tau;
636
637         /* final equilibrium depth */
638
639         for (i = 1; i <= 20; i += 2) {
640                 *(t[*m] + 1) += *(An[*m] + i) / i * exp(i * i * tim);
641         }
642         *(t[*m] + 1) *= 2.0 * yL * alpha * t0 * airy / M_PI;
643
644         /* heat flow and temperature structure */
645
646         for (i = 1; i <= 20; ++i) {
647                 *(t[*m] + 3) += *(An[*m] + i) * exp(i * i * tim) * i;
648                 *(t[*m] + 2) = *(An[*m] + i) * exp(i * i * tim);
649                 for (j = 6; j <= i2; ++j) {
650                         *(t[*m] + j) += *(t[*m] + 2) * sin(i * M_PI * zz[j-5] / yL);
651                 }
652         }
653
654         *(t[*m] + 3) = (kbase * t0 / yL) * (*(t[*m] + 3) * M_PI + 1.0);
655
656         for (j = 6; j <= i2; ++j) {
657                 *(t[*m] + j) = t0 * (zz[j-5] / yL + *(t[*m] + j) );
658         }
659
660         /* calculate results without lateral heat flow effects */
661
662         temp[*m][1] = subf[*m] - t[*m][1];
663         temp[*m][3] = t[*m][3] + hfc / *delta;
664         for (j = 6; j <= i2; j++) {
```

```
665                     temp[*m][j] = t[*m][j];
666                     if(write_temp) {
667                             if (pos[*m] == 70)
668                                     fprintf(ftemp, "%f %f\n", zz[j-5], temp[*m][j], *m);
669                     }
670             }
671
672             if(write_temp) {
673                     if (pos[*m] == 70)
674                             fprintf(ftemp, "\n");
675             }
676
677
678     } /* Tempers */
679
680
681     int Xflow (int *m, double t[][150], double temp[][150], double *width, double *tstep)
682     /* calculates lateral heat flow effects during stretching phase */
683     {
684             int     i, j;
685             double  x, d, errfc[110];
686
687             /* compute error functions for left side */
688
689             if (*m != 1) {
690                     d = width[*m] / 2.0;
691                     for (i = 1; i < *m; ++i) {
692                             x = d / (rootk * 2.0 * sqrt(*tstep));
693                             errfc[i] = erfc(x);
694                             d += width[*m - i];
695                     }
696
697                     /* add effect of left side boxes */
698
699                     for (i = 1; i < *m; ++i) {
700                             x = errfc[*m - i];
701                             temp[*m][1] -= x * (t[i][1] - t[i + 1][1]) / 2.f;
702                             temp[*m][3] += x * (t[i][3] - t[i + 1][3]) / 2.f;
703                             for (j = 6; j <= i2; ++j) {
704                                     temp[*m][j] += x * (t[i][j] - t[i + 1][j]) / 2.f;
705                             }
706                     }
707
708             }
709
710             /* compute error functions for right side */
711
712             if (*m != nbox) {
713                     d = width[*m] / 2.0;
714                     for (i = *m + 1; i <= nbox; ++i) {
715                             x = d / (rootk * 2.0 * sqrt(*tstep));
716                             errfc[i] = erfc(x);
717                             d += width[i];
718                     }
719
720                     /* add effect of right side boxes */
721
722                     for (i = *m + 1; i <= nbox; ++i) {
723                             x = errfc[i];
724                             temp[*m][1] -= x * (t[i][1] - t[i - 1][1]) / 2.f;
725                             temp[*m][3] += x * (t[i][3] - t[i - 1][3]) / 2.f;
726                             for (j = 6; j <= i2; ++j) {
727                                     temp[*m][j] += x * (t[i][j] - t[i - 1][j]) / 2.f;
728                             }
729                     }
730             }
731
732
733
734     } /* Xflow */
735
```



```
736
737     int Yflow (int *m, double t[][150], double temp[][150], double *widthf, double *time)
738     /* calculates lateral heat flow effects during post stretching phase */
739     {
740
741             int     i, j;
742             double  x, errfc[110];
743
744             /* compute error functions */
745
746             for (i = 1; i <= nbox; ++i) {
747                     x = (i - 0.5) * *widthf / (rootk * 2.0 * sqrt(*time));
748                     errfc[i] = erfc(x);
749             }
750
751             /* add effect of left side boxes */
752
753             if (*m != 1) {
754                     for (i = 1; i < *m; ++i) {
755                             x = errfc[*m - i];
756                             temp[*m][1] -= x * (t[i][1] - t[i + 1][1]) / 2.f;
757                             temp[*m][3] += x * (t[i][3] - t[i + 1][3]) / 2.f;
758                             for (j = 6; j <= i2; ++j) {
759                                     temp[*m][j] += x * (t[i][j] - t[i + 1][j]) / 2.f;
760                             }
761                     }
762             }
763
764             /* add effect of right side boxes */
765
766             if (*m != nbox) {
767                     for (i = *m + 1; i <= nbox; ++i) {
768                             x = errfc[i - *m];
769                             temp[*m][1] -= x * (t[i][1] - t[i - 1][1]) / 2.f;
770                             temp[*m][3] += x * (t[i][3] - t[i - 1][3]) / 2.f;
771                             for (j = 6; j <= i2; ++j) {
772                                     temp[*m][j] += x * (t[i][j] - t[i - 1][j]) / 2.f;
773                             }
774                     }
775             }
776
777     }
778
779
```

B.2 MATURE2

MATURE2 is a program for calculating the maturity index, either as time-temperature index, TTI (Waples, 1980), or the equivalent vitrinite reflectance, R_o. The input required are the burial history and the temperature gradient through time. Burial history is obtained by standard 1D backstripping (*e.g.* Allen and Allen, 1990). Although the modelling done in Chapter 6 uses the EASY%R_o model (Sweeney and Burnham, 1990; Wood, 1988), the program can also calculate TTI and R_o based on either the traditional Lopatin-Waples method or a chemical kinetics model (Wood, 1988; Hunt *et al.*, 1991; Hunt and Hennet, 1992). The following sections describe briefly the various methods of calculating TTI and R_o that have been implemented in the program.

Lopatin-Waples TTI

The Lopatin time-temperature index (here referred to as TTI_L) was introduced by Waples (1980) based on the theory proposed by Lopatin (1971) that the rate of vitrinite maturation doubles for every 10° C increase in temperature. The maturity attained by sediment during a finite period of heating is given by the length of time (Δt_i) that the sediment spent in a 10° C temperature interval, multiplied by a temperature factor 2^n. This is termed the "interval TTI". The total maturity or the cumulative TTI is given by the sum of all the interval TTI's:

$$TTI_L = \sum_{i=0}^{n} \Delta t_i 2^i \tag{B.14}$$

where n is the number of intervals. In Waples's (1980) definition, $i = 0$ corresponds to the temperature interval 100–110 °C.

Following Wood (1988), the temperature factor is defined as a continuous rather than as discrete 10 °C intervals:

$$TTI_L = \sum_{i=0}^{n} \Delta t_i \, 2^{(T/10)-10.5} \tag{B.15}$$

This equation sets $i = 0$ at 105 °C, the midpoint of Waples's arbitrarily defined interval 100-110 °C. If absolute temperature in K is used instead of °Celcius, the alternative expression is

$$TTI_L = \sum_{i=0}^{n} \Delta t_i \, 2^{(T/10)-37.815} \tag{B.16}$$

The interval TTI attained during a period from t_i to t_{i+1} is the integral form of equation B.16:

$$TTI_i = \frac{t_{i+1} - t_i}{(T_{i+1} - T_i)/10} \int_{T_i}^{T_{i+1}} 2^{(T/10)-37.815} \, dT \tag{B.17}$$

Note that the time interval has to be divided by $\frac{1}{10}$ of the temperature interval in order for the value to be the same as the Lopatin-Waples index.

Wood (1988) derived a cubic regression equation for the relationship between TTI and R_o based on the data of Waples (1980, his Table 4), and is used in the program to convert TTI_L to R_o in the program:

$$\log_{10} R_o = -0.006(\log_{10} TTI_L)^3 + 0.042(\log_{10} TTI_L)^2 + \log_{10} TTI_L - 0.397$$

TTI Based On Chemical Kinetics

It is now recognised that Lopatin's assumption that kerogen reaction rates double for every 10° C increase in temperature is too simplistic; in fact, reaction rates may double after about 3–5° C increase (Ungerer *et al.*, 1990). In recent years, methods based on chemical kinetics have gained popularity over the traditional Lopatin-Waples TTI method. Wood (1988) made a comparative study of TTI_L calculated using Waples method and TTI based on the Arrhenius equation (herein denoted as TTI_A), and concluded that thermal maturation trends in sediments are strongly controlled by heating rates. Wood's analysis suggests that TTI_L tends to underestimate thermal maturity at heating rates >1° C/Ma and overestimate it at heating rates significantly less than ~1° C/Ma. To overcome this, many workers have devised a method of modelling R_o using chemical kinetics (Hunt and Hennet,

1992). Below are a summary of the methods that have been implemented in the program MATURE2.

Kinetic models are based on the Arrhenius equation

$$k = Ae^{-E/RT} \tag{B.18}$$

where k is the reaction rate, A is the pre-exponential factor (1 Ma^{-1}), E is the activation energy (kJ mol^{-1}), R is the universal gas constant (0.008314 kJ mol^{-1} K^{-1}), and T is absolute temperature (K). Wood (1988) derived an expression for TTI_A:

$$TTI_A = \sum_{n=1}^{m} \frac{A}{q_n}\left(h_n e^{-E/RT_{n+1}} - h_{n+1}e^{-E/RT_n}\right) \quad \text{for} \quad T_n \neq T_{n+1}$$
$$+ \sum_{n=1}^{m}(t_{n+1} - t_n)Ae^{-E/RT_n} \quad \text{for} \quad T_n = T_{n+1}$$

where m is the total number of temperature intervals, and

$$h_n = \left(\frac{RT_n^2}{E + 2RT_n^2}\right) \qquad q_n = \frac{t_{n+1} - t_n}{T_{n+1} - T_n}$$

As for the Lopatin-Waples method described above, TTI_A is converted to R_o using the empirical relationship between TTI_L, TTI_A and R_o for specific values of A and E, depending on the kerogen composition. Wood (1988), for example, suggested the use of "average" Type III kerogen kinetic parameters (E=218 kJ mol^{-1}, $A = 5.45 \times 10^{26} Ma^{-1}$) and derived the following cubic regression equation for converting TTI_A to R_o:

$$\log_{10} R_o = -0.0001(\log_{10} TTI_A)^3$$
$$+ 0.003(\log_{10} TTI_A)^2 + 0.109(\log_{10} TTI_A) + 0.106$$

The program can be used to model different sets of parameters representing a range of kerogen types, based on the data of Hunt and Hennet (1992) (Table B.1). However, for each set of parameters, a different equation is needed to convert TTI_A to R_o. In MATURE2, only Woods average kinetics parameters are used.

Kerogen Type	E (kJ mol^{-1})	A (Ma^{-1})	relative reaction rate
IA	194	1.01×10^{25}	fast
IB	219	8.87×10^{26}	medium
IC	269	7.48×10^{30}	slow
IIA	143.5	7.017×10^{20}	fast
IIB	178.7	4.223×10^{23}	medium-fast
IIC	201.3	1.546×10^{25}	medium
IID	218.3	5.656×10^{26}	slow
III	230	3.98×10^{27}	medium
"average Type III"	218	5.45×10^{26}	slow

Table B.1. Arrhenius kinetic parameters (A and E) for various kerogen types (from Table 3.1 of Hunt and Hennet, 1992). The "average Type III" values are thosed used by Wood (1988) in his calibration of Lopatin-Waples TTI.

EASY%R_o Method

This method is also based on the Arrhenius rate equation (B.18) but, instead of using the kinetic parameters for a single reaction that is specific to one type of kerogen, it uses a set of 20 parallel reactions (Table B.2) with different Es, weighted by pre-determined stoichiometric factors (Sweeney and Burnham, 1990). The pre-exponential factor, A, used in the calculation is fixed at 1×10^{13} s^{-1}. The method is based on the calibration of R_o with the fraction of kerogen converted, F:

$$R_o = \exp(-1.6 + 3.7F)$$

The parameter F, which is a function of the reaction rate, is calculated according to the method outlined by Sweeney and Burnham (1990, p. 1568) as follows. The reaction rate can be described in terms of the Arrhenius equation:

$$\frac{\mathrm{d}C}{\mathrm{d}t} = -CA\exp(-E/RT)$$

where C is the concentration of kerogen undergoing reaction. In the EASY%R_o model, the reaction is represented by a set of parallel reactions with the same A

E (kJ mol^{-1})	Stoichiometric factor
142.3	0.03
150.6	0.03
159.0	0.04
167.4	0.04
175.7	0.05
184.1	0.05
192.5	0.06
200.8	0.04
209.2	0.04
217.6	0.07
225.9	0.06
234.3	0.06
242.7	0.06
251.0	0.05
259.4	0.05
267.8	0.04
276.1	0.03
284.5	0.02
292.9	0.02
301.2	0.01

Table B.2. Activation energies (E) in kJ mol^{-1} and their respective stoichiometric factors used in the EASY%R_o model (from Table 1 of Sweeney and Burnham, 1990). The pre-exponential factor A is fixed at 1.0×10^{13}s^{-1}.

but different Es. Hence,

$$\begin{aligned}\frac{\mathrm{d}C}{\mathrm{d}t} &= \sum_{i}^{n} \frac{\mathrm{d}C_i}{\mathrm{d}t} \\ &= -\sum_{i}^{n} C_i A \exp\left[-E_i/RT(t)\right]\end{aligned}$$

where C_i is the concentration of component i, while n is the total number of components ($n = 20$). The amount of kerogen i remaining after time t is the difference between its initial concentration and the integral of B.2 over t:

$$C_i = C_{io} - \int_0^t \left[\mathrm{d}C_i/\mathrm{d}t\right] \mathrm{d}t$$

The fraction of total reactants converted is given by:

$$\begin{aligned}F &= 1 - C/C_o \\ &= 1 - \sum_{i}^{n} \left[C_i/C_{oi}\right] f_i\end{aligned} \tag{B.19}$$

where f_i is the stoichiometric factor for component i as given in Table B.2, and C_o is the total concentration of all reactants. For implementation in the program, the relevant equations in Sweeney and Burnham (1990) are used.

```
1     /* mature2
2     Program to calculate VRo or time-temperature index (TTI) based on Lopatin-Waples or A
      rrhenius equation (Wood,1988; Sweeney and Burnham, 1990).
3     Data input consists of geohistory file output from backstripping program bcks3.
4     TTI calculated from temperature gradient input from file "grad" in the current direct
      ory
5     or based on stretching model in which case a beta factor needs to be specified.
6     Uses external functions contained in matlib.c, compiled as matlib.o
7     Mazlan Madon, Oxford, 7/11/94 */
8
9     #include <stdio.h>
10    #include <math.h>
11
12    void errmess(void)
13    {
14            printf("\n<mature2> computes organic maturation index, either the  time-tempe
      rature index (TTI) or Vitrinite Reflectance (VRo) using burial history data (from back
      stripping) and temperature history specified in input file with default name <grad> of
       calculated using stretching model assuming a value of beta factor. Calculation based
      on either Lopatin-Waples or any of the Kinetic (Arrhenius-type) models. Default is to
      use EASYRo (Sweeney & Burnham 1990). Command line syntax is as follows:\n\n");
15            printf("mature <burial history file> -O<output file> [-A<use kinetic model by
       specifying kerogen type (Hunt and Hennet 1992)] [-L <Lopatin-Waples TTI method]\n");
16            printf("Outputs depth vs VRo.\n\n");
17    }
18
19
20    void error(int type)
21    {
22            if (type == 1) {
23                    errmess();
24                    exit(0);
25            }
26            if (type == 2) {
27                    printf("Need to specify kerogen type for Arrhenius-type model.\nExiti
      ng.\n");
28                    exit(0);
29            }
30            if (type == 3) {
31                    printf("Cannot find input file.\nExiting.\n");
32                    exit(0);
33            }
34            if (type == 4) {
35                    printf("Cannot find temperature gradient file < grad >....\n");
36                    printf("Make sure it is in the current directory.\n");
37                    exit(0);
38            }
39    }
40
41
42    main (int argc, char *argv[])
43    {
44    #define TRUE 1
45    #define FALSE 0
46    #define max 20
47    #define surface_temp 21
48
49            FILE * fin, *fout, *fgrad;
50            char    modifier, kerogen_class;
51            int     i, j, n, kerogen_type, lopatinK, arrhenius, wood;
52            double  x, y, z;
53            double  A, E;
54            double  grad[max], age[max][max], depth[max][max], t[max], temp[max], tti[max
      ], vro[max];
55            extern void EasyRo (int *, double *, double *, double *, double *);
56            extern void Lopatin (int *, double *, double *, double *, double *);
57            extern void KineticPar (int *, int *, char *, double *, double *);
58            extern void KineticTTI (int *, double *, double *, double *, double *, double
       *, double *);
59
60            fin = fout = NULL;
```



```
61            lopatinK = arrhenius = wood = FALSE;
62
63            for (i = 1; i < argc; i++) {
64                    if (argv[i][0] == '-') {
65                            switch (argv[i][1]) {
66                            case 'O':
67                            case 'o':
68                                    fout = fopen(&argv[i][2], "w");
69                                    break;
70                            case 'A':
71                            case 'a':
72                                    sscanf(&argv[i][2], "%d%c",                     &kero
      gen_type, &kerogen_class);
73                                    arrhenius = TRUE;
74                                    break;
75                            case 'L':
76                            case 'l':
77                                    lopatinK = TRUE;
78                                    break;
79                            }
80                    } else
81                            fin = fopen(argv[i], "r");
82            }
83
84            if (argc < 3)
85                    error(1);
86            if (fin == NULL)
87                    error(3);
88            if (arrhenius)
89                    KineticPar(&wood, &kerogen_type, &kerogen_class, &E, &A);
90
91            /* READ INPUT FILES */
92
93            /* read burial history file from backstripping (output from bck3) */
94
95            i = 0;
96            while ( ( fscanf(fin, "%lf %lf %d", &x, &z, &n) ) != EOF) {
97                    *(age[i] + n) = x;
98                    *(depth[i] + n) = z;
99                    ++i;
100                   if (x == 0)
101                           i = 0;
102           }
103
104           /* read input geothermal gradient file */
105           fgrad = fopen("grad", "r");
106           for (i = 0; i <= n; ++i) {
107                   fscanf(fgrad, "%lf %lf", &x, &grad[i]);
108                   printf("age =%.1f grad=%.1f\n", x, grad[i]);
109           }
110           fclose(fgrad);
111
112           for (j = 0; j <= n; ++j) {
113                   for (i = 0; i <= j; ++i) {
114                           t[i] = age[0][j] - age[i][j];
115                           temp[i] = surface_temp + depth[i][j] * grad[i];
116                           if (arrhenius)
117                                   KineticTTI (&n, &E, &A, t, temp, tti, vro);
118                           else if (lopatinK)
119                                   Lopatin (&n, t, temp, tti, vro);
120                           else
121                                   EasyRo (&n, t, temp, tti, vro);
122
123                           if (!arrhenius || wood)
124                                   printf("%.3f\t%.3f\n", depth[i][j], vro[i]);
125                           else
126                                   printf("%.3f\t%.3f\n", depth[i][j], tti[i]);
127                   }
128                   printf("\n");
129                   fprintf(fout, "%.3f\t%.3f\n", depth[j][j], vro[j]);
130           }
```

```
131
132             fclose(fin);
133             fclose (fout);
134             exit(0);
135     }
136
137
```

```
1     /* functions used by mature.c and mature2.c for calculation of tti and vro
2     Mazlan Madon 28.8.1995 */
3     #include <math.h>
4
5     /* called by function EasyRo */
6
7     double  Calc (int i, double x)
8     {
9     #define num 20
10
11            static double   Rg = 0.001987;/*kcal/mol*/
12            static double   An = 1e13;
13            static double   a1 = 2.334733;
14            static double   a2 = 0.250621;
15            static double   b1 = 3.330657;
16            static double   b2 = 1.681534;
17
18            /*Activation energies in kcal/mol*/
19            static double   E[num] = {
20                    34.0, 36.0, 38.0, 40.0, 42.0,
21                    44.0, 46.0, 48.0, 50.0, 52.0,
22                    54.0, 56.0, 58.0, 60.0, 62.0,
23                    64.0, 66.0, 68.0, 70.0, 72.0            };
24            double  p, q;
25
26            p = E[i] / (Rg * x);
27            q = 1 - (((p * p) + (a1 * p) + a2) / ((p * p) + (b1 * p) + b2));
28            return( x * An * exp(-p) * q );
29
30    }
31
32
33    /* Calculates Easy%Ro (Sweeney & Burnham 1990, p. 1568) */
34
35    void EasyRo (int *n, double *t, double *temp, double *tti, double *vro)
36    {
37    #define num 20
38    #define max 20
39            static double   f[num] = {
40                    0.03, 0.03, 0.04, 0.04, 0.05,
41                    0.05, 0.06, 0.04, 0.04, 0.07,
42                    0.06, 0.06, 0.06, 0.05, 0.05,
43                    0.04, 0.03, 0.02, 0.02, 0.01            };
44            int     i, j;
45            double  qn;
46            double  w, I[num][max], dI[num][max], F[max];
47
48            for (j = 0; j <= *n; ++j) {
49                    for (i = 0; i < 20; ++i)
50                            I[i][j] = Calc(i, 273.15 + temp[j]);
51            }
52
53            for (j = 0; j <= *n; ++j) {
54                    if (temp[j] == temp[j-1])
55                            qn = 0.0000001;
56                    else
57                            qn = (temp[j] - temp[j-1]) / (t[j] - t[j-1]);
58                    w = 0;
59                    for (i = 0; i < 20; ++i) {
60                            if (j == 0)
61                                    dI[i][j] = 0.0;
62                            else
63                                    dI[i][j] = dI[i][j-1] + ( (I[i][j] - I[i][j-1]) / (qn
       / 3.1536e13) );
64                            w += f[i] * (1 - exp(-dI[i][j]));
65                    }
66                    F[j] = w;
67                    vro[j] = exp(-1.6 + 3.7 * F[j]);
68            }
69    }
70
```



```
71
72    /* function called by Lopatin (Wood, 1988; eq. 20)*/
73
74    double  Reflectance (double x)
75    {
76            double  a, b;
77
78            b = log10(x);
79            a = (-0.006 * pow(b, 3)) + (0.042 * pow(b, 2)) + (0.162 * b) - 0.397;
80            return(pow(10, a));
81    }
82
83
84    /* Calculate VRo based on Lopatin-Waples TTI method (Wood, 1988; eq. 8) */
85    void Lopatin (int *n, double *t, double *temp, double *tti, double *vro)
86    {
87            int     i;
88            double  qn, int_tti;
89
90            for (i = 0; i <= *n; ++i) {
91                    qn = (temp[i] - temp[i-1]) / (t[i] - t[i-1]);
92                    if (i == 0)
93                            tti[i] = 0.0;
94                    else {
95                            if (temp[i] == temp[i-1])
96                                    int_tti = (t[i] - t[i-1]) * pow(2, (((273.15 + temp[i
    ]) / 10) - 37.815));
97                            else
98                                    int_tti = (pow(10, (0.030 * (273.15 + temp[i]) - 10.2
    24)) - pow(10, (0.030 * (273.15 + temp[i-1])
99                                            -10.224))) * (1 / qn);
100                           tti[i] = tti[i-1] + int_tti;
101                   }
102                   if (tti[i] <= 0)
103                           vro[i] = 0.202;
104                   else
105                           vro[i] = Reflectance(tti[i]);
106
107           }
108
109   }
110
111
112   /* select and test for kinetic parameters (Wood, 1988; Hunt and Hennet, 1992)*/
113
114   void KineticPar (int *wood, int *kerogen_type, char *kerogen_class, double *E, double
       *A)
115   /* Units: E in kJ/mol, A in per Ma */
116   {
117           extern void error();
118
119           if (*kerogen_type == 1) {
120                   switch (*kerogen_class) {
121                   case 'a':
122                           *E = 194;
123                           *A = 1.01e25;
124                           break;
125                   case 'b':
126                           *E = 219;
127                           *A = 8.87e26;
128                           break;
129                   case 'c':
130                           *E = 269;
131                           *A = 7.48e30;
132                           break;
133                   default :
134                           error(2);
135                   }
136           } else if (*kerogen_type == 2) {
137                   switch (*kerogen_class) {
138                   case 'a':
```

```
                        *E = 143.5;
                        *A = 7.017e20;
                        break;
                case 'b':
                        *E = 178.7;
                        *A = 4.223e23;
                        break;
                case 'c':
                        *E = 201.3;
                        *A = 1.546e25;
                        break;
                case 'd':
                        *E = 218.3;
                        *A = 5.656e26;
                        break;
                default :
                        error(2);
                }
        } else if (*kerogen_type == 3) {
                *E = 230;
                *A = 3.98e27;
        } else {
                /* Wood's "average" Type III kinetics */
                *E = 218.;
                *A = 5.45e26;
                *wood = 1;
        }
        printf("Kinetic parameters: E=%.2f kJ/mol\nA=%.2e /Ma\n", *E, *A);

}


/* Called by KineticTTI */
#define R 0.008314 /* gas constant in kJ/mol/K */

double  Factor (double x, double z)
{
        double  a, b, c;

        a = R * x * x;
        b = z + (2 * R * x);
        c = exp(-z / (R * x));
        return (a * c / b);

}


/* function called by KineticTTI, to convert TTI to Ro, based on
Wood's average Type III kinetics; Wood (1988, eq. 21) */

double  type3_vro (double x)
{
        double  a, b;

        b = log10(x);
        a = (-0.0001 * pow(b, 3)) + (0.003 * pow(b, 2)) + (0.109 * b) + 0.106;
        return(pow(10, a));
}


/* Calculates TTI based on kinetic parameters (Wood, 1988; eq.15) */

void KineticTTI (int *n, double *E, double *A, double *t, double *temp, double *tti,
double *vro)
{
        int     i;
        double  qn, int_tti;

        for (i = 0; i <= *n; ++i) {
                qn = (temp[i] - temp[i-1]) / (t[i] - t[i-1]);
```



```
                if (i == 0)
                        tti[i] = 0.0;
                else {
                        if (temp[i] == temp[i-1])
                                int_tti = (t[i] - t[i-1]) * *A * exp( -*E / (R * (273
.15 + temp[i])));
                        else
                                int_tti = (*A / qn) * (Factor((273.15 + temp[i]), *E)
 - Factor((273.15 + temp[i-1]), *E) );
                        tti[i] = tti[i-1] + int_tti;
                }

                if (tti[i] <= 0)
                        vro[i] = 0.202;
                else
                        vro[i] = type3_vro(tti[i]);

        }


}
```

REFERENCES

Aadland, A.J., and Phoa, R.S.K. 1981. *Geothermal gradient map of Indonesia.* Indonesian Petroleum Association, Jakarta.

Achalabhuti, C. 1975. Petroleum geology of Thailand (Gulf of Thailand and South China Sea) – Summary. *Pages 251–255 of:* Halbouty, M.T., Maher, J.C., and Lian, H.M. (eds), *Circum-Pacific Energy and Mineral Resources.* Memoir, no. 25. American Association of Petroleum Geologists.

Ahmad, Munif Khoraini. 1993. Tertiary palynomorphs from Batu Arang, Malaysia. *Warta Geologi*, **19**, 116.

Allen, C.R., Gillespie, A.R., Yuan, Han, Sien, K.E., Zhang, B., and Zhu, C. 1984. Red River and associated faults, Yunnan Province, China: Quaternary geology, slip rates and seismic hazards. *Geological Society of America Bulletin*, **95**, 686–700.

Allen, P.A., and Allen, J.R. 1990. *Basin Analysis: Principles and Applications.* Blackwell, Oxford.

Armitage, J.H., and Viotti, C. 1977. Stratigraphic nomenclature — southern end Malay Basin. *Proceedings Indonesian Petroleum Association 6th Annual Convention, Jakarta, May 1977*, 69–94.

ASCOPE. 1981. *Tertiary sedimentary basins of the Gulf of Thailand and South China Sea: stratigraphy, structure, and hydrocarbon occurrences.* ASEAN Council on Petroleum.

Asquith, G.B. 1980. *Basic well-log analysis for geologists.* Methods in Exploration. American Association of Petrolem Geologists, Tulsa, OK.

Athy, L.F. 1930. Density, porosity and compaction of sedimentary rocks. *American Association of Petroleum Geologists Bulletin*, **14**, 1–24.

Audley-Charles, M.G., Ballantyne, P.D., and Hall, R. 1988. Mesozoic-Cenozoic rift-drift sequence of Asian fragments from Gondwanaland. *Tectonophysics*, **155**, 317–330.

Badley, M.E., Egeberg, T., and Nipen, O. 1984. Development of rift basin illustrated by the structural evolution of the Oseberg feature, Block 30/6, offshore Norway. *Journal of the Geological Society of London*, **41**, 639–649.

Bally, A.W., and Snelson, S. 1980. Realms of subsidence. *Canadian Society of Petroleum Geologists Memoir*, **6**, 1–94.

Barnett, J.A.M., Mortimer, J., Rippon, J.H., Walsh, J.J., and Watterson, J. 1987. Displacement geometry in the volume containing a single normal fault. *American Association of Petroleum Geologists Bulletin*, **71**, 925–937.

Barr, D. 1987. Structural/stratigraphic models for extensional basins of graben type. *Journal of Structural Geology*, **9**, 491–500.

Barton, P.J., and Wood, R. J. 1984. Tectonic evolution of North Sea basin: crustal stretching and subsidence. *Geophysical Journal of the Royal Astronomical Society*, **79**, 987–1022.

Bassi, G., Keen, C.E., and Potter, P. 1993. Contrasting styles of rifting: models and examples from the eastern Canadian margin. *Tectonics*, **12**, 639–655.

Bates, G.B., and Ong, G.B. 1991. *Pari-1 and Penyu-1 South China Sea, Malaysia, Biostratigraphy and depositional environments.* Technical Report. Robertson Singapore Pte Ltd.

Beauchamp, J. 1988. Triassic sedimentation and rifting in the High Atlas (Morrocco). *Pages 477–497 of:* Manspeizer, W. (ed), *Triassic-Jurassic Rifting: Part A*. Elsevier, Amsterdam.

Beaumont, C. 1981. Foreland basins. *Geophysical Journal of the Royal Astronomical Society*, **65**, 291–329.

Beaumont, C., Keen, C.E., and Boutilier, R. 1982. On the evolution of rifted continental margins; comparison of models and observations for Nova Scotia margin. *Geophysical Journal of the Royal Astronomical Society*, **70**, 667–715.

Beck, M.E.Jr. 1989. Block rotation in continental crust: examples from western North America. *Pages 1–16 of:* Kissel, C., and Laj, C. (eds), *Paleomagnetic Rotations and Continental Deformation.* Kluwer Academic Press.

Beddoes, L.R. 1980. Hydrocarbon plays in Tertiary basins of Southeast Asia. *Offshore South East Asia Conference, 26–29 Feb 1980, Singapore.*

Bertram, G.T., and Milton, N.J. 1989. Reconstructing basin evolution from sedimentary thickness; the importance of palaeobathymetric control with reference to the North Sea. *Basin Research*, **1**, 247–257.

Bignell, J.D., and Snelling, N.J. 1977. K-Ar ages of some basic igneous rocks from Peninsular Malaysia and Thailand. *Bulletin of the Geological Society of Malaysia*, **8**, 89–93.

Bishop, W.F. 1980. Structure, stratigraphy, and hydrocarbons offshore southern Kalimantan Indonesia. *American Association of Petroleum Geologists Bulletin*, **64**, 37–58.

Bond, G.C., and Kominz, M.A. 1984. Construction of tectonic subsidence curves for the lower Palaeozoic miogeocline, southern Canadian Rocky Mountains: implications for subsidence mechanisms, age of breakup and crustal thinning. *Geological Society of America Bulletin*, 155–173.

Bott, M.H.P. 1973. Inverse methods in the interpretation of magnetic and gravity anomalies. *Methods in Computational Physics*, **13**, 133–162.

Bott, M.H.P. 1982. Origin of the lithosphere tension causing basin formation. *Philosophical Transaction Royal Society of London*, **A305**, 319–324.

Bown, J.W., and White, R.S. 1995a. Finite duration rifting, melting and subsidence at continental margins. *Pages 31–54 of:* Banda, E., *et al.* (eds), *Ocean-Continent Boundaries.* Kluwer Academic Press, Amsterdam.

Bown, J.W., and White, R.S. 1995b. Effect of finite extension rate on melt generation at rifted continental margins. *Journal of Geophysical Research*, **100**, 18011–18029.

Braun, J., and Beaumont, C. 1989. A physical explanation of the relation between flank uplifts and the break-up unconformity at rifted continental margins. *Geology*, **17**, 760–764.

Brodie, J., and White, N. 1994. Sedimentary basin inversion due to igneous underplating; Northwest European shelf. *Geology*, **22**, 147–150.

Burov, E.B., and Diament, M. 1995. The effective elastic thickness (T*e*) of continental lithosphere: What does it really mean? *Journal of Geophysical Research*, **100**, 3905–3927.

Burrus, J. 1989. Review of geodynamic models for extensional basins; The paradox of stretching in the gulf of Lions (Northwest Mediterranean). *Bulletin de la société géologie de France*, **8**, 377–393.

Burton, C.K. 1973. Mesozoic. *Pages 97–141 of:* Gobbett, D.J., and Hutchison, C.S. (eds), *Geology of the Malay Peninsula.* Wiley Interscience, New York.

Burton, C.K., and Bignell, J.D. 1969. Cretaceous-Tertiary events in Southeast Asia. *Geological Society of America Bulletin*, **80**, 681–688.

Carslaw, H.S., and Jaeger, J.C. 1959. *Conduction of Heat in Solids.* Oxford University Press.

Cartwright, J.A. 1987. Transverse structural zones in continental rifts—an example from the Danish Sector of the North Sea. *In: Brooks, J. and Glennie, K. (eds.), Petroleum Geology of Northwest Europe. Graham and Trotman*, 441–452.

Cartwright, J.A., Trudgill, B.D., and Mansfield, C.S. 1995. Fault growth by segment linkage: an explanation for scatter in maximum displacement and trace length data from Canyonlands Grabens of SE Utah. *Journal of Structural Geology*, **17**, 1319–1326.

Chapman, R.E. 1983. *Petroleum Geology.* Elsevier, Amsterdam.

Chinbunchorn, N., Pradidtan, S., and Sattayarak, N. 1989. Petroleum potential of Tertiary intermontane basins in Thailand. *Proceedings International Symposium on Intermontane Basins: Geology and Resources. Chiang Mai, Thailand (30 January - 2 February 1989)*, 29–41.

Christie-Blick, N., and Biddle, K.T. 1985. Deformation and basin formation along strike-slip faults. *Pages 1–34 of:* Biddle, K.T., and Christie-Blick, N. (eds), *Strike-slip Deformation, Basin Formation and Sedimentation.* Special Publication, no. 37. Society of Economic Paleontologists and Mineralogists.

Cloetingh, S., and Kooi, H. 1992. Tectonics and global change — inferences from Late Cenozoic subsidence and uplift patterns in the Atlantic/Mediterranean region. *Terra Nova*, **4**, 340–350.

Clure, J. 1991. Spreading centres and their effect on oil generation in the Sunda Region. *Proceedings Indonesian Petroleum Association 20th Annual Convention, Jakarta, 8–10 Oct. 1991*, 37–50.

Cobbing, E.J., Mallick, D.I., Pitfield, P.E.J., and Teoh, L.H. 1986. The granite of the Southeast Asian tin belt. *Journal of the Geological Society of London*, **143**, 537–550.

Cochran, J.R. 1983. Effects of finite rifting times on the development of sedimentary basins. *Earth and Planetary Science Letters*, **66**, 289–302.

Coney, P.J., and Harms, T.A. 1984. Cordilleran metamorphic core complexes: Cenozoic extensional relics of Mesozoic compression. *Geology*, **12**, 550–554.

Coward, M. 1994. Inversion tectonics. *Pages 289–304 of:* Hancock, P.L. (ed), *Continental Deformation.* Pergamon, Oxford.

Cowie, P.A., and Karner, G.D. 1990. Gravity effect of sediment compaction: examples from the North Sea and the Rhine Graben. *Earth and Planetary Science Letters*, **99**, 141–153.

Cowie, P.A., and Scholz, C.H. 1992. Displacement-length scaling relationship for faults: Data synthesis and discussion. *Journal of Structural Geology*, **14**, 1149–1156.

Cowie, P.A., Vanneste, C., and Sornette, S. 1993. Statistical physics model for the spatiotemporal evolution of faults. *Journal of Geophysical Research*, **98**, 21809–21821.

Cox, K.G. 1993. Continental magmatic underplating. *Philosophical Transaction Royal Society of London*, **A342**, 155–166.

Crostella, A. 1981. Malacca Strait wrench fault controlled Lalang and Mengkapan oil fields. *Proceedings Offshore South East Asia Conference, Singapore*, **2**, 1–12.

Crowell, J.C. 1974. Origin of late Cenozoic basins in southern California. *Pages 190–204 of:* Dickinson, W.R. (ed), *Tectonics and Sedimentation.* Special Publication, no. 22. Society of Economic Paleontologists and Mineralogists.

Dain, A.Y. Le, Tapponnier, P., and Molnar, P. 1984. Active faulting and tectonics of Burma and surrounding region. *Journal of Geophysical Research*, **89**, 453–472.

Daines, S.R. 1985. Structural history of the W Natuna Basin and the tectonic evolution of the Sunda region. *Proceedings Indonesian Petroleum Association 14th Annual Convention, Jakarta, October 1985*, **1**, 39–61.

Daly, M.C. 1989. Rift basin evolution in Africa: the influence of reactivated steep basement shear zones. *Pages 309–334 of:* Cooper, M.A., and Williams, G.D. (eds), *Inversion Tectonics.* Special Publication, no. 44. Geological Society of London.

Daly, M.C., Hooper, B. G. D., and Smith, D.G. 1987. Tertiary plate tectonics and basin evolution in Indonesia. *Proceedings Indonesian Petroleum Association 16th Annual Convention, Jakarta, October 1987*, **1**, 399–428.

Daly, M.C., Cooper, M.A., Wilson, I., Smith, D.G., and Hooper, B.G.D. 1991. Cenozoic plate tectonics and basin evolution in Indonesia. *Marine and Petroleum Geology*, **8**, 2–21.

Dawers, N.H. 1993. Growth of normal faults: displacement-length scaling. *Geology*, **21**, 1107–1110.

de Bremaecker, J.C. 1983. Temperature, subsidence and hydrocarbon maturation in extensional basins, a finite element model. *American Association of Petroleum Geologists Bulletin*, **67**, 1410–1414.

Destro, N. 1995. Release faults: A variety of cross fault in linked extensional fault systems, in the Sergipe–Alagoas Basin, NE Brazil. *Journal of Structural Geology*, **17**, 615–629.

Dewey, J.F. 1980. Episodicity, sequence and style at convergent plate boundaries. *Geological Association of Canada Special Paper*, **20**, 553–573.

Dewey, J.F. 1982. Plate tectonics and the evolution of the British Isles. *Journal of the Geological Society of London*, **139**, 317–412.

Dewey, J.F. 1988. Extensional collapse of orogens. *Tectonics*, **7**, 1123–1139.

Dewey, J.F., Cande, S., and III, W.C. Pitman. 1989. Tectonic evolution of the India-Eurasia Collision Zone. *Eclogae Geologicae Helvetiae*, **82**, 717–734.

Dixon, T.H., Stern, R.J., and Hussein, I.E. 1987. Controls on Red Sea rift geometry by Precambrian structures. *Tectonics*, **6**, 551–571.

Ebinger, C.J., Karner, G.D., and Weissel, J.K. 1991. Mechanical strength of extended continental lithosphere: constraints from the western rift system, East Africa. *Tectonics*, **10**, 1239–1256.

Elliot, D. 1976. The energy balance and deformation mechanisms of thrust sheets. *Philosophical Transaction Royal Society of London*, **A283**, 289–312.

England, P., and Molnar, P. 1990. Right-lateral shear and rotation as explanation for strike-slip faulting in eastern Tibet. *Nature*, **344**, 140–142.

Eubank, R.T., and Makki, A.C. 1981. Structural geology of the Central Sumatra back-arc basin. *Proceedings of the Indonesian Petroleum Association 14th Annual Convention, Jakarta, May 1981*, 153–196.

Faccenna, C., Nalpas, T., Braun, J.P., and Davy, P. 1995. The influence of pre-existing thrust faults on normal fault geometry in nature and in experiments. *Journal of Structural Geology*, **17**, 1139–1149.

Feng, Chi-Chin, and Teng, Ta-Liang. 1983. Three-dimensional crust and upper mantle structure of the Eurasian continent. *Journal of Geophysical Research*, **88**, 2261–2272.

Flower, M.J., Harder, S.H., and McCabe, R.J. 1992. Tectonic implications of Cenozoic magmatism in Southeastern and Eastern Asia. *Symposium Tectonic Framework and Energy Resources of the Western Margin of the Western Pacific Basin, Kuala Lumpur, 29 Nov-2 Dec. 1992. Program and Abstracts*, 31.

Fowler, S., and McKenzie, D. 1989. Gravity studies of the Rockall and Exmouth Plateaux using SEASAT altimetry. *Basin Research*, **2**, 27–34.

Fuller, M., Haston, R., Jin-Lu, Lin, Richter, B., Schmidtke, E., and Almasco, J. 1991. Tertiary paleomagnetism of regions around the South China Sea. *Journal of Southeast Asian Earth Sciences*, **6**, 161–184.

Funahara, S., Nishikawa, N., Murata, F., Otofuji, Y., and Wang, Y. 1993. Clockwise rotation of the Red River Fault inferred from paleontology of Cretaceous rocks in the Shan-Thai-Malay block of western Yunnan. *Earth and Planetary Science Letters*, **117**, 29–42.

Gabel, J., Trzeski, R., Zwingmann, H., Chonglakmani, C., Helmcke, D., and Meischner, D. 1993. Triassic extensional basins in northern Thailand. *Late Orogenic Extension in Mountain Belts. Doc. BGRM Fr. No. 219. Abstracts of International Meeting, 4-6 March Montpellier*, 72.

Garfunkel, Z., and Ron, H. 1985. Block rotation and deformation by strike-slip faults 2. The properties of a type of macroscopic discontinuous deformation. *Journal of Geophysical Research*, **90**, 8589–8602.

Gatinsky, Y.G. 1986. Geodynamics of Southeast Asia in relation to the evolution of ocean basins. *Palaeogeography, Palaeoclimatology, Palaeoecology*, **55**, 127–144.

Gawthorpe, R.L., and Hurst, J.M. 1993. Transfer zones in extensional basins: their structural style and influence on drainage development and stratigraphy. *Journal of the Geological Society of London*, **150**, 1137–1152.

Gawthorpe, R.L., Fraser, A.L., and Collier, R. E. Ll. 1994. Sequence stratigraphy in active extensional basins: implications for the interpretation of ancient basin-fills. *Marine and Petroleum Geology*, **11**, 642–658.

Geological, Survey Department Malaysia. 1985. *Geological Map of Peninsular Malaysia, 8th Edition.* Technical Report. Director-General, Geological Survey of Malaysia.

Gibbs, A.D. 1984. Structural evolution of extensional basin margins. *Journal of the Geological Society of London*, **141**, 609–620.

Gibbs, A.D. 1989. Structural styles in basin formation. *Pages 81–93 of:* Tankard, A.J., and Balkwill, R.W. (eds), *Extensional Tectonics and Stratigraphy of the North Atlantic Margins.* Memoir, no. 46. American Association of Petroleum Geologists.

Gibling, M.R. 1988. Cenozoic lacustrine basins of Southeast Asia, their tectonic setting, depositional environment and hydrocarbon potential. *Pages 341–351 of:* Fleet, A.J., Kelts, K., and Talbot, M.R. (eds), *Lacustrine Petroleum Source Rocks.* Special Publication, no. 40. Geological Society of London.

Gilder, S.A., Coe, R.S., Wu, H., Kuang, G., Zhao, X., Wu, Q., and Tang, X. 1993. Cretaceous and Tertiary paleomagnetic results from Southeast China and their tectonic implications. *Earth and Planetary Science Letters*, **117**, 637–652.

Gillespie, P., Walsh, J.J., and Watterson, J. 1992. Limitations of displacement and dimension data from single faults and the consequence for data analysis and interpretation. *Journal of Structural Geology*, **14**, 1157–1172.

Ginger, D.C., Ardjakusuma, W.O., Hedley, R.J., and Pothecary, J. 1993. Inversion history of the West Natuna Basin: examples from the Cumi-Cumi PSC. *Proceedings Indonesian Petroleum Association 22nd Annual Convetion, October 1993*, 635–658.

Ginger, D.C., Pothecary, J., and Hedley, R.J. 1994. New insights into the inversion history of the West Natuna Basin. *American Association of Petroleum Geologists Bulletin*, **78**, 1142–1143.

Gobbett, D.J., and Hutchison, C.S. 1973. *Geology of the Malay Peninsula.* Wiley Interscience, New York.

Gobbett, D.J., and Tjia, H.D. 1973. Tectonic history. *Pages 308–334 of:* Gobbett, D.J., and Hutchison, C.S. (eds), *Geology of Peninsular Malaysia.* Wiley Interscience, New York.

Haile, N.S. 1973. The geomorphology and geology of the northern part of the Sunda Shelf and its place in the Sunda Mountain system. *Pacific Geology*, **6**, 73–89.

Haile, N.S., Beckinsale, R.D., Chakraborty, K.R., Hussein, A.H., and Hardjono, T. 1983. Palaeomagnetism, geochronology and petrology of the dolerite dykes and basaltic lavas from Kuantan, West Malaysia. *Bulletin of the Geological Society of Malaysia*, **16**, 71–85.

Hall, B.D., and White, N. 1994. Origin of anomalous Tertiary subsidence adjacent to North Atlantic continenal margins. *Marine and Petroleum Geology*, **11**, 702–714.

Hamilton, W. 1979. *Tectonics of the Indonesian region.* U.S. Geological Survey Professional Paper 1078.

Harbury, N.A., Jones, M.E., Audley-Charles, M.G., Metcalfe, I., and Mohamed, K.R. 1990. Structural evolution of Mesozoic Peninsular Malaysia. *Journal of the Geological Society of London*, **147**, 11–26.

Harder, S.H., McCabe, R.J., and Flower, M.F.J. 1992. A single mechanism for Cenozoic extension in and around Indonesia. *Symposium Tectonic Framework and Energy Resources of the Western Margin of the Western Pacific Basin, Kuala Lumpur, 29 Nov-2 Dec., 1992. Program and Abstracts*, 34.

Harding, T.P. 1985. Seismic characteristics and identification of negative flower structures, positive flower structures, and positive structural inversion. *American Association of Petroleum Geologists Bulletin*, **69**, 582–600.

Harding, T.P. 1990. Identification of wrench faults using subsurface structural data: criteria and pitfalls. *American Association of Petroleum Geologists Bulletin*, **74**, 1590–1609.

Hartley, R., Watts, A.B., and Fairhead, J.D. in press. Isostasy of Africa. *Earth and Planetary Science Letters.*

Hayes, D.E., Houtz, R.E., Jarrard, R.D., Morowski, C.L., and Watanabe, T. 1978. Crustal structure. *Pages 4–5 of:* Hayes, D.E. (ed), *Geophysical Atlas of East and Southeast Asian Seas.* Map and Chart Series, vol. MC-25. Geological Society of America.

Heidrick, T.L., and Aulia, K. 1993. A structural and tectonic model of the Central Plains Block, Central Sumatra Basin, Indonesia. *Proceedings Indonesian Petroleum Association 22nd Annual Convention, Jakarta, October 1993*, 285–318.

Helander, D. 1983. *Fundamentals of Formation Evaluation.* OGCI, Tulsa.

Hellinger, S.J., and Sclater, J.G. 1983. Some comments on two-layer extensional models for the evolution of sedimentary basins. *Journal of Geophysical Research*, **88**, 8251–8296.

Holt, W.E., Ni, J.F., Wallace, T.C., and Haines, A.J. 1991. The active tectonics of the Eastern Himalayan Syntaxis and surrounding regions. *Journal of Geophysical Research*, **96**, 14595–14632.

Huang, K., and Opdyke, N.D. 1991. Paleomagnetic results from the upper Carboniferous of the Shan-Thai-Malay Block of western Yunnan, China. *Tectonophysics*, **192**, 333–344.

Huang, K., and Opdyke, N.D. 1993. Palaeomagnetic results from Cretaceous and Jurassic rocks in south and southwest Yunnan: evidence for large clockwise rotations in the Indochina and Shan-Thai-Malay terranes. *Earth and Planetary Science Letters*, **117**, 507–524.

Huchon, P., Pichon, X. Le, and Rangin, C. 1994. Indochina Peninsula and the collision of India and Eurasia. *Geology*, **22**, 27–30.

Hunt, J.M., and Hennet, R.J.-C. 1992. Modeling petroleum generation in sedimentary basins. *Pages 21–52 of:* Whelan, J.K., and Farrington, J.W. (eds), *Organic Matter: Productivity, Accummulation, and Preservation in Recent and Ancient Sediments.* Columbia University Press, New York.

Hunt, J.M., Lewan, M.D., and Hennet, R.J.-C. 1991. Modeling oil generation with Time-Temperature Index Graphs based on Arrhenius equation. *American Association of Petroleum Geologists Bulletin*, **75**, 795–807.

Hutchinson, I. 1985. The effects of sedimentation and compaction on oceanic heat flow. *Geophysical Journal of the Royal Astronomical Society*, **82**, 439–459.

Hutchison, C.S. 1973. Metamorphism. *Pages 253–303 of:* Gobbett, D.J., and Hutchison, C.S. (eds), *Geology of the Malay Peninsula.* Wiley Interscience, New York.

Hutchison, C.S. 1975. Ophiolite in Southeast Asia. *Geological Society of America Bulletin*, **86**, 797–806.

Hutchison, C.S. 1984. Is there a satisfactory classification for Southeast Asian Tertiary basins? *Proceedings Offshore Southeast Asia Conference*, **5**, 6.64–6.76.

Hutchison, C.S. 1989a. *Geological Evolution of South-East Asia.* Oxford monographs on Geology and Geophysics, no. 13. Clarendon Press, Oxford.

Hutchison, C.S. 1989b. The Paleo-Tethyan realm and Indosinian orogenic system of Southeast Asia. *In: Sengor, A.M.C. (ed.) Tectonic evolution of the Tethyan Realm*, 585–643.

Hutchison, C.S. 1992a. The Eocene unconformity in Southeast and East Sundaland. *Bulletin of the Geological Society of Malaysia*, **32**, 69–88.

Hutchison, C.S. 1992b. Tectonic framework of the Southeast Asian Tertiary basins. *Symposium Tectonic Framework and Energy Resources of the Western Margin of the Western Pacific Basin, Kuala Lumpur, 29 Nov-2 Dec. 1992. Programs and Abstracts*, 20.

Huyghe, P., and Mugnier, J.-L. 1992. Short-cut geometry during structural inversions: competition between faulting and reactivation. *Bulletin de la société géologie de France*, **163**, 691–700.

Ingersoll, R.V., and Busby, C.J. 1995. Tectonics of sedimentary basins. *Pages 1–51 of:* Busby, C.J., and Ingersoll, R.V. (eds), *Tectonics of Sedimentary Basins.* Blackwell Science, Cambridge, MA.

Ismail, M.T., Abdullah, S. A., and Rudolph, K.W. 1994. Structural and sedimentary evolution of the Malay Basin. *American Association of Petroleum Geologists Bulletin*, **78**, 1148.

Issler, D.R. 1992. A new approach to shale compaction and stratigraphic restoration, Beaufort-Mackenzie Basin and Mackenzie Corridor, Northern Canada. *American Association of Petroleum Geologists Bulletin*, **76**, 1170–1189.

Jackson, J.A. 1987. Active normal faulting and crustal extension. *Pages 3–17 of:* Coward, M.P., Dewey, J.F., and Hancock, P.L. (eds), *Continental Extensional Tectonics.* Special Publication, no. 28. Geological Society of London.

Jackson, J.A., and McKenzie, D.P. 1983. The geometrical evolution of normal fault systems. *Journal of Structural Geology*, **5**, 471–482.

Jackson, J.A., and White, N.J. 1989. Normal faulting in the upper continental crust: observations from regions of active extension. *Journal of Structural Geology*, **11**, 15–36.

Jarvis, G.T. 1984. An extensional model of graben subsidence — the first stage of basin evolution. *Sedimentary Geology*, **40**, 13–31.

Jarvis, G.T., and McKenzie, D.P. 1980. The development of sedimentary basins with finite extension rates. *Earth and Planetary Science Letters*, **48**, 42–52.

Jolivet, L., Huchon, P., and Rangin, C. 1989. Tectonic settings of western Pacific marginal basins. *Tectonophysics*, **160**, 23–27.

Jones, F.W., and Majorowicz, J.A. 1987. Some aspects of the thermal regime and hydrodynamics of the western Canada sedimentary basin. *Pages 79–85 of:* Goff, J.C., and Willliams, B.P.J. (eds), *Fluid Flow in Sedimentary Basins and Aquifers.* Special Publication, no. 34. Geological Society of London.

Karner, G.D. 1991. Sediment blanketing and the flexural strength of extended continental lithosphere. *Basin Research*, **3**, 177–185.

Keen, C.E., and Beaumont, C. 1990. Geodynamics of rifted continental margins. *Pages 391–472 of:* Keen, M.J., and William, G.L. (eds), *Geology of Continental Margin of Eastern Canada.* Memoir, vol. 2. Geological Survey of Canada.

Keen, C.E., Beaumont, C., and Boutilier, R. 1981. Preliminary results of a thermomechanical model for the evolution of Antlantic-type continental margins. *Pages 123–128 of: Geology of Continental Margins.* Supplement, vol. 4. 26th International Geological Congress, Colloque C3.3.

Keen, C.E., MacLean, B.C., and Kay, W.A. 1991. A deep seismic reflection profile across the Nova Scotia continental margin, offshore eastern Canada. *Canadian Journal of Earth Sciences*, **28**, 1112–1120.

Kingston, D.R., Dishroon, C.P., and Williams, P.A. 1983. Global basin classification system. *American Association of Petroleum Geologists Bulletin*, **67**, 2175–2193.

Kirby, G.A., Morley, R.J., Humphreys, B., and eleven others. 1993. A re-evaluation of the regional geology and hydrocarbon prospectivity of the onshore central North Sumatra Basin. *Proceedings Indonesian Petroleum Association 22nd Annual Convention, Jakarta, October 1993*, 243–260.

Kooi, H., Cloetingh, S., and Burrus, J. 1992. Lithospheric necking and regional isostasy at extensional basins. 1. Subsidence and gravity modeling with an application to the Gulf of Lions margin (SE France). *Journal of Geophysical Research*, **B12**, 17553–17571.

Kusznir, N.J., and Ziegler, P.A. 1992. The mechanism of continental extension and sedimentary basin formation: a simple-shear/pure shear flexural cantilever model. *Tectonophysics*, **215**, 117–131.

Lacassin, R., Leloup, P.H., and Tapponnier, P. 1993. Bounds on strain in large Tertiary shear zones of SE Asia from boudinage restoration. *Journal of Structural Geology*, **15**, 677–692.

Latin, D.M., and Waters, F.G. 1992. Basaltic magmatism in the North Sea and its relationship to lithospheric extension. *Tectonophysics*, **208**, 77–90.

Leeder, M.R., and Gawthorpe, R.L. 1987. Sedimentary models for extensional tilt-block/half-graben basins. *Pages 139–152 of:* Coward, M.P., Dewey, J.F., and Hancock, P.L. (eds), *Continental Extensional Tectonics.* Special Publication, no. 28. Geological Society of London.

Letouzey, J. 1990. Fault reactivation, inversion and fold-thrust belt. *Pages 101–128 of:* Letouzey, J. (ed), *Petroleum in Mobile Belts.* Technip, Paris.

Letouzey, J., and Kimura, M. 1985. Okinawa Trough genesis: structure and evolution of a backarc basin developed in a continent. *Marine and Petroleum Geology*, **2**, 111–130.

Letouzey, J., Werner, P., and Marty, A. 1990. Fault reactivation and structural inversion; backarc and intraplate compressive deformations; examples of the eastern Sunda shelf (Indonesia). *Tectonophysics*, **183**, 341–362.

Liu, Guojiang. 1994. Tectonic modelling in the Björnöya West Basin of the Western Barents Sea. *Geophysical Prospecting*, **42**, 277–302.

Loke, M.H., Lee, C.Y., and van Klinken, G. 1983. Interpretation of regional gravity and magnetic data in Peninsular Malaysia. *Bulletin of the Geological Society of Malaysia*, **16**, 1–22.

Lopatin, N.V. 1971. Temperature and geologic time as factors in coalification. *Izv. Akad. Nauk USSR Ser. Geol.*, **3**, 95.

Lucazeau, F., and Douaran, S. Le. 1985. The blanketing effect of sediments in basins formed by extension: A numerical model. Application to the Gulf of Lion and Viking Graben. *Earth and Planetary Science Letters*, **74**, 92–102.

Lumadyo, E., McCabe, R., Harder, S., and Lee, T. 1993. Borneo: a stable portion of the Eurasian margin since the Eocene. *Journal of Southeast Asian Earth Sciences*, **8**, 225–231.

Lyle, M., and Ness, G.E. 1991. The opening of the Gulf of California. *Pages 403–423 of:* Dauphin, J.P., and Simoneit, B.R.T. (eds), *The Gulf and Peninsular Province of the Californias.* Memoir, no. 47. American Association of Petroleum Geologists.

MacDonald, A.S., Barr, S. M., Dunning, G.R., and Yaowanoiyothin, W. 1993. The Doi Inthanon metamorphic core complex in NW Thailand: age and tectonic significance. *Journal of Southeast Asian Earth Sciences*, **8**, 117–125.

MacDonald, G.J.F. 1965. Geophysical deductions from observations of heat flow. *Pages 191–210 of:* Lee, W.H.K. (ed), *Terrestrial Heat Flow.* Monograph, vol. 8. American Geophysical Union.

Madon, Mazlan B.Hj. 1992. Depositional setting and origin of berthierine oolitic ironstones in the lower Miocene Terengganu Shale, Tenggol Arch, offshore Peninsular Malaysia. *Journal of Sedimentary Petrology*, **62**, 899–916.

Maluski, H., Lacassin, R., Leloup, P.H., Tapponnier, P., Briais, A., Bunopas, S., Hinthong, C., and Siribhaki, K. 1993. Mid-Oligocene left-lateral shear along the Wang Chao fault zone (NW Thailand). *Terra Abstracts, EUG VII Strasbourg 4–8 April 1993*, 262.

Marrett, R., and Allmendinger, R.W. 1991. Estimates of strain due to brittle faulting: sampling of fault population. *Journal of Structural Geology*, **13**, 735–737.

Matsubayashi, O., and Uyeda, S. 1980. Estimation of heat flow in certain exploration wells in offshore area of Malaysia. *United Nations ECAFE, CCOP Technical Bulletin*, **13**, 11–22.

McCabe, R., Celaya, M., Cole, J., Han, H.C., Ohnstad, T., Paijitprapon, V., and Thitipawan, V. 1988. Extension tectonics: the Neogene opening of the north-south trending basins of Thailand. *Journal of Geophysical Research*, **93**, 11899–11910.

McCabe, R., Harder, S., Cole, J.T., and Lumadyo, E. 1993. The use of paleomagnetic studies in the understanding the complex Tertiary tectonic history of East and Southeast Asia. *Journal of Southeast Asian Earth Sciences*, **8**, 257–268.

McKenzie, D. 1978. Some remarks on the development of sedimentary basins. *Earth and Planetary Science Letters*, **40**, 25–32.

McKenzie, D.P., and Bickle, M.J. 1988. The volume and composition of melt generated by extension of the lithosphere. *Journal of Petrology*, **29**, 625–679.

McKenzie, D.P., and Jackson, J.A. 1986. A block model of distributed deformation by faulting. *Journal of the Geological Society of London*, **143**, 349–353.

McNutt, M.K., Diament, M., and Kogan, M.G. 1988. Variations of elastic plate thickness at continental thrust belts. *Journal of Geophysical Research*, **93**, 8825–8838.

Metcalfe, I. 1988. Origin and assembly of Southeast Asian continental terranes. *Pages 101–118 of:* Audley-Charles, M.G., and Hallam, A. (eds), *Gondwana and Tethys.* Special Publication, no. 37. Geological Society of London.

Metcalfe, I. 1989. Triassic sedimentation in the Central Basin of Peninsular Malaysia. *Pages 173–186 of: Proceedings of the International Symposium on Intermontane Basins: Geology and Resources, 30 Jan–2 Feb 1989.* Chiang Mai University.

Metcalfe, I. 1991. Late Palaeozoic and Mesozoic palaeogeography of Southeast Asia. *Palaeogeography, Palaeoclimatology, Palaeoecology*, **87**, 211–221.

Mitchell, A.H.G. 1981. Phanerozoic plate boundaries in mainland SE Asia, the Himalayas and Tibet. *Journal of the Geological Society of London*, **138**, 109–122.

Mitchum, R.M., Vail, P.R., and Thompson, S. 1977. Seismic stratigraphy and global changes of sea-level, part 2: The depositional sequence as the basic unit for stratigraphic analysis. *Pages 53–62 of:* Payton, C.E. (ed), *Seismic Stratigraphy — Applications to Hydrocarbon Exploration.* Memoir, no. 26. American Association of Petroleum Geologists.

Mohd, Firdaus Abdul Halim. 1993. *A study of geothermics in the Malaysian sedimentary basins.* PRSS Project No. 104/89.

Molnar, P., and Lyon-Caen, H. 1989. Fault plane solutions of earthquake and active tectonics of the Tibetan Plateau and its margins. *Geophysical Journal International*, **99**, 123–153.

Morley, C.K. 1989. Extension, detachments, and sedimentation in continental rifts (with particular reference to East Africa). *Tectonics*, **8**, 1175–1192.

Morley, C.K. 1995. Developments in the structural geology of rifts over the last decade and their impact on hydrocarbon exploration. *Pages 1–32 of:* Lambiase, J.J. (ed), *Hydrocarbon Habitats in Rift Basins.* Special Publication, vol. 80. Geological Society of London.

Morley, R.J., Azmi, Y., Awalludin, H., Bahari, M.N., and Munif, K. Ahmad. 1994. *Concepts and methods with respect to the application of biostratigraphy within the Malay Basin.* Technical Report. Petronas Research unpublished report.

Moulds, P.J. 1989. Development of the Bengkalis Depression, central Sumatra, and its subsequent deformation — a model for other Sumatran grabens? *Proceedings Indonesian Petroleum Association 18th Annual Convention*, **I**, 217–245.

Muraoka, H., and Kamata, H. 1983. Displacement distribution along minor fault traces. *Journal of Structural Geology*, **5**, 483–485.

Murphy, R.W. 1975. Tertiary basins of Southeast Asia. *Southeast Asia Petroleum Exploration Society Proceedings*, **2**, 1–36.

Murphy, R.W. 1989. *Individual contribution to*: Inversion tectonics - a discussion. *Geological Society of London Special Publication No*, **44**, 336–337.

Naylor, M.A., Mandl, G., and Sijpesteijn, C.H.K. 1986. Fault geometries in basement-induced wrench faulting under different initial stress states. *Journal of Structural Geology*, **8**, 737–752.

Ngah, Khalid. 1975. *Stratigraphic and structural analyses of the Penyu Basin, Malaysia.* Masters thesis, Oklahoma State University.

Nilsen, T.H., and Sylvester, A.G. 1995. Strike-slip basins. *Pages 425–457 of:* Busby, C.J., and Ingersoll, R.V. (eds), *Tectonics of Sedimentary Basins.* Blackwell Science, Cambridge, MA.

Otofuji, Y., Inoue, Y., Funahara, S., Murata, F., and Zhang, X. 1990. Paleomagnetic study of eastern Tibet — deformation of the Three River region. *Geophysical Journal International*, **103**, 85–94.

Packam, G.H. 1993. Plate tectonics and the development of sedimentary basins of the dextral regime in western Southeast Asia. *Journal of Southeast Asian Earth Sciences*, **8**, 497–511.

Parker, R. 1972. The rapid calculation of potential anomalies. *Geophysical Journal of the Royal Astronomical Society*, **31**, 447–455.

Peacock, D.C.P., and Sanderson, D.J. 1991. Displacement, segment linkage and relay ramp in normal fault zones. *Journal of Structural Geology*, **13**, 721–733.

Peacock, D.C.P., and Sanderson, D.J. 1994. Geometry and development of relay ramps in normal fault systems. *American Association of Petroleum Geologists Bulletin*, **78**, 147–165.

Peltzer, G., and Tapponnier, P. 1988. Formation and evolution of strike-slip faults, rifts, and basins during the India-Asia collision: an experimental approach. *Journal of Geophysical Research*, **93**, 15085–15117.

Pigott, J.D, and Sattarayak, N. 1993. Aspects of sedimentary basin evolution assessed through tectonic subsidence analysis. Example: northern Gulf of Thailand. *Journal of Southeast Asian Earth Sciences*, **8**, 407–420.

Pitman, W.C., and Andrews, J.A. 1985. Subsidence and history of small pull-apart basins. *Pages 45–49 of:* Biddle, K.T., and Christie-Blick, N. (eds), *Strike-slip Deformation, Basin Formation and Sedimentation.* Special Publication, no. 37. Society of Economic Paleontologists and Mineralogists.

Polachan, S., and Sattayarak, N. 1989. Strike-slip tectonics and the development of Tertiary basins in Thailand. *Proceedings International Symposium on Intermontane Basins: Geology and Resources. Chiang Mai, Thailand (30 January - 2 February 1989)*, 243–253.

Polachan, S., Pradidtan, S., Tongtaow, C., Janmaha, C., Intarawirti, K., and Sangsuwan, C. 1991. Development of Cenozoic basins in Thailand. *Marine and Petroleum Geology*, **8**, 84–97.

Pradier, B., Landais, P., Rochdi, A., and Davis, A. 1992. Chemical basis of fluorescence alteration of crude oils and kerogens—II. Fluorescence and infrared microspectrometric analysis of vitrinite and liptinite. *Organic Geochemistry*, **18**, 241–248.

Press, W.H., Teukolsky, S.A., Vetterling, W.T., and Flannery, B.P. 1992. *Numerical Recipes in C: The Art of Scientific Computing, 2nd Edition.* Cambridge University Press.

Raiga-Clemenceau, J., Martin, J.P., and Nicoletis, S. 1988. The concept of acoustic formation factor for more accurate porosity determination from sonic transit time data. *The Log Analyst*, **29**, 54–60.

Ramli, Mohd Nazri. 1988. Stratigraphy and paleofacies development of Carigali's operating areas in the Malay Basin, South China Sea. *Bulletin of the Geological Society of Malaysia*, **22**, 153–188.

Ramli, Nik. 1986. *Oligocene and Miocene sedimentology in the southeastern part of the Malay Basin, offshore West Malaysia.* Ph.D. thesis, University of Oxford.

Rangin, C., Jolivet, L., Pubellier, M., *et al.* 1990. A simple model for the tectonic evolution of Southeast Asia and Indonesia region for the past 43 m.y. *Bulletin de la société géologie de France*, **8**, 889–905.

Reading, H.G. 1980. Characteristics and recognition of strike-slip fault systems. *Pages 7–26 of:* Ballance, P.F., and Reading, H.G. (eds), *Sedimentation in Oblique-Slip Mobile Zones.* Special Publication, no. 4. International Association of Sedimentologists.

Remus, D., Webster, M., and Keawkan, K. 1993. Rift architecture and sedimentology of the Petchabun intermontane basin, central Thailand. *Journal of Southeast Asian Earth Sciences*, **8**, 421–432.

Rexilius, J.P., Hos, D.P.C., Powell, S.L., and Islam, M.A. 1992. *Biostratigraphic reports on Block PM14 wells, offshore West Malaysia: Cherating-1, Merchong-1, Rhu-1/1A and Rumbia-1.* Technical Report. International Stratigraphic Consultants Pty Ltd.

Richter, B., Fuller, M., Schmidtke, E., Myint, U. Tin, Ngwe, U. Tin, Win, U. Mya, and Bunopas, S. 1993. Paleomagnetic results from Thailand and Myanmar: implications for the interpretation of tectonic rotations in Southeast Asia. *Journal of Southeast Asian Earth Sciences*, **8**, 247–255.

Roberts, A., and Yielding, G. 1994. Continental extensional tectonics. *Pages 223–250 of:* Hancock, P.L. (ed), *Continental Deformation.* Pergamon, Oxford.

Roberts, A.M., Badley, M.E., Price, J.D., and Huck, I.W. 1990. The structural history of a transtensional basin: Inner Moray Firth, NE Scotland. *Journal of the Geological Society of London*, **147**, 87–103.

Roberts, A.M., Yielding, G., Kusznir, N.J., Walker, I., and Dorn-Lopez, D. 1993. Mesozoic extension in the North Sea: constraints from flexural backstripping, forward modelling and fault populations. *Pages 1123–1136 of:* Parker, J.R. (ed), *Petroleum Geology of Northwest Europe: Proceeding of the 4th Conference.* Geological Society of London.

Roberts, S., and Jackson, J.A. 1991. Active normal faulting in Central Greece: an overview. *Pages 125–142 of:* Roberts, A.M., Yielding, G., and Freeman, B. (eds), *The Geometry of Normal Faults.* Special Publication, no. 56. Geological Society of London.

Rodgers, D.A. 1980. Analysis of pull-apart basin development produced by en echelon strike-slip faults. *Pages 27–41 of:* Ballance, P.F., and Reading, H.G. (eds), *Sedimentation in Oblique-Slip Mobile Zones.* Special Publication, no. 4. International Association of Sedimentologists.

Roques, D., Rangin, C., Lepvrier, C., and Huchon, P. 1995. Da Nang Area structural analysis: An onshore-offshore integrated study of central Vietnam. *Geological Society of London Petroleum Group Conference: Petrolem Geology of Southeast Asia, London, 26-27th September 1995*, Abstract.

Rosendahl, B.R. 1987. Architecture of continental rifts with special reference to East Africa. *Annual Reviews of Earth and Planetary Science*, **15**, 445–503.

Rowley, D.B., and Sahagian, D. 1986. Depth-dependent stretching: A different approach. *Geology*, **14**, 32–45.

Royden, L., and Keen, C.E. 1980. Rifting processes and thermal evolution of the continental margin of eastern Canada determined from subsidence curves. *Earth and Planetary Science Letters*, **51**, 342–361.

Ru, Ke, and Pigott, J.D. 1987. Episodic rifting and subsidence in the South China Sea. *American Association of Petroleum Geologists Bulletin*, **70**, 1015–1024.

Ruppel, C., Kogan, M.G., and McNutt, M.K. 1993. Implications of new gravity data for Baikal Rift Zone structure. *Geophysical Research Letters*, **20**, 1635–1638.

Rutherford, K.J., and Qureshi, M.K. 1981. *Geothermal gradient map of SE Asia. 2nd Edition.* Southeast Asia Petroleum Exploration Society/ Indonesian Petroleum Association.

Ryall, J.C. 1982. Some thoughts on the crustal structure of Peninsular Malaysia — results of a gravity traverse. *Bulletin of the Geological Society of Malaysia*, **15**, 9–18.

Sanchez-Zamora, O., Doguin, P., Couch, R.W., and Ness, G.E. 1991. Magnetic anomalies of the northern Gulf of California: structural and thermal interpretations. *Pages*

377–401 of: Dauphin, J.P., and Simoneit, B.R.T. (eds), *The Gulf and Peninsular Province of the Californias.* Memoir, no. 47. American Association of Petroleum Geologists.

Sandwell, D.T., and Smith, W.H.F. 1992. Global marine gravity from ERS-1, Geosat and Seasat reveals new tectonic fabric. **EOS**, *Transactions of the American Geophysical Union*, **73 (43)**, 133.

Schärer, U., Tapponnier, P., Lacassin, R., Leloup, P.H., Dulai, Z., and Shaocheng, J. 1990. Intraplate tectonics in Asia: a precise age for large-scale Miocene movement along the Ailao Shan – Red River shear zone, China. *Earth and Planetary Science Letters*, **97**, 65–70.

Schärer, U., Tapponnier, P., and Xiachan, L. 1993. Precise dating of Tertiary strike-slip movement in the Red River shear belt. *Terra Abstracts, EUG VII Strasbourg 4–8 April 1993*, 268.

Schärer, U., Zhang, L.-S., and Tapponnier, P. 1994. Duration of strike-slip movements in large shear zones: The Red River belt, China. *Earth and Planetary Science Letters*, **126**, 379–397.

Schmidtke, E., Fuller, M., and Haston, R. 1990. Paleomagnetic data from Sarawak, Malaysian Borneo and the Late Mesozoic tectonics of Sundaland. *Tectonics*, **9**, 123–140.

Schreurs, G. 1994. Experiments on strike-slip faulting and block rotation. *Geology*, **22**, 567–570.

Sclater, J.G., and Christie, P.A.F. 1980. Continental stretching: an explanation of the post-mid-Cretaceous subsidence of the central North Sea basin. *Journal of Geophysical Research*, **85**, 3711–3739.

Scott, D.L., Braun, J., and Etheridge, M.A. 1994. Dip analysis as a tool for estimating regional kinematics in extensional terranes. *Journal of Structural Geology*, **16**, 393–401.

Şengör, A.M.C. 1979. Mid-Mesozoic closure of Permo-Triassic Tethys and its implications. *Nature*, **279**, 590–593.

Şengör, A.M.C. 1987. Tectonics of the Tethysides: orogenic collage development in a collisional setting. *Annual Reviews of Earth and Planetary Science*, **15**, 213–244.

Şengör, A.M.C., and Burke, K. 1978. Relative timing of rifting and volcanism on Earth and its tectonic implications. *Geophysical Research Letters*, **5**, 419–421.

Şengör, A.M.C., and Hsü, K.J. 1984. The Cimmerides of eastern Asia: history of the eastern end of the Paleo-Tethys. *Memoir de la société géologie de France*, **147**, 139–167.

Seoparjadi, R.A., Nayoan, G.A.S., L.R. Beddoes, Jr., and James, W.V. 1975. Exploration play concepts in Indonesia. *Proceedings 9th World Petroleum Congress, Tokyo*, **3**, 51–64.

Shelton, J.W. 1984. Listric normal faults: An illustrated summary. *American Association of Petroleum Geologists Bulletin*, **68**, 801–815.

Sibson, R.H. 1995. Selective fault reactivation during basin inversion: potential redistribution through fault-valve action. *Pages 3–20 of:* Buchanan, P.G., and Buchanan, P.G. (eds), *Basin Inversion.* Special Publication, no. 88. Geological Society of London.

Singh, D. Santokh, Chu, L.H., and Teoh, L.H. 1984. The Stong Complex: A reassessment. *Bulletin of the Geological Society of Malaysia*, **17**, 61–77.

Situmorang, B., and Yulihanto, B. 1985. The role of strike-slip faulting in structural development of the North Sumatra Basin. *Proceedings of the Indonesian Petroleum Association 14th Annual Convention, Jakarta, October 1985*, 21–38.

Situmorang, B., Guntur, A., Yulihanto, B., Himawan, R., and Jacob, T. Gamal. 1991. Structural development of the Ombilin Basin, West Sumatra. *Proceedings Indonesian Petroleum Association 20th Annual Convention, Jakarta, October 1991*, 1–16.

Stauffer, P.H. 1968. The Kuala Lumpur Fault Zone: a proposed major strike-slip fault across Malaya. *Newsletter of the Geological Society of Malaysia*, **15**, 2–4.

Steckler, M.S. 1985. Uplift and extension at the Gulf of Suez: indications of induced mantle convection. *Nature*, **317**, 135–139.

Steckler, M.S., and Watts, A.B. 1978. Subsidence of the Atlantic-type continental margin off New York. *Earth and Planetary Science Letters*, **41**, 1–13.

Stephenson, R.A., Nakiboglu, S.M., and Kelly, M.A. 1989. Effects of asthenosphere melting, regional thermoisostasy, and sediment loading on the thermomechanical subsidence of extensional sedimentary basins. *Pages 17–27 of:* Price, R.A. (ed), *Origin and Evolution of Sedimentary Basins and their Energy and Mineral Resources.* Monograph, no. 48. American Geophysical Union.

Su, Daquan, White, N., and McKenzie, D. 1989. Extension and subsidence of the Pearl River Mouth Basin, northern South China Sea. *Basin Research*, **2**, 205–222.

Sweeney, J.J., and Burnham, A.K. 1990. Evaluation of a simple model of vitrinite reflectance based on chemical kinetics. *American Association of Petroleum Geologists Bulletin*, **74**, 1559–1570.

Talwani, M., Worzel, J.L., and Landisman, M. 1959. Rapid gravity computations for two-dimensional bodies with application to the Mendocino Fracture Zone. *Journal of Geophysical Research*, **64**, 49–59.

Tan, D.N.K., and Lamy, J.M. 1991. Tectonic evolution of the NW Sabah margin since the late Eocene. *Bulletin of the Geological Society of Malaysia*, **27**, 241–260.

Tapponnier, P., and Molnar, P. 1976. Slip-line field theory and large-scale continental tectonics. *Nature*, **264**, 319–324.

Tapponnier, P., Peltzer, G., Dain, A.Y. Le, and Armijo, R. 1982. Propagating extrusion tectonics in Asia: new insights from simple experiments with plasticine. *Geology*, **10**, 611–616.

Tapponnier, P., Peltzer, G., and Armijo, R. 1986. On the mechanics of the collision of India and Asia. *Pages 115–157 of:* Coward, M.P., and Ries, C. (eds), *Collision Tectonics.* Special Publication, no. 19. Geological Society of London.

Taylor, B., and Hayes, D.E. 1980. The tectonic evolution of the South China Basin. *Pages 89–104 of:* Hayes, D.E. (ed), *The Tectonic and Geologic Evolution of Southeast Asian Seas and Islands.* Geophysical Monograph, vol. 23. American Geophysical Union.

ten Brink, U.S., and Ben-Avraham, Z. 1989. The anatomy of a pull-apart basin: seismic reflection observations of the Dead Sea Basin. *Tectonics*, **8**, 333–350.

TEXACO, Exploration Penyu Inc. 1992. *The significance of the Rhu oil discovery, PM-14, offshore Peninsular Malaysia: A preliminary summary.* unpublished report, ER:TEXACO:1:92-01.

Thamrin, M. 1985. An investigation of relationship between the geology of Indonesian sedimentary basins and heat flow density. *Tectonophysics*, **121**, 45–62.

Tjia, H.D. 1972. Strike-slip faults in West Malaysia. *24th International Geological Congress Section 3*, 255–262.

Tjia, H.D. 1993. *Inversion tectonics in the Malay Basin: evidence and timing of events.* Technical Report. PRSS Report RP5-93-04.

Trudgill, B., and Cartwright, J. 1994. Relay-ramp forms and normal-fault linkages, Canyonlands National Park, Utah. *Geological Society of America Bulletin*, **106**, 1143–1157.

Turcotte, D.L., and Schubert, G. 1982. *Geodynamics: Applications of Continuum Mechanics to Geological Problems.* Wiley, New York.

Ungerer, P., Burrus, J., Doligez, B., Chénet, P.Y., and Bessis, F. 1990. Basin evaluation by integrated two-dimensional modeling of heat transfer, fluid flow, hydrocarbon generation, and migration. *American Association of Petroleum Geologists Bulletin*, **74**, 309–335.

van der Beek, P. 1995. *Tectonic evolution of continental rifts: inferences from numerical modelling and fission track thermochronology.* Ph.D. thesis, Free University, Amsterdam.

Vendeville, B., and Cobbold, P.R. 1988. How normal faulting and sedimentation interact to produce listric fault profiles and stratigraphic wedges. *Journal of Structural Geology*, **10**, 649–659.

Villemin, T., Angelier, J., and Sunwoo, C. 1992. Fractal distribution of fault lengths and offsets: Implications on brittle deformation: The Lorraine Coal Basin (NE France). *In:* Barton, C., and Point, P. La (eds), *Fractals and their use in the Petroleum Industry.* Book Series. American Association of Petroleum Geologists.

Wajzer, M.R., Barber, A.J., Hidayat, S., and Suharsono. 1991. Accretion, collision and strike-slip faulting: the Woyla Group as a key to the tectonic evolution of North Sumatra. *Journal of Southeast Asian Earth Sciences*, **6**, 447–461.

Walsh, J.J., and Watterson, J. 1987. Distribution of cumulative displacement and of seismic slip on a single normal fault surface. *Journal of Structural Geology*, **9**, 1039–1046.

Walsh, J.J., and Watterson, J. 1988. Analysis of the relationship between displacement and dimensions of faults. *Journal of Structural Geology*, **10**, 239–247.

Wan, Ismail Wan Yusoff. 1984. Heat flow study in the Malay Basin. *Pages 77–87 of: Combined Proceedings of the Joint ASCOPE/CCOP Workshops on Heat Flow (1981).* Technical Publication, vol. 15. CCOP.

Wan, Ismail Wan Yusoff. 1990. Heat flow in offshore Malaysian basins. *Pages 39–54 of: Proceedings CCOP Heat Flow Workshop III.* Technical Publication, vol. 21. CCOP.

Waples, D.W. 1980. Time and temperature in petroleum formation: Application of Lopatin's method to petroleum exploration. *American Association of Petroleum Geologists Bulletin*, **64**, 916–926.

Waples, D.W. 1994. Basin modelling: How well have we done? *Geological Society of London Petroleum Group Conference on Basin Modelling, 1–2 Nov. 1994, London*, **Abstract Volume**.

Waples, D.W., and Ramly, M. in press. A simple statistical method for correcting and standardizing heat flows and subsurface temperatures derived from log and test data. *In:* Teh, G.H. (ed), *Proceedings AAPG International Conference 1994: Southeast Asian Basins: Oil and Gas in the 21st Century, Kuala Lumpur.* Geological Society of Malaysia.

Waples, D.W., Ramly, M., and Leslie, W. in press. Implications of vitrinite-reflectance suppression for the tectonic and thermal history of the Malay Basin. *In:* Teh, G.H. (ed), *Proceedings AAPG International Conference 1994: Southeast Asian Basins: Oil and Gas in the 21st Century, Kuala Lumpur.* Geological Society of Malaysia.

Watts, A.B. 1978. An analysis of isostasy in the world's oceans: 1. Hawaiian-Emperor Seamount Chain. *Journal of Geophysical Research*, **83**, 5989–6004.

Watts, A.B. 1982. Tectonic subsidence, flexure amd global changes of sea level. *Nature*, **297**, 469–472.

Watts, A.B. 1988. Gravity anomalies, crustal structure and flexure of the lithosphere at the Baltimore Canyon Trough. *Earth and Planetary Science Letters*, **89**, 221–238.

Watts, A.B. 1992. The effective elastic thickness of the lithosphere and the evolution of foreland basins. *Basin Research*, 4, 169–178.

Watts, A.B., and Marr, C. 1995. Gravity anomalies and the thermal and mechanical structure of rifted continental margins. *In:* Banda, E., *et al.* (eds), *Rifted Ocean-Continent Boundaries.* Kluwer Academic Publishers.

Watts, A.B., and Ryan, W.B.F. 1976. Flexure of the lithosphere and continental margin basins. *Tectonophysics*, **36**, 25–44.

Watts, A.B., and Thorne, J. 1984. Tectonics, global changes in sea level and their relationship to stratigraphical sequences at the US Atlantic continental margin. *Marine and Petroleum Geology*, **1**, 319–339.

Watts, A.B., and Torné, M. 1992. Crustal structure and the mechanical properties of extended continental lithosphere in the Valencia Trough. *Journal of the Geological Society of London*, **149**, 813–827.

Watts, A.B., Bodine, J.H., and Bowin, C.O. 1978. Free air gravity field. *Pages 5–6 of:* Hayes, D.E. (ed), *Geophysical Atlas of East and Southeast Asian Seas.* Map and Chart Series, vol. MC-25. Geological Society of America.

Watts, A.B., Karner, G.D., and Steckler, M.S. 1982. Lithospheric flexure and the evolution of sedimentary basins. *Philosophical Transaction Royal Society of London*, **A305**, 249–281.

Weissel, J.K., and Karner, G.D. 1989. Flexural uplift of rift flanks due to mechanical unloading of lithosphere during extension. *Journal of Geophysical Research*, **94**, 13919–13945.

Wernicke, B. 1985. Uniform-sense simple shear of the continental lithosphere. *Canadian Journal of Earth Sciences*, **22**, 108–125.

Wernicke, B.R., and Burchfiel, B.C. 1982. Modes of extensional tectonics. *Journal of Structural Geology*, **141**, 634–649.

Wheildon, J., Morgan, P., Williamson, K.H., Evans, T.R., and Swanberg, C.A. 1994. Heat flow in the Kenya Rift Zone. *Tectonophysics*, **236**, 131–149.

White, J.M.Jr., and Wing, R.S. 1978. Structural development of the South China Sea with particular references to Indonesia. *Proceedings Indonesian Petroleum Association 7th Annual Convention, Jakarta, June 1978*, 159–178.

White, N., and Latin, D. 1993. Lithospheric stretching from subsidence analyses in the North Sea 'triple junction'. *Journal of the Geological Society of London*, **150**, 473–488.

White, N., and McKenzie, D. 1988. Formation of "steer's head" geometry of sedimentary basins by differential stretching of crust and mantle. *Geology*, **16**, 250–253.

White, N.J., Jackson, J.A., and McKenzie, D.P. 1986. The relationship between the geometry of normal faults and that of the sedimentary layers in their hanging walls. *Journal of Structural Geology*, **8**, 897–909.

White, R.S., and McKenzie, D. 1989. Magmatism at rift zones: the generation of volcanic continental margins and flood basalts. *Journal of Geophysical Research*, **94**, 7685–7729.

Wilkins, R.W.T., Wilmhurst, J.R., Russell, N.J., Hladky, G., Ellacott, M.V., and Buckingham, C. 1992. Fluorescence alteration and the suppression of vitrinite reflectance. *Organic Geochemistry*, **18**, 629–640.

Wilkins, R.W.T., Wilmhurst, J.R., Hladky, G., Ellacot, M.V., and Buckingham, C.P. 1995. Should fluorescence alteration replace vitrinite reflectance as a major tool for thermal maturity determination in oil exploration? *Organic Geochemistry*, **22**, 191–209.

Williams, H.H., Fowler, M., and Eubank, R.T. 1995. Characteristics of selected Paleogene and Cretaceous lacustrine source basins of Southeast Asia. *Pages 241–282 of:* Lambiase, J.J. (ed), *Hydrocarbon Habitat of Rift Basins.* Special Publication, no. 80. Geological Society of London.

Williams, P.R., Supriatna, S., and Harahap, B. 1986. Cretaceous melange in west Kalimantan and its tectonic implications. *Bulletin of the Geological Society of Malaysia*, **19**, 69–78.

Williams, P.R., Johnston, C.R., Almond, R.A., and Simamora, W.H. 1988. Late Cretaceous to Early Tertiary structural elements of West Kalimantan. *Tectonophysics*, **148**, 279–297.

Windley, B.F., and Allen, M.B. 1993. Mongolian Plateau; evidence for a late Cenozoic mantle plume under central Asia. *Geology*, **21**, 295–298.

Wongsosantiko, A., and Wirojudo, G.K. 1984. Tertiary tectonic evolution and related hydrocarbon potential in the Natuna area. *Proceedings of the Indonesian Petroleum Association 13th Annual Convention, Jakarta, August 1975*, 202–211.

Wood, B.G.M. 1985. The mechanics of progressive deformation in crustal plates - A working model for Southeast Asia. *Bulletin of the Geological Society of Malaysia*, **18**, 55–99.

Wood, D.A. 1988. Relationship between thermal maturity indices calculated using Arrhenius equation and Lopatin method: implications for petroleum exploration. *American Association of Petroleum Geologists Bulletin*, **72**, 115–134.

Woodcock, N.H., and Fischer, M. 1986. Strikes-slip duplexes. *Journal of Structural Geology*, **8**, 725–735.

Yan, C., and Courtillot, V. 1989. Widespread Cenozoic (?) remagnetization in Thailand and its implications for the India–Asia collision. *Earth and Planetary Science Letters*, **93**, 113–122.

Yeats, R.S. 1983. Large-scale Quaternary detachments in Ventura Basin, southern California. *Journal of Geophysical Research*, **88**, 569–583.

Zhang, Z.-M., Liou, G., and Coleman, R.G. 1989. The Mesozoic and Cenozoic tectonism in Eeastern China. *Pages 124–139 of:* Ben-Avraham, Z. (ed), *The Evolution of the Pacific Ocean Margin.* Oxford University Press.